Investigations of Spectral Properties in Power Systems

Felix Koeth

Communauté UNIVERSITÉ Grenoble Alpes

THÈSE

Pour obtenir le grade de

DOCTEUR DE LA COMMUNAUTÉ UNIVERSITÉ GRENOBLE ALPES

Spécialité : **GENIE ELECTRIQUE**

Arrêté ministériel : 25 mai 2016

Présentée par

Felix KOETH

Thèse dirigée par **Nicolas RETIERE**

préparée au sein **Laboratoire de Génie Electrique**
dans **l'École Doctorale EEATS**

Etude des propriétés spectrales des graphes des réseaux électriques.

Investigations of Spectral Graph Properties in Power Systems

Thèse soutenue publiquement le **19 décembre 2019**,
devant le jury composé de :

Monsieur Didier Georges
Professeur des Universités, Grenoble-INP, Président

Monsieur Ettore Bompard
Professeur des Universités, Politecnico di Torino, Rapporteur

Monsieur Philippe Jacquod
Professeur des Universités, HES-SO Valais-Wallis, Rapporteur

Monsieur Jose Luis Dominguez
Charge de Recherche, IREC Barcelona, Examinateur

Monsieur Jean-Guy Caputo
Maitres de conférénce - INSA Rouen, Invitée

Monsieur Nicolas Retiere
Professeur des Universités, Université Grenoble Alpes, Directeur de thèse

Contents

List of Figures

List of Tables

List of Abbreviations

SP	**S**tructure **P**reserving
EP	**E**igenvalue **P**roblem
GEP	**G**eneralized **E**igenvalue **P**roblem
QEP	**Q**uadratic **E**igenvalue **P**roblem
ODE	**O**rdinary **D**ifferential **E**quation
CC	**C**onnected **C**omponents

List of Symbols

$\imath$	imaginary unit, $\sqrt{-1}$	
L	Laplacian matrix	
A	adjacency matrix	
M^T	Transpose of matrix M	
M^{-1}	Inverse of matrix M	
$M^\dagger$	Pseudo inverse of matrix M (Moore–Penrose inverse)	
$n_\mathcal{S}$	Cardinality of set $\mathcal{S}$	
$\lvert x \rvert$	absolute value of x	
$\lVert v \rVert$	norm of v (generally the 2-norm)	
I_n	$n \times n$ identity matrix	
J_n	$n \times n$ matrix of all ones	
$\mathcal{V}$	Set of vertices	
$\mathcal{E}$	Set of edges	
$\mathcal{G}(\mathcal{V}, \mathcal{E})$	Graph consisting of vertices $\mathcal{V}$ and edges $\mathcal{E}$	
$\mathcal{P}$	Set of generators (Producers)	
$\mathcal{C}$	Set of loads (Consumers)	
P_B	Bus power (either consumed or produced)	
P	active power	W ($\mathrm{J\,s^{-1}}$)
Q	reactive power	W ($\mathrm{J\,s^{-1}}$)
V	Voltage	V
I	Current	A
Y	Nodal admittance matrix	S
M	Inertia	
D	Damping	
ω	angular frequency	$\mathrm{rad\,s^{-1}}$
θ	bus phase angle	rad
α	generator phase angle	rad
δ_{ij}	Kronecker delta	
λ_k	k-th eigenvalue	

$\mathcal{S}$	Sets are written in a calligraphic font
C	Complex numbers are written in a sans serif font
$\boldsymbol{V}$	Vectors are written in a bold font
$\mathrm{Im}(\mathsf{x})$	imaginary part of x
$\mathrm{Re}(\mathsf{x})$	imaginary part of x
$(\boldsymbol{x})_{\mathcal{S}} = \boldsymbol{x}_{\mathcal{S}}$	Elements of x corresponding to the set $\mathcal{S}$

General Introduction - Overview

The world is becoming increasingly complex. Hundreds of years ago, many people almost never left their villages. Advances in transportation made people to be *global citizens*, travelling the world for work and leisure. Companies, previously focused on a city or area now span the world. In the globalised economy, goods are produced in some parts of the world and sold in another. Modern communication, especially the internet, allows people to meet and interact with people around the world at any time. This complexity can be described by networks [1]. Humans have social networks, connecting them with family, friends, colleagues or acquaintances. Large enterprises can be seen as a large network of employees, properties and products. Communication is based both on a real world networks which transfer data, and on abstract networks like friends on social media. The rising complexity can be described by changes in the structure of the underlying networks. We are able to meet more people from different cultures, which can wildly expand and widen our social network.

Networks are also of vital important in many fields of natural science. The brain is a complex network of neurons, connected by synapses. The structure of these connections are responsible for thinking and memory [2, 3]. Networks can also be used to describe the the complicated physiological and biochemical properties of cells [4]. A combination between the social networks and biological systems is the modelling of virus spreads [5]. A fundamental tool in the science of stochastic processes are the Markov chains. They model random processes with the important property that their future development only depends on the current state and not on the past [6]. There is a direct link between Markov chains and networks [7]. They can be used for the long time simulation of molecular dynamics [8] or to model the states of ion channels in neurons [9, 10].

Another network of major importance is the power system. It is responsible to generate, transfer and consume electrical energy. The power system is the largest man made structure [11] and spans over whole continents. From home appliances, communication including the internet to many industrial processes, electrical energy is vital for modern life. But this network has to undergo significant changes.

Climate change is one of the main problems the world is facing, socially and ecologically [12]. Greenhouse gases are directly responsible for the rise of temperature worldwide. The production of heat and electricity is responsible for almost 60% of the greenhouse gas emissions [13]. With increased electric mobility and heating, the demand for electric energy will further rise. Moving to renewable energy production, like wind or solar, is a necessity. These energy sources will be more intermittent and less centralised than the conventional sources [14]. A larger usage of power electronics and converters will decrease the inertia of the system, which might lead to destabilisation [15]. All of these changes and challenges will reshape the network.

In any field, dynamics on networks are usually especially important [16]. For example, the aforementioned neurons emit a time varying action potential, which travels through the network. All neurons in the network can react to this signal and fire accordingly. Schooling fish can be seen as a network between fishes. The movement of each fish affects the movement of neighbouring fish. This results in an interesting interplay, where the individual dynamics affect the whole system, but the system also influences the individual behaviour.

The dynamics of power systems are crucial for the stability of the system. Dynamical instabilities are the main cause of large incidences, such as costly blackouts in the system. Hence, this work focuses on the dynamics of power systems and especially the influence of the geometry of the system on these dynamic properties. To tackle the complexity of the system, we will not use the normal simulation based approaches common in engineering to investigate the main drivers of the dynamics. Instead, we will use spectral graph theory to make the links between the dynamics and the geometry of the system. We use this method to transform the geometry of the network into the geometry of the eigenvectors of the system, which then describe the dynamics of the system.

Thesis Outline

This thesis is divided into six main chapters. Roughly, the first two chapters are the introduction and the mathematical background. Chapters 3 and 4 are the application of spectral graph theory to power systems research, focusing on static and dynamic properties. Chapter 5 is a theoretical investigation of a phenomenon observed in both dynamic and static power system research. In general, all sections can be read individually. A more detailed overview about the contents of each section is given here:

- **Chapter 1** introduces the impact of geometry in networks and explains the modelling background of power systems. The chapter finishes with a literature review about stability problems in power systems and the role of geometry in these studies.
- **Chapter 2** explains spectral graph theory, a method to investigate graphs. Many methods and results from graph theory and spectral graph theory are introduced and explained for simple graphs. Also, the application of spectral graph theory in power system research is reviewed.
- **Chapter 3** gives a short example of spectral power flow, which solves the DC power flow problem using spectral methods. This method can be used to decompose the flow into different modes and investigate the flows in each line separately. It is shown how these flows depend on the eigenvalues and eigenvectors of the underlying network.
- **Chapter 4** is focused on spectral methods in dynamical power systems. First, the small signal problem is introduced as a quadratic eigenvalue problem. The properties of the quadratic eigenvalue problem are introduced and investigated with respect to the power system studies. Numerical tests to investigate the impact of the machine parameters (mainly the damping and the inertia of the generators) and the underlying network are performed. Finally, a new eigenvalue perturbation method is proposed to relate the solutions of the quadratic eigenvalue problem with the easier generalised eigenvalue problem.
- **Chapter 5** investigates localisation, a phenomenon observed in the previous two chapters. First, necessary definitions are given and simple example cases are investigated. Next, two eigenvector bounds are derived mathematically, which can be used to describe localisation. These bounds are extensively tested on a real power system test case to show how the bounds successfully predict and explain localisation.
- **Chapter 6** concludes this thesis and gives an outlook about further research directions.

The main contributions in this thesis are found in Chapter 5. The eigenvector bounds derived therein are a new tool to investigate localisation in graphs. The application to simplified systems and a real world example show that these tools lead to a functional method to work with localisation problems in graphs. While the focus on this work were power systems, these methods and results might also be applied to other fields where the eigenvectors of graphs are important.

Résumé en français

Introduction et contexte

Le système électrique joue un rôle essentiel pour assurer un niveau de vie élevé dans de grandes parties du monde. En raison des défis du changement climatique, le système électrique doit s'adapter, par exemple en intégrant davantage de sources d'énergie renouvelables. Le système électrique est un système vaste et complexe. Ce travail tente d'étudier l'influence des propriétés topologiques du réseau sur le comportement statique et dynamique du système.

Pour les systèmes simplifiés, le comportement dynamique du système peut être décrit par l'équation d'oscillation, donnée comme:

$$\begin{aligned} M_i\ddot{\theta}_i + D_i\dot{\theta}_i &= P_{B,i} - \sum_{j=1}^{n} a_{ij}\sin\big(\theta_i - \theta_j\big) \quad i \in \mathcal{V}_\mathcal{P} \\ D_i\dot{\theta}_i &= P_{B,i} - \sum_{j=1}^{n} a_{ij}\sin\big(\theta_i - \theta_j\big) \quad i \in \mathcal{V}_\mathcal{C} \end{aligned} \tag{1}$$

Nous pouvons linéariser le système pour les petites perturbations $\Delta\theta$ autour d'un point de fonctionnement θ^* :

$$M\ddot{\Delta\theta} + D\dot{\Delta\theta} = P_B - L\Delta\theta \tag{2}$$

Ici, L est la matrice laplacienne du graphe sous-jacent du système. La linéarisation met en évidence l'interaction entre la topologie du réseau, encodée en L, et le comportement dynamique du système électrique. Si les dérivées temporelles sont considérées comme nulles, $\ddot{\Delta\theta} = \dot{\Delta\theta} = 0$, on trouve les équations de flux de puissance, données comme :

$$P_B = L\Delta\theta \tag{3}$$

On trouvera plus de détails dans chapter 1 et chapter 2.

Flux de puissance spectrale

Comme nous l'avons vu dans la section précédente, les équations linéarisées de flux de puissance peuvent être utilisées pour trouver les phases θ en utilisant la matrice

laplacienne L et les puissances P_B. Nous pouvons projeter les solutions de θ et de la puissance P sur la base formée par les vecteurs propres ϕ, correspondant aux valeurs propres λ de L. Cela décompose le système en différents modes, qui correspondent aux oscillations spatiales des puissances dans le système. Les projections sont données sous la forme :

$$P = \sum_{k=1}^{n} \underbrace{\frac{\phi_k \cdot P}{\phi_k \cdot \phi_k^T}}_{=:p_k} \phi_k = \sum_{k=1}^{n} p_k \phi_k \tag{4}$$

$$\boldsymbol{\theta} = \sum_{k=1}^{n} o_k \boldsymbol{\phi}_k \tag{5}$$

Où p_k et o_k décrivent comment P et θ sont répartis sur les différents modes. Résoudre les équations de flux de puissance équivaut à trouver que $p_k = \frac{o_k}{\lambda_k}$. En utilisant cette décomposition, nous pouvons décomposer les flux dans chaque ligne à chaque mode. Les flux F_k sont donnés sous la forme :

$$F_k = B \frac{p_k}{\lambda_k} \nabla \boldsymbol{\phi}_k \tag{6}$$

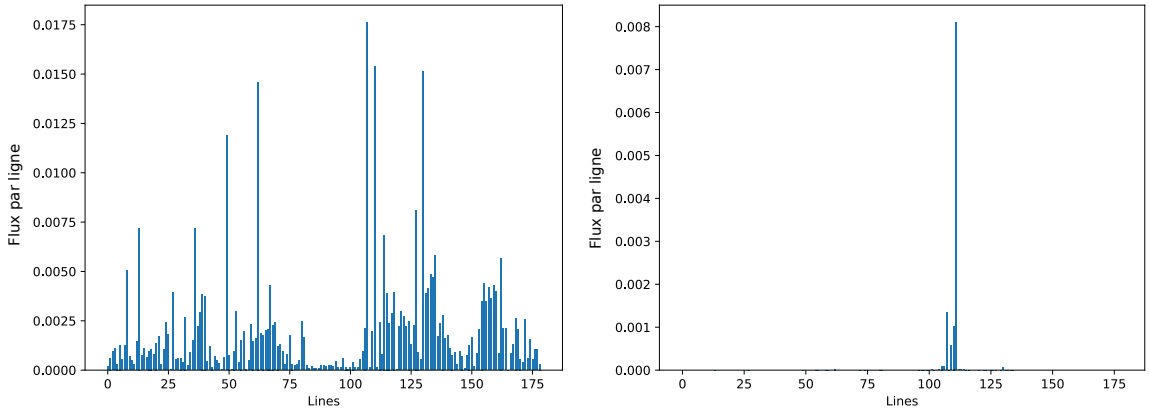

(A) $k = 2$ (B) $k = 118$

FIGURE 1: Flux par ligne pour la deuxième plus petite et la plus grande valeur propre.

Dans fig. 1, nous montrons les flux pour la deuxième plus petite et la plus grande valeur propre du cas de test IEEE 118. Nous pouvons voir qu'à la petite valeur propre, les flux sont répartis sur de nombreuses lignes. Pour la grande valeur propre, les flux sont confinés à une seule ligne. La raison de ce phénomène est le vecteur

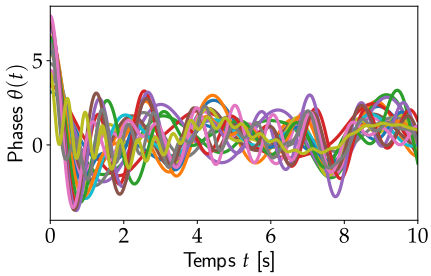

FIGURE 2: Oscillations du modèle de système électrique linéarisé.

propre localisé ϕ au mode 118, qui est presque nul partout sauf pour deux nœuds, où les flux apparaissent. Vous trouverez plus d'informations sur l'application de la théorie des graphes spectraux sur les flux de puissance dans chapter 3.

Propriétés spectrales des systèmes d'énergie dynamiques

Dans cette section, nous voulons étudier les propriétés de l'équation dynamique linéarisée, donnée dans eq. (2). Cette équation peut être résolue par un problème quadratique de valeurs propres avec les matrices M, D, L as :

$$\left(\lambda^2 M + \lambda D + L\right)\phi = 0 \tag{7}$$

La réponse temporelle peut être calculée à partir des valeurs propres λ et des vecteurs propres ϕ du problème quadratique des valeurs propres. Les valeurs propres décrivent les fréquences des oscillations, les vecteurs propres la participation de chaque nœud à une fréquence donnée. La réponse temporelle pour le cas de test IEEE 118 est indiquée dans fig. 2.

Nous nous intéressons à la façon dont les valeurs propres et les vecteurs propres dépendent des M, des D et des L. Une enquête simple est présentée dans fig. 3. Ici, les valeurs propres sont indiquées après avoir perturbé M et D. Les valeurs propres originales sont en bleu, les valeurs propres perturbées en gris. Nous pouvons voir que M influence le système beaucoup plus fortement que D. De plus, les valeurs propres plus importantes sont plus fortement perturbées, dans les deux cas.

Cette forte perturbation aux modes élevés correspond à nouveau à des valeurs propres localisées. Pour plus de détails sur les propriétés spectrales du problème des valeurs propres quadratiques dans les applications de réseaux électriques, voir chapter 4.

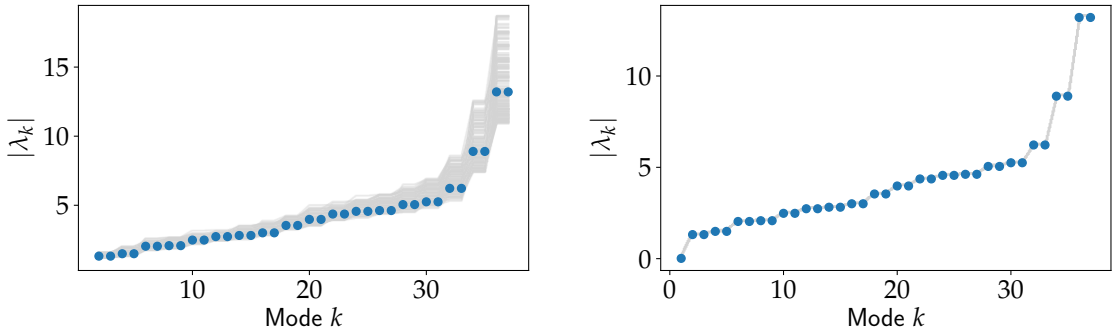

(A) Modification de l'inertie (B) Modification de l'amortissement

FIGURE 3: Spectres du cas d'essai IEEE 118 avec inertie modifiée aléatoirement M et paramètre d'amortissement D.

Vecteurs propres localisés

Comme nous l'avons observé dans les sections précédentes, les vecteurs propres de la matrice laplacienne peuvent être utilisés pour étudier les comportements importants dans un système de pouvoir. Une caractéristique commune observée dans les modèles dynamiques et statiques de réseaux électriques sont les vecteurs propres localisés, ce qui signifie que les vecteurs propres sont petits partout sauf pour quelques nœuds. En termes mathématiques, on dit qu'un vecteur propre ϕ est localisé dans le sous-graphe $\mathcal{S}$ if :

$$\phi_i = \begin{cases} \mathcal{O}(1) & \text{if} \quad i \in \mathcal{S} \\ \mathcal{O}(\epsilon) & \text{else} \end{cases}$$

Dans cette thèse, nous dérivons deux limites de vecteurs propres et montrons comment ces limites peuvent être utilisées pour prédire et étudier des vecteurs propres localisés. La première borne, appelée paysages du graphique, délimite la composante de chaque vecteur propre à chaque nœud et est donnée sous la forme :

$$\frac{|\phi_i|}{|\phi|_{\max}} \leq \begin{cases} h_i = \left|\frac{1}{\lambda}\right| \sum_{j=1}^{n} |L_{ij}| \\ l_i = |\lambda| \sum_{j=1}^{n} \left|L_{ij}^{\dagger}\right| \end{cases} \tag{8}$$

La deuxième borne limite les vecteurs propres d'un sous-graphe $\mathcal{S}$ et dépend d'un vecteur v, qui est la solution de l'équation discrète de Laplace $Lv = 0$ sur $\mathcal{S}$. La borne est donnée par :

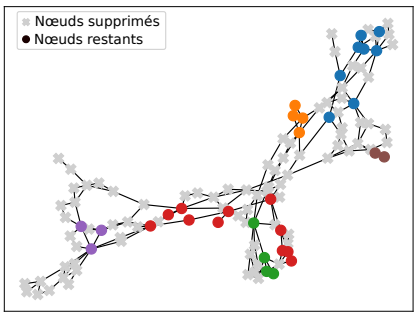

FIGURE 4: Nœuds restants après la suppression des nœuds en utilisant les paysages.

$$\|\phi\|_{\mathcal{S}} \leq \left(1 + \max_{\lambda_{\mathcal{S}}} \left|\frac{\lambda}{\lambda - \lambda_{\mathcal{S}}}\right|\right) \|v\|_{\mathcal{S}} \tag{9}$$

Où $\lambda_{\mathcal{S}}$ sont les valeurs propres de la matrice laplacienne limitées aux lignes et colonnes correspondant à $\mathcal{S}$.

La première borne peut être utilisée pour trouver des sous-graphiques candidats à la localisation. Ces sous-graphes sont trouvés en supprimant tous les nœuds ayant un très petit paysage, où aucune localisation ne peut apparaître. Un exemple est présenté dans fig. 4. Ici, la plupart des nœuds sont supprimés, mais nous nous attendons à ce que la localisation apparaisse à des valeurs propres élevées pour les nœuds restants.

Pour trouver à quels modes la localisation λ apparaît, on peut utiliser la deuxième borne. La localisation est liée à la résonance, où $\lambda_{\mathcal{S}}$. Environ Il s'avère que pour les sous-graphiques de fig. 4 (sauf pour un faux positif), la localisation apparaît exactement aux modes où λ est le plus proche d'un $\lambda_{\mathcal{S}}$. La preuve des limites présentées et une enquête plus approfondie se trouve dans chapter 5.

Discussion

Nous avons vu que les méthodes spectrales sont un outil puissant pour étudier le comportement dynamique et statique des systèmes d'alimentation, notamment en ce qui concerne les propriétés topologiques. Nous avons également étudié la localisation, qui est un comportement important. Deux limites et méthodes ont été

dérivées pour étudier la localisation. La poursuite du développement de ces méthodes et leur extension à des modèles plus grands et plus réalistes constituent une orientation de recherche prometteuse, sur la base de ces résultats.

Chapter 1

Geometry and Power Systems

1.1 The Role of Geometry

All networks,whether they are social, biological or technical, have one common feature: their behaviour is shaped by the geometry of the network, meaning how how the different elements are connected together. For instance, the geometry of the power system can be changed by introducing new transmission lines, which will impact the stability of the system. Many interesting features of the network depend hence more on the shape of the network than the properties of the individual parts. Understanding the geometry and thus the interactions in the system can guide actions in improving the overall system.

To highlight the role of geometry in a power system, two simple examples focusing on very small electrical circuits are first presented.

Four Resistors A simple way to understand the role of geometry in an electrical network is presented here. We consider a network of four identical resistors with resistance R. We want to know the effective resistance between two nodes. In fig. 1.1, the circuits for nine different configurations are shown.

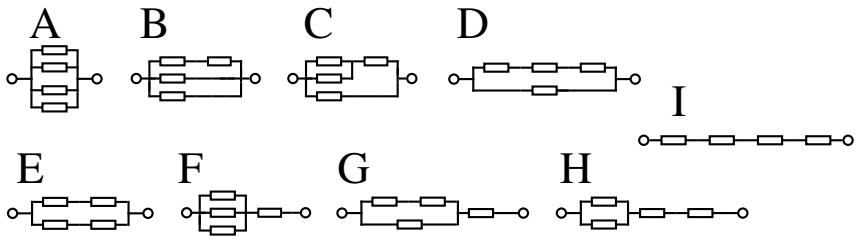

FIGURE 1.1: Nine possible networks with four identical resistors with resistance R.

Using the well known laws for resistances in serial and parallel circuits [17], we can simply calculate the total resistance for those nine configurations. The results

are shown in table 1.1. In [18], it is shown that these nine values are all possible values for four identical resistors.

Circuit	A	B	C	D	E	F	G	H	I
R_{total}	$\frac{1}{4}R$	$\frac{2}{5}R$	$\frac{3}{5}R$	$\frac{3}{4}R$	$1R$	$\frac{4}{3}R$	$\frac{5}{3}R$	$\frac{5}{2}R$	$4R$

TABLE 1.1: Total resistance for all circuits with four identical resistors from fig. 1.1.

The large difference in the values of the total resistance show how important the geometry of a network is, even in a very simple network. We can observe a difference of factor 16 in the total resistance. The results presented in table 1.1 can calculated in a more general way as the *effective resistance* of a resistor graph.

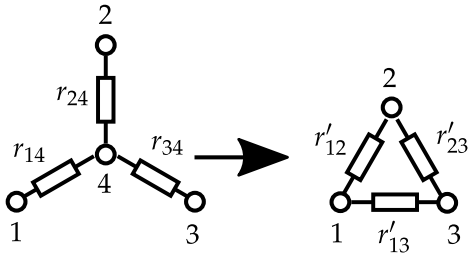

FIGURE 1.2: Schematic drawing of the start delta transformation.

Star Delta Transformation A famous example in the theory of electrical networks is the star delta transformation [19], which is depicted in fig. 1.2. The star network on the left can be transformed to the triangle on the right. The electrical properties of the systems, when investigated at the three nodes 1, 2 and 3 are equivalent in both systems, if the reduced resistances r' are calculated by:

$$r'_{12} = \frac{r_{14}r_{34} + r_{24}r_{34} + r_{14}r_{24}}{r_{14}} = \frac{r'}{r_{14}}$$
$$r'_{13} = \frac{r_{14}r_{34} + r_{24}r_{34} + r_{14}r_{24}}{r_{34}} = \frac{r'}{r_{34}}$$
$$r'_{23} = \frac{r_{14}r_{34} + r_{24}r_{34} + r_{14}r_{24}}{r_{24}} = \frac{r'}{r_{24}}$$

This process is a simple case of the more general Kron reduction in electrical networks [20, 21, 22]. A powerful application of the Kron reduction in dynamical power system models is discussed later in section 4.1.2.

Both examples show the influence of geometry in simple electrical circuits, but also how graph theoretical thinking can help in solving problems in these systems.

We now introduce how a power system can be modelled and used to relate dynamical and topological properties.

1.2 Power Systems

In this section, modelling foundations of the power system are explained. We want to pay attention to the geometrical properties of the power system. The power system connects the producer of energy with the consumer. Thus, the power system has three different main functions:

1. Production of energy - The generators which produce electrical energy.
2. Transportation of energy - The transmission lines, which transport the energy from the producers to the consumers.
3. Consumption of energy - The loads, which will use the electrical energy. Here, all from industrial factories to the power supply at private buildings are considered.

All three parts combine to a complex and large system. It spans from large power plants, over multiple countries, to buildings and factories. If we want to understand and investigate this complex system, we have to find mathematical models for all main functions in the system. In this work, we try to investigate and understand the fundamental properties in a general way. Thus, we usually investigate simplified power system models. More general and accurate models of the power systems are described in detail in the main textbooks on power systems [11, 23]. An explanation of the simplified models presented here can be found in [24].

1.2.1 Transmission of Energy - Power Flow

The largest part of the power system are the transmission lines, which are responsible for transportation and distribution of electrical energy in the system. For example, the main transmission lines of Germany is drawn on the map in fig. 1.3a. To describe the transmission of energy, we use the power flow equations. The complex current injected at a node i is given as $\mathbf{I}_i$. From Kirchhoff's current law [25], we know that this current is identical to the sum of currents of all branches which end at node i. The complex nodal voltages are called $\mathbf{V}_i$. Using Ohm's law, we can relate the currents and voltages as:

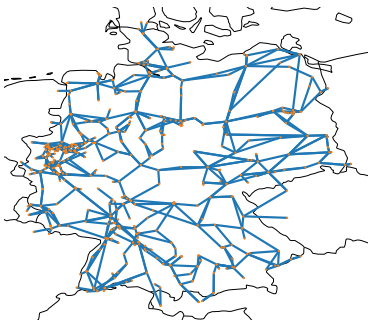

(A) German transmission grid

FIGURE 1.3: Example transmission system in Germany (made with PYPSA, [26]).

$$\mathbf{I} = \mathsf{Y}\mathbf{V} \tag{1.1}$$

Where Y is the nodal admittance matrix. The matrix elements Y_{ij} are non zero if the nodes i and j are connected and are equal to the admittance between the nodes. If i and j are not connected, the matrix elements are zero. The values on the main diagonal are called the *self-admittances* and are equal to the sum of all admittances connected to the corresponding node. If all shunt admittances are ignored, as usually done in the simplified models [20], the values on the main diagonal are identical to the row sum of all non-diagonal terms [27]. The complex power S at node i can be partitioned in the real and complex power P and Q, respectively:

$$\mathsf{S}_i = \boldsymbol{P}_i + \imath \boldsymbol{Q}_i = \mathbf{V}_i \mathbf{I}_i^*$$

Using the Voltage phase angle θ, we express the complex voltages in polar form as $\mathbf{V}_i = V_i \exp(\imath \boldsymbol{\theta}_i)$, where V_i is the Voltage magnitude or simply Voltage of the node. The nodal admittance matrix can be separated in the conductance G and the susceptance B as $\mathsf{Y} = G + \imath B$.

$$\boldsymbol{P}_i + \imath \boldsymbol{Q}_i = V_i \exp(\imath \boldsymbol{\theta}_i) \sum_{j=1}^{n} V_j \mathsf{Y}_{ij} \exp\left(-\imath \boldsymbol{\theta}_j\right)$$

Separating these equations in the real and imaginary parts lead to the well known power flow equations:

$$\begin{aligned} \boldsymbol{P}_i &= \sum_{j=1}^{n} V_i V_j \left(G_{ij} \cos\left(\boldsymbol{\theta}_i - \boldsymbol{\theta}_j\right) + B_{ij} \sin\left(\boldsymbol{\theta}_i - \boldsymbol{\theta}_j\right) \right) \\ \boldsymbol{Q}_i &= \sum_{j=1}^{n} V_i V_j \left(G_{ij} \sin\left(\boldsymbol{\theta}_i - \boldsymbol{\theta}_j\right) - B_{ij} \cos\left(\boldsymbol{\theta}_i - \boldsymbol{\theta}_j\right) \right) \end{aligned} \tag{1.2}$$

We define three different types of buses in the network:

1. PV buses: The buses connected to generators are usually modelled as PV buses, where the power output P and Voltage V are constant.

2. PQ buses: At all other buses, the active and reactive power consumption P and Q are considered to be known and constant. Usually, the power is consumed at these buses and they are also called load buses.

3. Slack bus: One generator bus is usually considered to be the reference or slack bus, where the Voltage V and the phase $\theta = 0$ are fixed. The angle of this bus serves as a reference point for all other buses.

Using the power flow equations eq. (1.2) and the definition of the buses, the other unknowns, for example the Voltage angles and phases at the load buses, can be calculated. Solving the power flow equations is a complex problem in the field of power system engineering and research. Especially finding the optimal solution (optimal load flow) is still a very active research field with recent developments (for example in [28]). The system described by (1.2) is nonlinear, possibly very large and maybe ill-conditioned, which makes the computation of solutions difficult. Many simplifications, computational schemes and algorithms to directly solve the equations have been proposed in literature [29].

DC Power Flow

When high accuracy is not necessary, simplifications of the equations are usually employed. The probably most famous simplification, especially used in transmission systems, are the DC power flow approximations [30]. The assumptions for DC power flow are:

1. Neglecting reactive power flow and assume all voltage magnitudes to be constant.

2. Assuming that the resistances are small compared to the susceptance $G \ll B$.

3. The difference of voltage phases is small, so that we can use $\sin(\boldsymbol{\theta}_i - \boldsymbol{\theta}_j) \approx \boldsymbol{\theta}_i - \boldsymbol{\theta}_j$ and $\cos(\boldsymbol{\theta}_i - \boldsymbol{\theta}_j) \approx 1$.

With those simplifications, the real part of the power flow equations simplifies to:

$$\boldsymbol{P} = -B\boldsymbol{\theta} \tag{1.3}$$

Where $\boldsymbol{\theta}$ is the vector of phase angles. Equation (1.3) is a linear equation which only depends on the susceptance matrix B (the imaginary part of the admittance matrix) and the nodal powers P.

1.2.2 Generation of Energy - Swing Equation

In the power system, electricity is classically generated by turning mechanical energy into electrical energy [1]. The mechanical energy, for example wind energy in wind parks or heated steam in thermal power plants, is injected into a generator. Inside the generator, a *rotor* then rotates against the stationary *stator*. Both the rotor and the stator are equipped with conductors. The rotors conductors produce a magnetic field, which in turn induces a current in the stator. The resulting current is the AC current injected and used throughout the power system.

To analyse the dynamics of the generator, the *swing equations* are used. We define the rotor angle as $\boldsymbol{\alpha}$. The angle is referred to a fixed reference frame. The mechanical laws of motion for rotating systems can be used to describe the dynamics of the system. The total power acting on the rotor consists of [24, 31]:

- $\boldsymbol{P}_M$: The mechanical input working on the turbine of the generator.
- $\boldsymbol{P}_D = D\dot{\boldsymbol{\alpha}}$: The damping power, which consists of the mechanical damping, electrical damping effects from the damper windings and possible control effects.
- $\boldsymbol{P}_e$: The electrical power withdrawal due to the electrical load.

Together with Newtons law, we arrive at the well known swing equation:

$$M\ddot{\boldsymbol{\alpha}} + D\dot{\boldsymbol{\alpha}} = \boldsymbol{P}_M - \boldsymbol{P}_e \tag{1.4}$$

[1] PV or power electronic sources will be ignored here.

With the inertia M of the generator. The electrical power $\boldsymbol{P}_e$ results from power flow equations section 1.2.1. The description of the generator dynamics here is very simplified. The rotor/stator interactions, damping and control included in a real generator are much more complex than in eq. (1.4). Usually, this model is used with other simplifications. Often, the reactive power flow and voltage dynamics are neglected, as in the DC power flow approximations. This simple model is considered to be valid for the first swing of a generator [32].

1.2.3 Consumption of Energy - Load Models

Finding suitable models for load can be very complicated, as different loads can have very different dynamical behaviour. For example, an electrical motor has a very different frequency behaviour than a transformer connected to the grid. Also, the stochastic nature of loads might have to be included in the models. For the investigations here, a simplified load model can be used. Usually, three different models are considered [24, 33]:

1. The effective network model: All loads are modelled as passive, constant impedances. In this case, all load nodes can be removed from the system and an effective network only consisting of the generators, based on the Kron reduction [20], is sufficient to describe dynamics.

2. The synchronous machine model: Loads are modelled as electrical machines. The load dynamics then resemble that of generators, with the swing equation, but with negative power output. Usually, all buses between the generators and machines are also removed from the network using the Kron reduction.

3. The structure preserving model: Here, all buses are modelled as frequency dependent loads with $P_L = P_{L,0} + D\dot{\theta}$. The name indicates that because of the active nature of the loads, the network is not Kron reduced and the original topological structure of the nodal admittance matrix is preserved [34].

Together with the previous sections, the full system of equations which describes the dynamics of a simplified power system are given as [33]:

$$\begin{aligned} M_i\ddot{\boldsymbol{\theta}}_i + D_i\dot{\boldsymbol{\theta}}_i &= \boldsymbol{P}_{B,i} - \sum_{j=1}^{n} a_{ij}\sin\left(\boldsymbol{\theta}_i - \boldsymbol{\theta}_j\right) \quad i \in \mathcal{V}_{\mathcal{P}} \\ D_i\dot{\boldsymbol{\theta}}_i &= \boldsymbol{P}_{B,i} - \sum_{j=1}^{n} a_{ij}\sin\left(\boldsymbol{\theta}_i - \boldsymbol{\theta}_j\right) \quad i \in \mathcal{V}_{\mathcal{C}} \end{aligned} \tag{1.5}$$

With the coupling matrix given element wise as $a_{ij} = B_{ij}V_iV_j$. The power vector $\boldsymbol{P}_B$ is the mechanical input or electrical load at each bus, depending on the type of bus. This general form can be used for all load models described before, with a appropriate choice of the parameters and the sets $\mathcal{V}_\mathcal{P}$ and $\mathcal{V}_\mathcal{C}$. For example, in the SP model, all load nodes are in $\mathcal{V}_\mathcal{C}$ and all generator nodes are in $\mathcal{V}_\mathcal{P}$. The model described in eq. (1.5) is a nonlinear dynamical system. The nonlinearity results in a very rich and complex behaviour, but also in difficulties in mathematical treatments. For many nonlinear systems, only numerical solutions can be used to investigate the system. Still, this model can be used to investigate and explain many important properties of the power system. In the next section, an overview over the vast literature related to power system research especially focusing on geometry is given.

1.3 The Role of Geometry in Power System Stability

In this section, we want to give a brief overview about the role of geometry in power systems stability. The models presented in the previous section and their complex variants [11, 23] have been used extensively to study the stability of power systems. Generally, three different classes of stability are considered [35]:

1. Rotor angle stability, the ability of the machines in the power system to remain synchronised or return to a synchronised state after perturbations or faults.

2. Frequency stability, the ability of the system to maintain a steady frequency after strong perturbations.

3. Voltage stability, the ability of the system to keep steady voltages at each bus after disturbances.

In this work, we mostly focus on rotor angle stability. This problem has been further divided into two problems, namely:

- *Small signal stability:* The response of the system to small perturbations around an operating point. As the perturbations are sufficiently small, the systems equations can be linearised. Usually, oscillations around this operating point are then observed. These oscillations need to be damped and decrease over time. Small signal stability can have long range interactions with inter area mode oscillations or local effect, called local plant mode oscillations.

- *Transient stability:* Large perturbations, where a stronger perturbation results in an excursion in the state space. The system is supposed to return to a synchronised operating mode after the perturbation. This stability depends on the systems ability to synchronise, but also the strength and duration of the disturbance.

Early work mainly investigated the stability of the system using energy functions [36] or Lyapunov methods [37]. These studies usually investigated single generators or very small systems, for example the single generator infinite bus system. The structure of the network and its influence where usually discarded. Attempts to consider a full network with the Lyapunov methods were later developed [34] and it was noted that the geometry of the network had to be taken into account. With advantages in computational power, time domain simulations became possible in power system stability studies [38]. One advantage is that computer simulations can take much more complex models into account, while *mathematical* models are often extremely simplified. The topology can also easily be considered for these simulations. One problem with computational simulations is that they are generally very specific to a certain topology and parameter set. Mathematical results are more general and can often be adopted to different scenarios without any problems [39].

In later years, the influence of the structure of networks on their properties became a bigger focus of the research. Especially the topological and statistical properties of networks were of interest. For example, it was shown that power systems may have small world and scale free behaviour. An overview about the many features and studies about the topological properties of power systems as complex networks can be found in [40].

Especially the interplay of topology and dynamics were of great interest [16]. The general focus of these investigations was usually synchronisation [41, 42] or stability (mainly transient stability) [43, 44] of those systems.

Synchronisation is found in a system consisting of dissimilar coupled agents. If the coupling *overcomes* the dissimilarity, the system synchronises. Synchronisation is directly linked to transient stability of a power system. In the community, a mixture of theoretical and statistical studies including computer simulations were usually performed and many interesting results have been reported. It has for example been shown that additional lines might destabilise the system [45] or results in more overloaded lines [46]. This is a power system equivalent to Braess' paradox, usually found in traffic networks. Braess' paradox means that additional roads might result in a decrease in traffic flow, even if the number of vehicles stays constant [47].

Weaker links in power systems such as dead ends and trees has also attracted a special attention [48, 49].

Recently, the dynamical properties of cascading failures has also been considered [50, 51]. It has been shown that failures of some lines can have cascading effects affecting the whole system, while other failures stay locally. While this makes it clear that the topology plays a role in cascading failures, a complete understanding of which topology promotes stability and which promotes failures remains to be seen.

Complexity and Spectral Solving

While the previous results show great advantages in the confronting stability to structural properties of power systems, many challenges remain open. One main problem for all investigations, be mathematically, statistically or with computer simulations, is the huge complexity of the system. The dynamics of a power system happen on very different time and length scales (a schematic drawing of the scales and the related problems is shown in fig. 1.4). The length scales range from thounsands of kilometers over whole continents to only less than a meter, on distribution or device level. The power system has thousands of devices, connected with a complex grid and with different behaviours and parameters. The power system is also inherently non linear, which further increases the complexity, as nonlinearities can easily result in chaotic behaviour on itself [52].

One way to address the problem of complexity is the spectral analysis. We can use spectral analysis to decompose the system into different time and length scales and investigate these scales individually. This analysis can be much easier than the calculation of all scales together. The remainder of this thesis will hence mostly focus on the concept of spectral graph theory, which is the application of spectral decomposition on graphs.

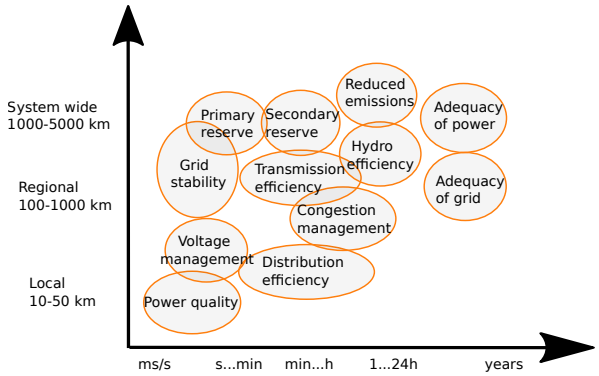

FIGURE 1.4: Overview over time and length scales related to power system operation and design. Adopted from [53]

Chapter 2

Spectral Graph Theory

The mathematical basis to investigate the topology and structure of complex networks is graph theory. This chapter, which serves as the theoretical background of this thesis, gives a general overview about graph theory and especially spectral graph theory. Spectral graph theory investigates eigenvalues and eigenvectors of graphs. Most of the results are presented here are found in [54] or various lecture notes from Daniel Spielman [55]. Another useful resource is [56], where many results especially of spectral properties on regular graphs and special geometries are found. Many definitions from general or algebraic graph theory have to be used in spectral graph theory as well. Those well known definitions and results can be found in various textbooks about graph theory, for example [57, 58, 59].

2.1 Fundamental Properties of Graphs

Graphs are mathematical objects, which model the *relations* between objects. A graph $\mathcal{G}$ consists of a set of vertices $\mathcal{V}$ (sometimes called nodes), and their relations encoded in a set of edges (sometimes called links or lines) $\mathcal{E}$. The vertices are the objects. For example, in a social network, all people considered are the vertices. If two people are friends, an edge between those two vertices exist. If two vertices have an edge between them, they are called connected. We define the size of the graph as the number of vertices.

2.1.1 Simple Graphs

In this work, we focus on a special case of graphs, called (weighted) simple graphs. This means that the edges of every graph fulfils the following properties:

1. Undirected edges. The edge between nodes i and j is identical to the edge between j and i.

2. No self loops. Edges cannot start and end at the same vertex.

3. Single edges. For each pair of nodes, only one edge exist.

4. Weighted edge: Every edge has a real weight $e_{i,j}$ between the nodes i and j. This weight indicates the *strength* of the connection between the nodes. The larger the value is, the closer the nodes are to each other. For electrical networks, the admittance between two nodes would be equivalent to the edge weight of the underlying graph[1].

An unweighted graph is equivalent to a weighted graph where each edge has a weight of one. In the spectral analysis, an edge weight of zero between nodes is identical to a non connection. If two nodes are not connected, the weight can be assumed to be zero. It is often very helpful to visualise graphs. In fig. 2.1, two examples graphs are drawn. The blue circles indicate the nodes, while the black lines indicate edges. Figure 2.1a is a simple graph, which shows the relationships between Florentine families in the 15th century [60]. The non-simple graph fig. 2.1b has directed edges (indicated by the arrows), self loops and multiple lines between edges.

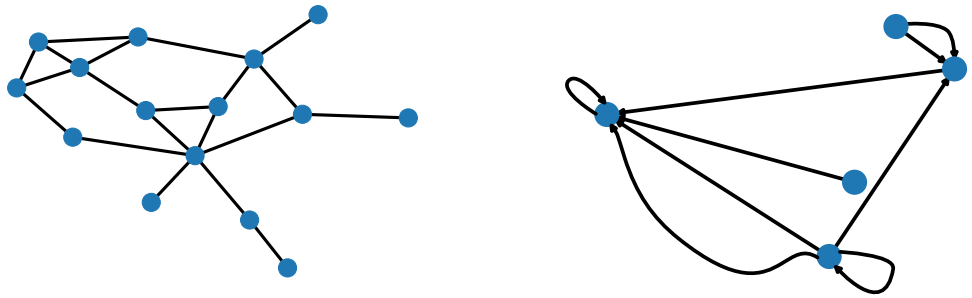

(A) Simple graph (B) Non-simple Graph

FIGURE 2.1: Graphical representation of a simple graph and a directed multigraph with self loops. The blue circles are the nodes, the black line the edges. Arrows indicate a directed line, ending in a certain node.

2.1.2 Networks and Graphs

In this thesis, both the term network and graph is used, sometimes interchangeably. In general, we consider a graph to be a mathematical object while the network is a physical, real world object [61]. Graphs can be used to mathematically describe networks. The main difference between is the science behind both objects:

[1] We usually consider only positive, real edge weights in the remainder.

1. Graph theory deals with fundamental properties and relationships between classes of graphs.

2. Network science investigates properties of concrete graphs and how they relate with the real world examples they are based on. Network science or theory often utilises the tools and ideas developed in graph theory.

We do exactly that, using graph theoretical and network science to investigate properties of real work systems.

2.1.3 Paths and Connected Graphs

An important concept in the analysis of graphs are *paths*. A path $\mathcal{P}(\mathcal{V}_\mathcal{P}, \mathcal{E}_\mathcal{P})$ is defined by a distinct sequence of vertices $\mathcal{V}_\mathcal{P}$ and a corresponding set of edges $\mathcal{E}_\mathcal{P}$, where each vertex is connected to the next vertex in the sequence. A related concept of *walks* allows for non distinct sequences of vertices or edges. A directed path is defined similarly, just with directed edges.

Paths allow us to define a *connected* graph. If a graph has a path including every vertex, this graph is connected. This means that from every vertex in the graph, all other vertexes can be reached, just by following some edges in the graph. For example, the simple graph from fig. 2.1a is connected. If the graph is directed, as in fig. 2.1b, the definition is more complicated. This graph is *weakly connected*, which means that replacing all directed edges with undirected edges would result in a connected graph. This graph is not *strongly connected* though, as for example no edge terminates in the top right vertex.

2.1.4 Subgraphs and Connected Components

An *vertex induced* subgraph $\mathcal{S}(\mathcal{V}_\mathcal{S}, \mathcal{E}_\mathcal{S})$ of a graph $\mathcal{G}(\mathcal{V}, \mathcal{E})$ is defined by the graph with a vertex set $\mathcal{V}_\mathcal{S} \subset \mathcal{V}$ and with the subset of edges $\mathcal{E}_\mathcal{S}$ which start and end in $\mathcal{V}_\mathcal{S}$ [57]. While in principle, different definitions of a subgraph can be found (for example, the subset of edges can be chosen), this work will consider subgraphs to always be induced subgraphs with respect to a vertex set. Subgraphs are also not necessarily connected, even when the graph is connected. The connected components of a graphs are the largest connected subgraphs. When the graph is connected, the connected component is the full graph itself. For example, fig. 2.2 shows a graph on the left with two subgraphs (with the orange and green nodes). The orange subgraph is connected, the green one is not. This graph has only one connected component. On the right side, another graph is shown, which is formed by removing all blue

vertices from the left graph. Then, the graph has three connected components, indicated by the circles around the subgraphs.

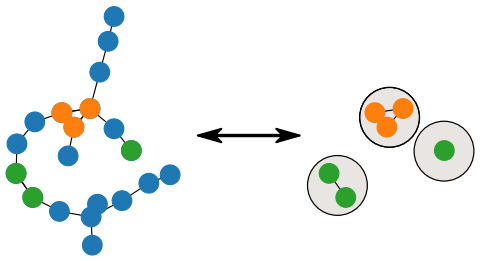

FIGURE 2.2: Left: A random graph with two different subgraphs (in orange and green). The orange subgraph is connected, the green one is not. Right: A second graph, where all blue vertices are removed. Three connected components are found.

2.1.5 Properties and Metrics of Graphs

In this section, some important metrics, often used in graph theory and network science are used. To illustrate, we use the simple real world graph of the Florentine families, as shown in fig. 2.1a.

Vertex Degree

The vertex degree, or simply degree, is the number of edges connected to each vertex. A vertex with a degree of zero is called isolated, as it is not connected to any other vertex. We can also define the weighted degree, which is just the sum of all weights of the edges connected to the vertex.

Degrees indicate how well connected a vertex is. Vertices with a degree of one are also called end vertex, as they are on the outside of the graph. In fig. 2.3a, the degrees of the Florentine family graph are shown by the node colour. The most connected graph in grey has a degree of six, which is much larger than the other nodes. This vertex corresponds to the famous Medici family, the most influential and richest family of Florence at the same.

An interesting basic result of graph theory, related to the degree is the handshaking lemma. It states that in every graph, the sum of all degrees is an even number. The name comes from the fact that when a group of people shake hands, the total number of hands shaken is an even number, as two hands are involved in each handshake. In fact, in the previous graph, the total number of degrees is 40.

The average degree can be used to describe how *dense* a network is. The higher the average degree, the more connections each vertex will have. The average degree

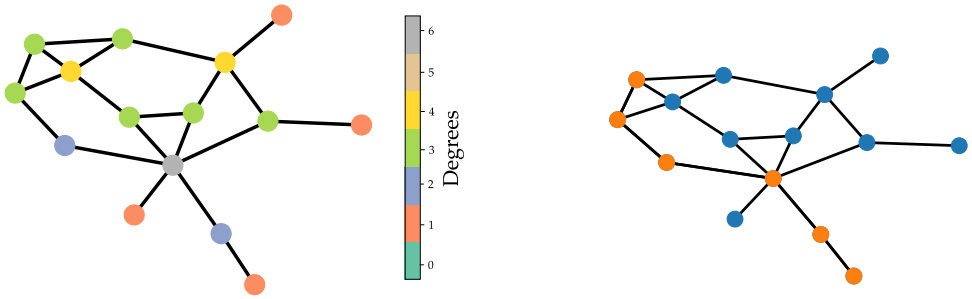

(A) Degrees (B) Diameter

FIGURE 2.3: Vertex degree and diameter of the Florentine families graph.

of the Florentine families from fig. 2.3a is 2.67, while the average degree graph on the left from fig. 2.2 is 2.0. This graph is clearly less connected than the Florentine family graph.

Shortest Path and Diameter

Methods to characterise the extend of a graph are often based on the shortest path. The shortest path between two nodes is the path with the least amount of vertices between the two nodes. This can be used to calculate the *diameter* of network. The diameter is defined as the length of the longest shortest path between any pair of nodes. The diameter of the Florentine families graph is 5. In fig. 2.3b, the orange vertices indicate a shortest path of length five. In contrast, the graph previously shown in fig. 2.2 is more radial. The diameter is 13 and the longest shortest path is shown in section 2.1.5, with the orange vertices label the path as before. Similarly, the average shortest path length can be calculated. The average shortest path is found by calculating the shortest path between all vertices of the graph and calculates the average. It measures the average distance between vertices. For the Florentine family graph, the average shortest path length is approximately 2.6. For the graph on the left in fig. 2.2, the average shortest path length is around 5.3, which is more than double the average shortest path length of the Florentine family graph.

2.1.6 Examples for Graphs

In this section, some typical graphs and properties are shown. All of these examples can be used as motives to build larger networks. At first, some typical graphs considered in mathematical graph theory are shown. Afterwards, random graphs, which are more common in network science as they resemble real world networks are introduced. Those graphs are more irregular and complicated in nature.

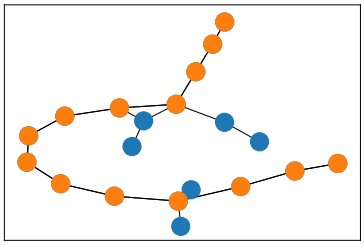

FIGURE 2.4: Diameter of the more radial graph from fig. 2.2. The orange nodes are the vertices of the longest shortest path in the graph.

Basic Graphs

In fig. 2.5, some examples for typical graphs are shown.

1. **Tree**: A tree graph is a graph where any two nodes are only connected by a single *path*. This means that no loops exist in this graph.
2. **Cyclic**: If the graph is not a tree, it has a cycle.
3. **Complete**: The complete graph of size n has n vertices and each vertex is connected to every other vertex
4. **Ring**: In a ring graph, each vertex is connected to its n nearest neighbours. This example is a 2-Ring.

The last two graphs are other examples for cyclic graphs. They are also *regular* graph, which means that every vertex has the same degree (the degree is two for the ring and five for the complete graph).

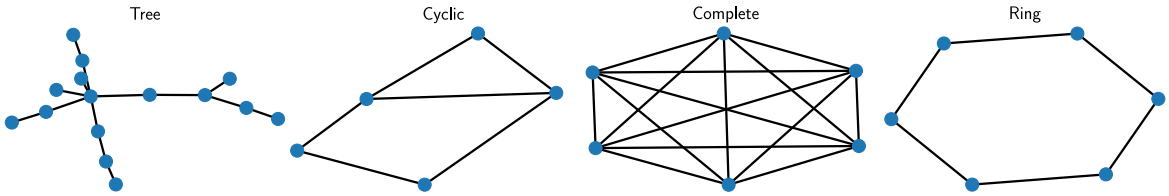

FIGURE 2.5: Examples for basic graphs.

Random Graphs

Real world networks are often not as regular as the examples described in the previous section. Thus, random networks are often used [61]. While many different type of random networks exist, we focus on two examples here, namely the Erdős–Rényi and the Watts–Strogatz graph.

The creation process for both graphs is shown in fig. 2.6:

1. Erdős–Rényi: A set of vertices with the given size n is chosen. Then, all possible edges of the complete graph with n vertices are considered. For every edge, a random number is chosen. If the random number is smaller than a given threshold p, the edge is added to the graph.

2. Watts–Strogatz: We start with a ring graph with n vertices, connected to its m nearest neighbours. For every edge, a random number is chosen. If a given probability p is lower than this random number, than one of the vertices connected to the edge will be randomly replaced by another vertex.

Obviously, the number of edges is constant in the Watts–Strogatz graph. The Erdős–Rényi graph is often used in graph theory, due to its pure randomness. The Watts–Strogatz model is a often used to model *small world* effects. It has a relatively local structure (as every node is connected to it neighbours), but also some *shortcuts* to other parts of the graph. This means that the average shortest path of these networks is often relatively small. In the real world, this has been reported as a low degree of separation which has been reported in many real world networks [2]. For example, it is believed that every human is connected to every other human by six social interactions, which means that the diameter of the graph of all human beings is only six.

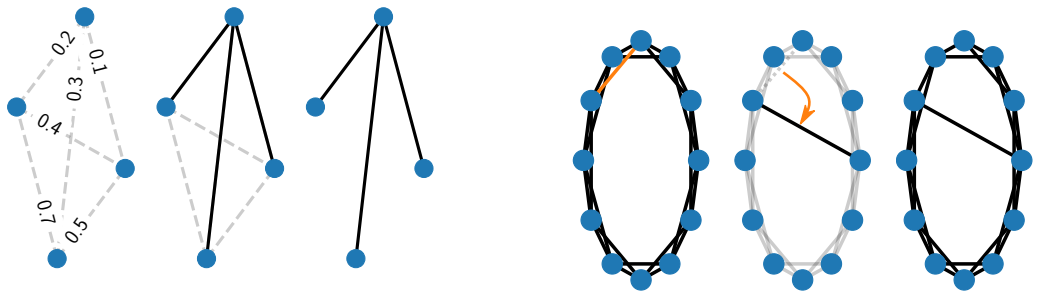

(A) Erdős–Rényi (B) Watts–Strogatz

FIGURE 2.6: Creating process of random graphs. The numbers on the edges of the Erdős–Rényi graph correspond to the random number, a threshold of 0.35 is used to create edges.

The impact of the random parameter p in both random graph types is illustrated in fig. 2.7. For the Erdős–Rényi graph, a higher value of p results in more edges included in the graph. While for low p, the graph is usually very sparse, a very large p will resemble a complete graph. In our example, the graph is not connected for $p = 0.1$. The Watts–Strogatz is an almost regular ring graph for low p. The

larger the p, the more random the graph and further away from an ordered graph it becomes.

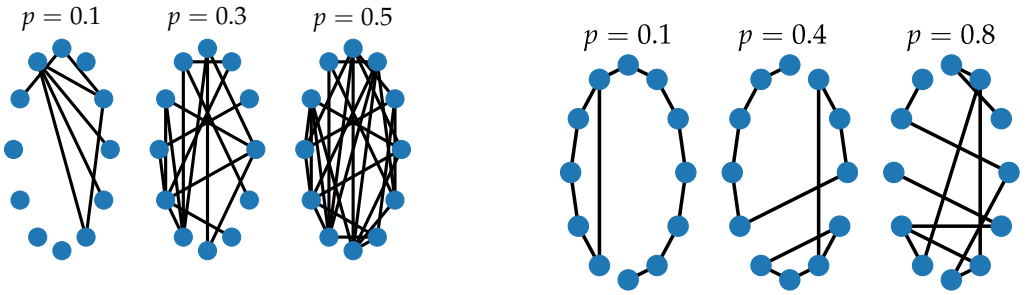

(A) Erdős–Rényi (B) Watts–Strogatz

FIGURE 2.7: Influence of the random parameter p on random graphs.

2.1.7 Graph Matrices

Graph theory, especially spectral graph theory, depends on matrices which describe the graphs. Multiple matrices have been discussed in Literature [56, 62], which might serve different purposes. We focus on three main matrices here.

All of these definitions are valid for a simple graph (as before). We define the size of the graph $n = |\mathcal{V}|$ as the number of vertices.

Adjacency Matrix

The obvious way to describe the network by a matrix is probably the incidence matrix A. For this, the n vertices of $\mathcal{G}$ are labelled from 1 to n. The symmetric $n \times n$ matrix A is component wise defined by the edge weights. So, for all vertices i and j, the matrix components $a_{ij} = e_{ij}$ for the edge weight e_{ij} between these vertices. If i and j are not adjacent to each other (which means, there is no connection), we set $e_{ij} = 0$.

For an undirected graph, the adjacency matrix is symmetric and we can see that the row sum is identical to the degree of this vertex.

Incidence Matrix

The incidence matrix $\tilde{I}$ of a graph describes the edges of a graph. It is a $n \times |\mathcal{E}|$ matrix, where the rows are indexed by the vertices and the columns are indexed by the edges. When a vertex i is connected to a vertex e, then $\tilde{I}_{i,e} = 1$ and zero otherwise.

More useful for this work is the directed incidence matrix I. This matrix is defined similarly, but we set $I_{i,e} = 1$ when the edge e ends in i and $I_{i,e} = -1$ when i is the end point of e. For an undirected graph, the start and end points of the vertices can be chosen arbitrary. Sometimes, the directed incidence matrix for an undirected graph is called the oriented Laplacian matrix.

Laplacian Matrix

In many cases [63, 20, 64, 65], the most interesting matrix in network science applications is the Laplacian matrix L. This matrix is again a $n \times n$ matrix, indexed by the vertices. Element-wise, we can define the Laplacian matrix as:

$$L_{ij} = \begin{cases} -e_{ij} & \text{if} \quad i \neq j \\ \sum_{j \neq i} e_{ij} & \text{else} \end{cases} \tag{2.1}$$

Which means that, using K as the diagonal matrix with the (weighted) degrees of the corresponding vertex on the diagonal, the Laplacian is also given as:

$$L = K - A$$

Using the previous definition of the oriented incidence matrix, we can also find the following relationship between the incidence matrix and the Laplacian matrix [56, 33]:

$$L = II^T \quad \text{or for weighted Graphs:} \quad L = I\text{diag}\left(e_{(i,j)\in\mathcal{E}}\right) I^T$$

Where $\text{diag}\left(e_{(i,j)\in\mathcal{E}}\right)$ is a diagonal matrix, with the edge weights on the main diagonal. The order of the weights corresponds to the order of edges in the incidence matrix. The first row of the incidence matrix corresponds to the first value on the diagonal and so forth. This also indicates the relationship between the Laplacian matrix and a quadratic form for any vector $\boldsymbol{x}$ [54]:

$$\sum_{(a,b)\in\mathcal{E}} e_{ab} \left(\boldsymbol{x}_a - \boldsymbol{x}_b\right)^2 = \boldsymbol{x}^T L \boldsymbol{x} \tag{2.2}$$

This work focuses on the Laplacian matrix as defined before. In some contexts, this matrix is called the *combinatorial* Laplacian matrix [66]. Sometimes two related matrices are investigated [62]:

$$\mathcal{L} = K^{-1/2} L K^{-1/2} \quad \text{(symmetric) normalized Laplacian} \tag{2.3}$$

$$\Delta_L = K^{-1} L \quad \text{discrete Laplace operator or random walk normalized Laplacian} \tag{2.4}$$

Depending on the studies, these matrices have some distinct advantages. This work only focuses on the combinatorial Laplacian matrix and will simply call it the Laplacian matrix of a Graph.

2.2 Spectral Properties of Graphs

Spectral graph theory is a powerful tool to investigate properties of the graphs, using the graph matrices presented previously. We focus here on the eigenpairs of the Laplacian matrix L, which are the solutions λ and $\boldsymbol{\phi}$ of:

$$L\boldsymbol{\phi} = \lambda\boldsymbol{\phi} \tag{2.5}$$

Where λ are the eigenvalues and $\boldsymbol{\phi}$ the eigenvectors of the matrix L. We can also define the left eigenvector $\boldsymbol{\psi}$ as the solution to:

$$\boldsymbol{\psi} L = \boldsymbol{\phi}\lambda \tag{2.6}$$

With the same eigenvalue λ. From the definition of the Laplacian and the fact that we have an undirected graph with $e_{ij} = e_{ji}$, we know that L is a symmetric real matrix. This means that L has only real eigenvalues and the eigenvectors can be used to form a basis [67]. It also follows that the left eigenvector is the transpose of the right eigenvector [68]. Thus, we generally consider only the right eigenvector. As every scalar multiplication of an eigenvector is another eigenvector, we usually fix each eigenvector by normalisation. To make the eigenvectors comparable, we normalise the eigenvectors so that the two-norm of each eigenvector is equals to one.

From the definition of the Laplacian matrix in eq. (2.1), we can easily see that the Laplacian matrix has zero column sum. This means that the vector $\boldsymbol{\phi}_0 = (1, 1 \dots 1)^T$ spans the null space, as:

$$L\boldsymbol{\phi}_0 = \left(\sum_{j \neq i} e_{0j} - \sum_{j \neq i} e_{0j}, \dots \right)^T = (0, 0, \dots, 0)^T$$

This also implies that the Laplacian has the zero eigenvalue, corresponding to the eigenvector $\boldsymbol{\phi}_0$. From the quadratic form eq. (2.2), we can clearly see that the Laplacian matrix is positive semi definite, if all edge weights are positive. Thus, we can order all eigenvalues as:

$$\lambda_1 = 0 \leq \lambda_2 \leq \lambda_3 \leq \dots \leq \lambda_n$$

The number of zero eigenvalues is identical to the number of connected components in the graph [56, Proposition 1.3.7]. As the graphs considered in this work are generally connected, the spectra usually have a single zero eigenvalue.

As L is a normal matrix (every real valued symmetric matrix is normal [69, pp. 7–1]), we know that the eigenvectors for distinct eigenvalues are orthogonal [67, Chapter 7]. This means that for any eigenvector $\boldsymbol{\phi} \neq \boldsymbol{\phi}_0$, the sum over all eigenvector components vanishes, as:

$$\boldsymbol{\phi} \cdot \boldsymbol{\phi}_0 = \sum_{i=1}^{n} \boldsymbol{\phi}_i = 0 \tag{2.7}$$

Which is independent of the normalisation of $\boldsymbol{\phi}$.

2.2.1 The Laplacian Pseudo Inverse

A famous result of eigenvalues is that the determinant of a matrix is given by the product of eigenvalues [67]. For the Laplacian matrix, this means that the determinant is zero:

$$\det L = \prod_i \lambda_i = 0$$

If the determinant of a matrix is zero, this matrix is non invertible or singular. The pseudo inverse of the Laplacian matrix is an important tool in spectral analysis. The most common used pseudo inverse is the (regularised) Moore-Penrose inverse $L^\dagger$. For a normal, positive semi definite matrix, the pseudo inverse can be calculated with the eigenvalue decomposition of a matrix L[2] [70]:

$$L = U \underbrace{\begin{pmatrix} \lambda_1 & & & \\ & \lambda_2 & & \\ & & \ddots & \\ & & & \lambda_n \end{pmatrix}}_{=:\Lambda} U^T \quad \leftrightarrow \quad L^\dagger = U \underbrace{\begin{pmatrix} 0 & & & \\ & \frac{1}{\lambda_2} & & \\ & & \ddots & \\ & & & \frac{1}{\lambda_n} \end{pmatrix}}_{=:\Lambda^\dagger} U^T$$

Where U is the matrix consisting of the eigenvectors of L and Λ is the diagonal matrix with the eigenvalues of L on the diagonal. From this definition, we can see that the pseudo inverse has the same eigenvectors as the original matrix and the eigenvalues are just the reciprocals of the original eigenvalue, except for the zero eigenvalue. We can also see from the definition that the pseudo inverse is a symmetric and real matrix, if L is symmetric and real.

Using the spectral decomposition, one can also show that the pseudo inverse has the other properties of a Laplacian matrix, namely [65]:

- Zero row sum.
- Positive diagonal and negative off diagonal entries.

Thus, the Laplacian pseudo inverse is a again a Laplacian matrix. It is important to remember the pseudo inverse does not *invert* the Laplacian matrix. Still, using the fact that both matrices have zero column sum can be used to show the following inversion property of the Laplacian pseudo inverse [70]:

$$LL^\dagger = L^\dagger L = \mathrm{I}_n - \frac{1}{n}\mathrm{J}_n \tag{2.8}$$

With the identity matrix I_n and the matrix of all ones J_n. We can clearly see that L and $L^\dagger$ commute.

[2] More generally, this is done with the singular value decomposition [67, Section 5.12]. For a normal, positive definite matrix, the eigenvalue decomposition and the singular value decomposition are identical.

2.2.2 Algebraic Connectivity

The first non-zero eigenvalue of a graph (here λ_2) is often called the algebraic connectivity. It has been shown that the algebraic connectivity is a good way to measure how *connected* a graph is [71]. For an unweighted graph, the following interesting properties for the algebraic connectivity found in [72] are listed here:

1. If $\mathcal{G}$ is a complete graph with n vertices: $\lambda_2(\mathcal{G}) = n$
2. If $\mathcal{G}$ has n vertices and is not a complete graph: $\lambda_2(\mathcal{G}) \leq n - 2$
3. If $\mathcal{G}$ is a ring graph with n vertices: $\lambda_2(\mathcal{G}) = 2\left(1 - \cos\frac{2\pi}{n}\right)$
4. If $\mathcal{G}_1$ is obtained by removing edge from $\mathcal{G}$: $\lambda_2(\mathcal{G}_1) \leq \lambda_2(\mathcal{G})$
5. If $\mathcal{G}_1$ is obtained by adding edge to $\mathcal{G}$: $\lambda_2(\mathcal{G}) \leq \lambda_2(\mathcal{G}_1) \leq \lambda_2(\mathcal{G}) + 2$

These examples show the connection between the algebraic connectivity and the connectivity of the graph. For example, by definition, the complete graph is the most connected graph. The conditions show that the complete graph has the largest algebraic connectivity for a given number of vertices.

Results like the last two generally hold true for the weighted case as well (as long as we only allow positive edge weights). For example, the algebraic connectivity of $\mathcal{G}_1$ after inserting a weighted edge with edge weight e_{ij} between the vertices i and j results in [63]:

$$\lambda_2(\mathcal{G}_1) = \lambda_2(\mathcal{G}) + e_{ij}\left(\phi_{2,i} - \phi_{2,j}\right)^2$$

Where $\phi_{2,i}$ is the i-th component of the eigenvector ϕ_2 of $\mathcal{G}$, corresponding to the eigenvalue λ_2. Obviously, from this follows that $\lambda_2(\mathcal{G}_1) \leq \lambda_2(\mathcal{G})$, as for the unweighted case.

2.2.3 Nodal Domains

Another interesting property are nodal domains. Nodal domains are the maximum connected subgraphs, whose nodes have eigenvector components with the same sign. For the zero eigenvalue, all nodes have the same eigenvector components, so the whole graph is defined as having a single nodal domain. In mathematical terms, a (strong) nodal domain is the maximum induced subgraph $\mathcal{W}$ of $\mathcal{G}$ with $\phi_i\phi_j > 0$ for all $i, j \in \mathcal{W}$. These domains are either positive (if $\phi_i > 0$ for all $i \in \mathcal{W}$) or

negative. A weak nodal domain is defined similarly, just allowing for equality with zero.

The number of nodal domains of an eigenvector ϕ are called $\mathrm{SND}(\phi)$ or $\mathrm{WND}(\phi)$ for strong and weak nodal domains, respectively. These numbers can be bounded similarly to the Courant nodal domain theorem in the continuous case [73, 74] and depends on the order of the eigenvalue. For the k-th eigenvector with eigenvalue multiplicity m_k, the number of nodal domains is bounded as:

$$\mathrm{SND}(\phi_k) \leq k + m_k - 1 \quad \text{and} \quad \mathrm{WND}(\phi_k) \leq k$$

In fig. 2.8, two graphs and the corresponding (strong) nodal domains are shown. In fig. 2.8a, the eigenvector of the algebraic connectivity is used, so we observe two nodal domains. In fig. 2.8b, the third eigenvalue (or second nonzero eigenvalue) is used, so up to three nodal domains can be found. Those three nodal domains can also be observed.

Of special interest are the nodal domains and eigenvectors of the algebraic connectivity. The eigenvector is often called the Fiedler vector and is used to partition the graph in two sets [71]. In [75], it is shown that using spectral methods, especially the Fiedler vector, is a good method to find a good cut of the graph, where the nodes are partitioned into useful, separated partitions.

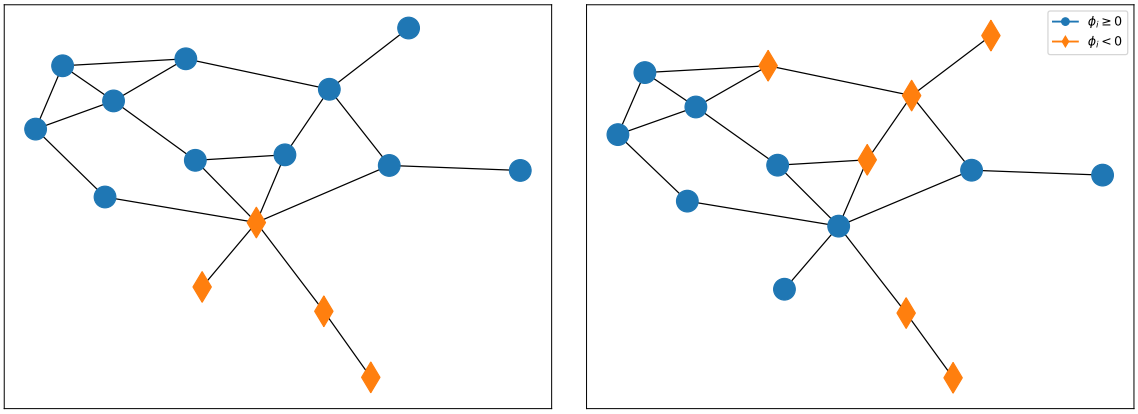

(A) Fiedler eigenvector (B) Second eigenvector

FIGURE 2.8: Examples showing the nodal domains on the Florentine families graph.

2.2.4 Coherency

A further property of the eigenvectors of a graph, which is related to nodal domains, is coherency. Coherency means that some eigenvectors for a given graph have, for a set of connected nodes, similar components. The problem of coherent clusters is directly related to nodal domains, as coherency is only possible inside a nodal domain. One exception would be a coherent cluster with very small components, which might be distributed around zero and thus cross the nodal domain boundaries. While some theory for the number of nodal domains exist, the number and shape of coherent clusters is generally even harder to predict. Even inside a single nodal domain, multiple coherent clusters might exist. Under certain conditions, coherency can be predicted by [63, Theorem 5.3]. The referenced theorem can be summarised as follows:

> If a graph can be partitioned into n_q partitions, where each partition has intra area connections of link strength $\mathcal{O}(1)$ and inter area link strengths of $\mathcal{O}(\epsilon)$, then:
>
> 1. There are $n - n_q$ eigenvalues of order $\mathcal{O}(1)$.
> 2. The remaining n_q eigenvalues are of order $\mathcal{O}(\epsilon)$.
> 3. The eigenvectors corresponding to the q slow eigenvalues exhibit approximate coherency.

An example showing this behaviour is provided in [63, Example 5.8]. This example is exactly recreated in fig. 2.9a, where the node colour corresponds to the eigenvector components of the Fiedler eigenvector. The graph is divided into four partitions, which are connected according to the requirements of the theorem. Calculating the eigenvectors, we can clearly see the coherency in the four clusters. We can also observe two nodal domains, where the two four node clusters and the two other clusters have different signs.

It should be noted that this is only a sufficient, but not a necessary condition for coherency. For example, the unweighted graph shown with the eigenvector component of the algebraic connectivity in fig. 2.9b exhibits coherency (and two nodal domains) as well. Interestingly, right side of fig. 2.9b is actually the Florentine families graph again. In both plots, the algebraic connectivity is used. We see a very different behaviour inside the cluster at the Fiedler eigenvector, where the connection results in a very coherent behaviour, instead of the nodal domains observed before.

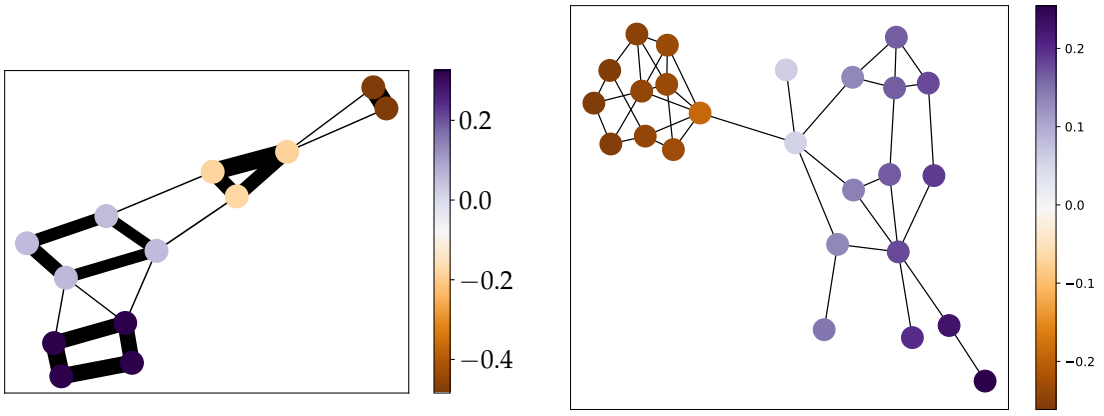

(A) Weighted graph (B) Unweighted graph

FIGURE 2.9: Two example graphs which exhibit coherency in the Fiedler eigenvector. The node colour is calculated from the eigenvector components.

2.3 Spectral Graph Theory on Power Systems

2.3.1 Small Signal Stability

The first application of spectral graph theory was usually done to investigate (slow) coherency and its application to network partitioning [76]. It has been shown that spectral methods can decompose the system into multiple modes. The eigenvectors of this decomposition result in a *mode shape* [77], which describes how the mode is distributed in the system. This was used to find coherent areas, where at a given mode, all generators behave similarly. The generators in a coherent cluster where often aggregated to a single generator, which simplified the analysis of the whole system significantly [78]. The coherency was mostly observed at small eigenvalues, which corresponds to low frequencies (hence the name *slow* coherency). On larger scale, these coherent clusters rotate against each other. The resulting inter area oscillations[3] can severely disturb the power system and are directly linked to some blackout occurrences [79]. The main focus of many research papers in this field is to find and identify these partitions efficiently and correctly, which means that many articles are focused on algorithmic problems [80].

A different approach to the studies of slow coherency is shown in [63]. Instead of trying to identify clusters in a given network, this work investigates the mathematical background of slow coherency and derived sufficient conditions for the emergence of coherency (these conditions were already presented in section 2.2.4).

[3]Very interesting videos showing these oscillations can be found on `http://fnetpublic.utk.edu/index.html`

In general, the work focuses on the structure of the eigenvectors and how they relate to the topology of the network. In contrast to other investigations, the analysis here was valid for dissimilar generators and allows for passive load nodes. One main drawback is that it is only valid for undamped oscillatory networks. The damping of the oscillation has been identified as vital for the stability of the system [35], especially in small signal stability. The oscillations in the afromentioned study thus never decay. Still, the results give insight about the distribution and shape of these oscillations, especially the coherency.

The elegant analysis of a linearised power system model in [21] highlights the role of the damping for the stability of the system. It was shown that the small signal stability of the system depends on the second smallest eigenvalue of the Laplacian and the dissipation (damping divided by inertia) of the system. Using a master stability function framework, a parameter set with maximum stability, depending on the second smallest eigenvalue and the machine parameters was identified. A similar, but more detailed analysis is found in [65]. This study explores the stability of multiple special cases. It was argued that the undamped case can only be marginally stable, which means that the oscillations do not grow, but also do not decay. In both investigations, the network is modelled as a set of generators without loads and with identical machine parameters. Also, both studies exclusively investigate the eigenvalues of the system, which define the stability. The eigenvectors, which are important for the clustering and the distribution of oscillations in the system are ignored.

2.3.2 Transient Stability

While the previous applications of spectral graph theory focus on small signal stability, links between transient stability and spectral graph theory have been identified.

In recent works, the applications of the spectral decomposition of the Laplacian matrix of a graph to vulnerability studies and disturbance propagation has been performed [81, 82]. It has been shown that the RoCoF (rate of change of frequency) of a perturbation directly depends on the eigenvectors of the Laplacian matrix and that the values of the Fiedler vector shape the propagation of disturbances over the system. The RoCoF is a typical measure to investigate the strengths of a fault in the power system.

Synchronisation is also linked to spectral properties of the graph. A provable bound for the existence of a synchronised solution is given as [32]:

$$\lambda_2(L) \geq \left\| I^T \boldsymbol{P}_B \right\|_2 \tag{2.9}$$

Where $\lambda_2(L)$ is the algebraic connectivity of the network, I the oriented incidence matrix and $\boldsymbol{P}_B$ the dissimilarity of the system. In the dynamical system presented here, it is the inherent frequency with which each generator oscillates. The product $I^T \boldsymbol{P}_B$ is a vector where each line corresponds to the difference of a pair of dissimilarities which is connected by an edge of the underlying graph. The spectral properties, linked to the algebraic connectivity, is directly linked to these results. While this condition is sufficient, it has been shown to be a conservative bound. A tighter bound has been proposed in [83, 33]:

$$\left\| I^T L^\dagger \boldsymbol{P}_B \right\|_\infty \leq 1 \tag{2.10}$$

The proof of this bound is not complete yet, numerical and mathematical investigations show that it is accurate and very tight for many networks and different conditions. This condition means that the maximum of the vector $L^\dagger \boldsymbol{P}_B$ over any transmission line has to be less than one for a synchronised solution to exist. The topological properties are encoded in the pseudo inverse $L^\dagger$. Due to the links with the eigenvalue decomposition of the Laplacian matrix, the pseudo inverse of the Laplacian can be seen as a spectral property of the graph. While this condition is easy to calculate, it can be difficult to understand from a geometrical point of view. Especially, it is not clear how the Laplacian matrix $L^\dagger$ depends on the geometrical features of the system. Interestingly though, the condition also links the synchronisation problem with the DC power flow problem. The vector $L^\dagger \boldsymbol{P}_B$ can be interpreted as a solution for the voltage phases of eq. (1.3). This means that the condition of synchronisation is identical with a upper bound on the voltage phase differences over any transmission line.

Another interesting result, are the fixed point equations also found in [33]. It can be shown that the synchronised phases $\boldsymbol{\theta}$ of a dynamical power system can be calculated as:

$$I^T \boldsymbol{\theta} = \arcsin\left(I^T L^\dagger \boldsymbol{P}_B \right)$$

Exploring the properties of $L^{\dagger}\boldsymbol{P}_B$ thus not only gives insight about the synchronisation of the system, but also about the values of the phases in a synchronised state.

More details of the spectral properties of $L^{\dagger}$ have been developed in [64]. In there, explicit formulas for the pseudo inverse for some simple geometries (for example, the complete and the path graph) are given. For further development of the properties of the pseudo inverse, the eigenvectors of the Laplacian matrix have to be understood.

2.3.3 Conclusion

Spectral properties are a powerful tool to quantify graph properties in a mathematical concise way. This overview shows how important the spectral properties are in the investigation of power systems. They play a major role for synchronisation, transient stability and small signal stability.

While most publications focus on the eigenvalues of the Laplacian matrix, we want to highlight the role of the eigenvectors. The strong condition for synchronisation presented earlier depends on the pseudo inverse of the Laplacian, which is build by the eigendecomposition of the Laplacian matrix and thus linked with the eigenvectors.

In chapter 4, we will analyse the small signal stability of a power system. In the literature, eigenvectors have been identified as being of major importance, for example for slow coherency or localised oscillations [84]. The best results were found for undamped systems, especially in [63]. The lack of damping (and thus, dissipation of energy), which has been described as being of major importance for the stability, is a drawback of this study. Investigating the effects of missing damping and trying to extend the results is the main goal of chapter 4.

While this work is motivated by dynamical studies, we first investigate the static power flow problem from a spectral point of view. The static problem is generally easier to investigate. It also allows us to make very clear connections between the behaviour of the system and the eigenvectors and show that spectral analysis is a powerful tool for power flow studies. The static analysis is also a further motivation for chapter 5, as well as linked with synchronisation studies as shown by the condition presented in eq. (2.10).

Chapter 3

Spectral Analysis of power flow

3.1 Methodology and Theory

In this section, we want to present how to investigate the power flow properties of a simple system by its spectral properties. This allows us to make powerful observation about the behaviour of the system and to link geometrical and spectral properties with the load flow results. Most of the analysis here is based on previous studies, especially [85]. The theoretical framework is also derived in [86, 46], with further applications therein.

This method is based on the DC power flow equations eq. (1.3), derived in section 1.2.1. The susceptance B in eq. (1.3) can be seen as a weighted laplacian matrix of the underlying network and we use $B = -L$ in the remainder of this section, as we are interested at the properties of the graph encoded in the Laplacian. Important properties of laplacian matrices have been discussed in section 2.2. We know that the Laplacian matrix L is singular, so eq. (1.3) cannot be solved directly. One option is to use the pseudo inverse $L^\dagger$, to solve for the voltage phase as:

$$\boldsymbol{\theta} = L^\dagger \boldsymbol{P} \tag{3.1}$$

In the remainder, the k-th eigenvectors and eigenvalues of L are called λ_k and $\boldsymbol{\phi}_k$, respectively. As the eigenvectors of L form a basis, we can project the real power $\boldsymbol{P}$ on the eigenvectors:

$$\boldsymbol{P} = \sum_{k=1}^{n} \underbrace{\frac{\boldsymbol{\phi}_k \cdot \boldsymbol{P}}{\boldsymbol{\phi}_k \cdot \boldsymbol{\phi}_k^T}}_{=:p_k} \boldsymbol{\phi}_k = \sum_{k=1}^{n} p_k \boldsymbol{\phi}_k \tag{3.2}$$

This projection can be used to decompose the power into the modes of the system. The power at every mode k depends on the scalar projection p_k and the eigenvector $\boldsymbol{\phi}_k$. We can use the previous equation to express the power at each node i as:

$$\boldsymbol{P}_i = \sum_{k=1}^{n} p_k \left(\boldsymbol{\phi}_k\right)_i$$

In a balanced system, the power consumption and generation is balanced, which means that the sum over all nodal power vanishes $\sum_{i=1}^{n} \boldsymbol{P}_i = 0$. This leads to:

$$0 = \sum_{i}^{n} P_i = \sum_{i}^{n}\sum_{k}^{n} p_k \left(\boldsymbol{\phi}_k\right)_i = \sum_{i}^{n} p_1 \left(\boldsymbol{\phi}_1\right)_i + \sum_{k=2}^{n} p_k \sum_{i}^{n} \left(\boldsymbol{\phi}_k\right)_i$$

From eq. (2.7), we know that the sum over all eigenvector components is zero, except for $\boldsymbol{\phi}_1$. From this, it is clear that $p_1 = 0$. Similar to the powers, we can decompose the voltage phases $\boldsymbol{\theta}$ in the spectral domain using the same eigenvectors $\boldsymbol{\phi}_k$ with the scalar projection o_k:

$$\boldsymbol{\theta} = \sum_{k=1}^{n} o_k \boldsymbol{\phi}_k \tag{3.3}$$

Using the DC load flow equation eq. (1.3), we see that:

$$\sum_{k=1}^{n} p_k \boldsymbol{\phi}_k = L \sum_{k=1}^{n} o_k \boldsymbol{\phi}_k = \sum_{k=1}^{n} \lambda_k o_k \boldsymbol{\phi}_k$$

As the eigenvectors are orthogonal, we can clearly see that $o_k = \frac{p_k}{\lambda_k}$ for all $k \neq 1$. This system is undetermined, as we cannot define o_1 in this case. The factor o_1 is related to the reference angle of the system, which can be chosen arbitrary. For simplicity, we set $o_1 = 0$.

Flows over Transmission Lines

The flow over a transmission line $\boldsymbol{F}$ can be expressed as:

$$\boldsymbol{F} = Y_L \nabla \boldsymbol{\theta} \tag{3.4}$$

Where Y_L is a diagonal matrix with the lines admittances on the diagonal and ∇ is the difference of the vertices of the edges in a graph. This means that ∇ is identical to the transpose of the oriented incidence matrix I presented in section 2.1.7. Using the spectral decomposition of $\boldsymbol{\theta}$, the line flows can be calculated with:

$$\boldsymbol{F} = Y_L \sum_{k=1}^{n} \frac{p_k}{\lambda_k} \nabla \boldsymbol{\phi}_k \tag{3.5}$$

The individual terms of the sum in the previous equation allow us to investigate the flow over the lines at each individual modes k_0 as:

$$\boldsymbol{F}_{k_0} = Y_L \frac{p_{k_0}}{\lambda_{k_0}} \nabla \boldsymbol{\phi}_{k_0}$$

From these equations, it is clear how the power flows of a DC power flow problem are directly linked to the spectral properties of the Laplacian matrix of the underlying network. Especially the flow between two vertices is directly linked to the difference of their eigenvector components.

3.2 Numerical Results

Using the theoretical results from the previous section, we know want to explore the spectral properties of a power flow problem. We focus our attention to the IEEE 118 test case [87]. The IEEE 118 test cases has 118 nodes (hence the name) and is supposed to represent a part of the Midwestern US grid.

3.2.1 Spectral Properties of the IEEE 118 Test System

At first, we want to present the spectral properties of the Laplacian matrix of the IEEE 118 test case. The eigenvalues are shown in fig. 3.1a. As we discussed previously, all eigenvalues are positive as L is a positive semi definite matrix. The zero eigenvalue is omitted here. We also show the Fiedler vector, corresponding to the smallest nonzero eigenvalue drawn on the network in fig. 3.1b. As predicted by

the theory, we observe two nodal domains, which divide the graph into two large clusters (a smaller one on the right and a large cluster on the left).

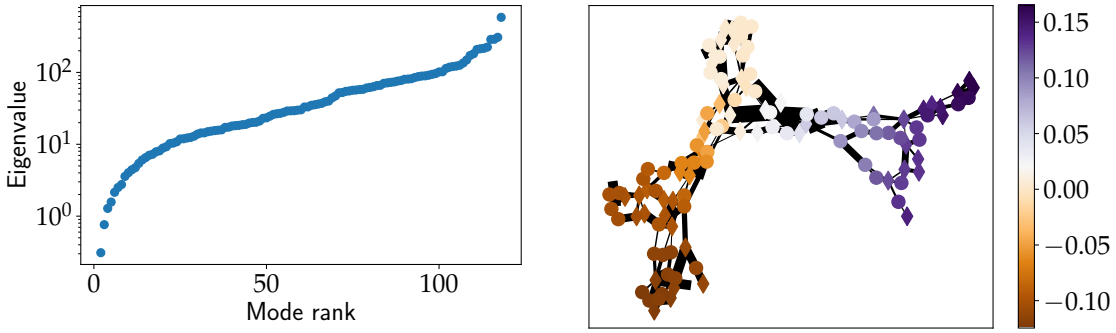

(A) Eigenvalues (B) Fiedler vector

FIGURE 3.1: Ordered eigenvalues and Fiedler vector drawn on a graph plots for the IEEE 118 test system. In the network, the diamonds represent generators, while the circles represent loads.

The eigenvector components for all nodes and all modes are shown in fig. 3.2. We can see a general trend. For small modes, we can see large clusters with large eigenvector components, often very similar. We can also see that most nodes have a non zero eigenvector component. While the indexing of the nodes does not directly corresponds to the representation in the system, we can also observe some coherent clusters or nodal domains. For the second smallest eigenvalue, the negative nodal domain can be observed for small indices, while the large indices correspond to the positive domain. On the other hand, especially at the highest modes, we see that only very few nodes have a non zero eigenvector component. At the largest eigenvalue, we can see that only two modes have a non vanishing eigenvector component. This difference between the low and high modes are a major factor in the analysis of the thesis and play a role the steady-state and dynamic behaviours of power systems. We will first to investigate the more simple case of the steady-state loadflow.

3.2.2 Powerflow Decomposition

To investigate the power flow in the modes, we first calculate the spectral projections p_k and o_k. The power decomposition is shown in fig. 3.3a. We can see that the power is distributed over the whole range of modes. The highest values are found for high modes, around 100. At the whole range, some modes have very little influence in the total power as the values of p_k are very small. On the other hand, the decomposition of the phases $\boldsymbol{\theta}$ are plotted in fig. 3.3b. Clearly, the phases are mostly dominated by

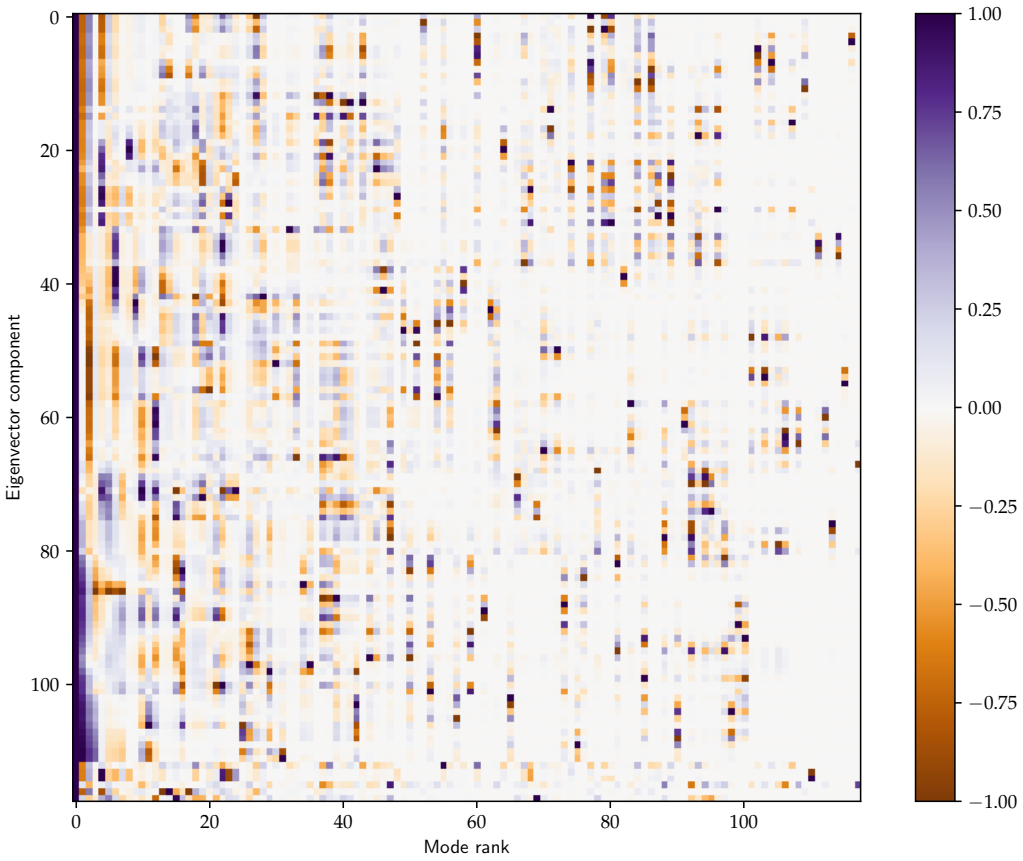

FIGURE 3.2: Eigenvector components of the IEEE 118 test case. The colour code corresponds to the value at a given node and mode. It should be noted that these eigenvectors are normalised so that their largest value is equal to one, for better visualisation.

the lowest modes and the high modes do not influence the phases a lot. We know that $o_k = \frac{p_k}{\lambda_k}$. As the eigenvalues grow very large for large k, as seen in fig. 3.3b, this is the expected behaviour.

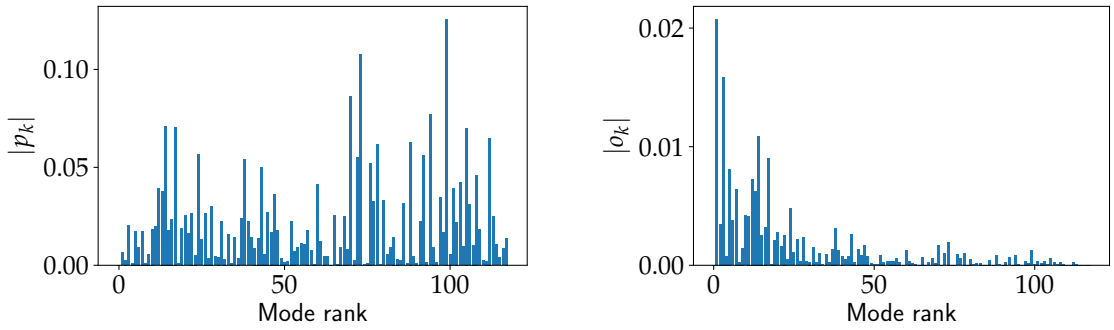

(A) Power decomposition (B) Phase decomposition

FIGURE 3.3: Scalar projections p_k and o_k to project the power and voltage phase on the eigenbasis of the laplacian matrix of the IEEE 118 system.

We can see how the decomposition influences the power flow solutions in fig. 3.4. In the left panel, we show the voltage phases calculated with the DC power flow calculation. The eigenvectors corresponding to the largest values o_k are shown, except the Fiedler vector already presented in fig. 3.1b. Investigating the voltage phases, we clearly see how distinct the left and the right side of the network are. This clustering is very similar to the nodal domains for the smallest nonzero eigenvalue shown before. In the right cluster, the voltage phases are further divided in two clusters. These clusters can be seen at ϕ_4. On the lower side of the left cluster, a branch with a very different phases in contrast to the rest can be observed. This branch can also be observed at mode $k = 15$. We see that some of the most prominent features of the voltage phases can be described by just a few modes.

3.2.3 Flows in Line

Now, we focus our attention to the flows on lines in the system. At first, we can investigate the flows in each individual line in the system. The IEEE 118 test case has 179 edges. In fig. 3.5a, the total flow in each line (for all modes) is shown. Clearly, some lines are loaded much more than the other lines. Especially lines 23, 112 and 162 are highly loaded, while some other lines have almost no flow in them. The highly loaded lines are especially important for the power system operation. On the other hand, we can calculate for each line the maximum power transferred at a single mode. This example is shown in fig. 3.5b- We can clearly see that the peak at line

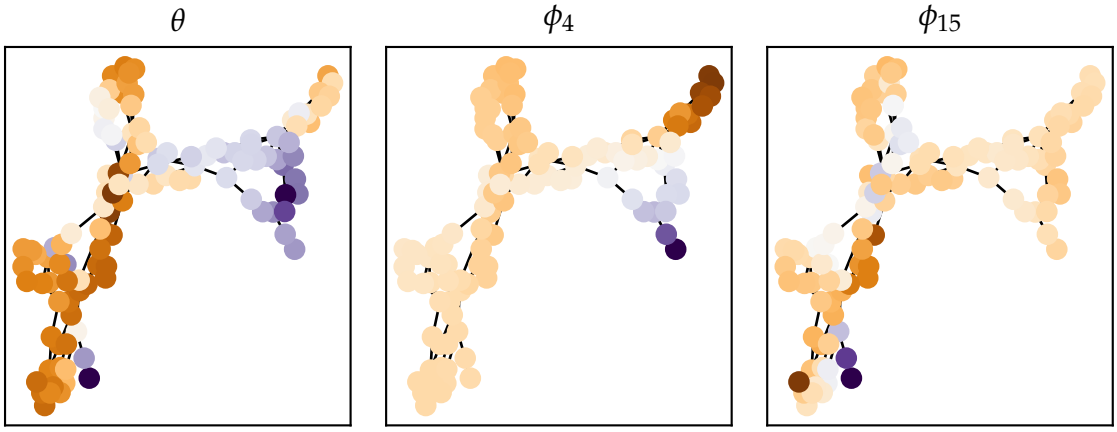

FIGURE 3.4: Phases and most dominant modes of the IEEE 118 test case.

23 vanishes, while the peak at 112 is still observable. This means that line 112 has a large amount of flow at a single mode, while the flow in line 23 is a consequence of many modes. In fact, in 25% of the total flow in line 112 happens at a single mode, while less than 11% of the flow in line 23 are a consequence of the most dominant mode..

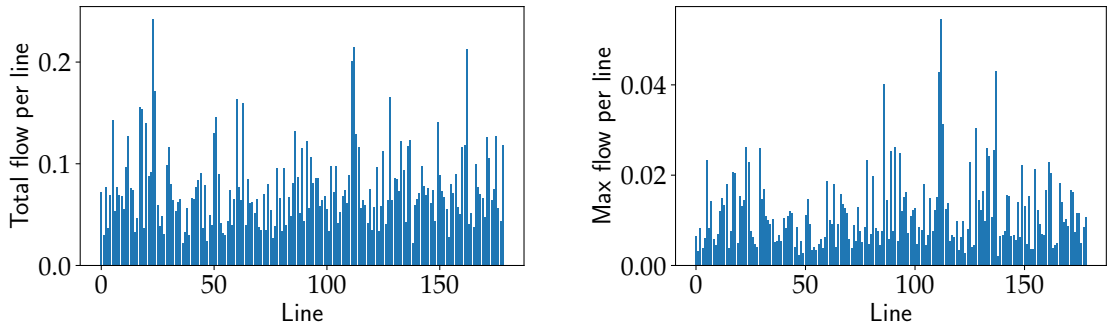

(A) Total flow

(B) Maximum flow

FIGURE 3.5: Total and maximum power flow in each transmission line in the IEEE 118 test case.

We can do a similar analysis, this time focusing on the flow per mode. This means that we calculate the flows in all the lines of the system at each 118 modes and the results are shown in fig. 3.6. The total flows are shown in fig. 3.6a. The total amount of power flow at each mode seem to decrease for larger modes and the highest peak is observed at mode 15. Again, we can calculate the maximum power in any line for each mode, which is shown in fig. 3.6b. In general, we see that maximum flows per line does not decrease as much with increasing modes as the

total flow. This means that for higher modes, the flows are more concentrated on single lines. We can also observe that some new peaks appear, for example mode 18. While this mode already has a large total flow, it also has one line which has a very high flow at a single line.

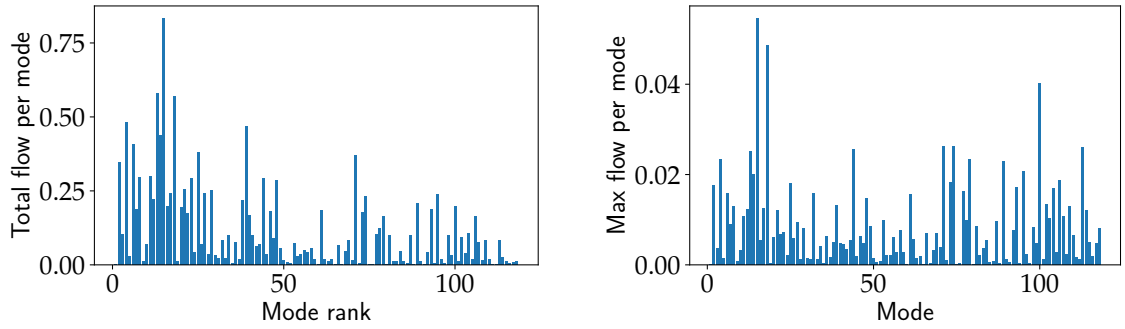

(A) Total flow (B) Maximum flow

FIGURE 3.6: Total and maximum power flow at each mode in the IEEE 118 test case.

The percentage of the maximum flow to the total flow per mode is shown in fig. 3.7a. Here, we can clearly see the increase for high modes. This means that for higher modes, the flow is limited to less lines. The largest values was found at mode 110, where almost 80% of the flow is found at a single line.

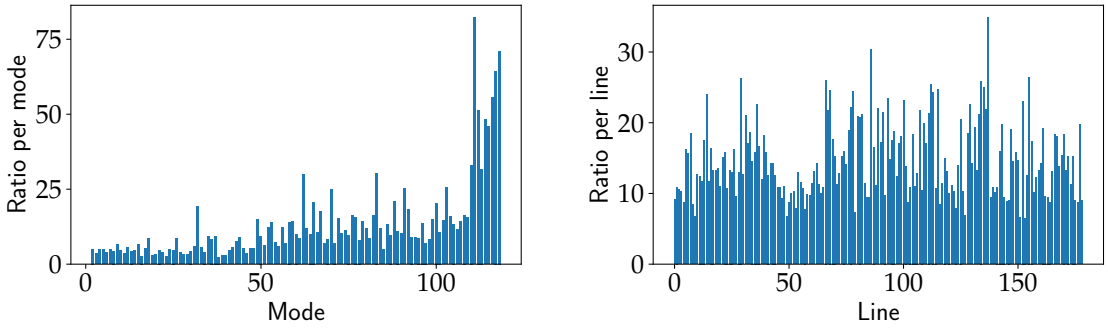

(A) Per mode (B) Per Line

FIGURE 3.7: Percentage of total flow to maximum for each line per mode or for each mode per line of the IEEE 118 test case.

We can investigate this difference in more detail by calculating the mode decomposition of power flows line per line. Two cases are shown in fig. 3.8. These cases correspond to the Lines with the lowest and the highest values in fig. 3.7b. On line 153, the flows are separated over multiple lines. At the other hand, almost all flow in Line 137 happens at two single modes.

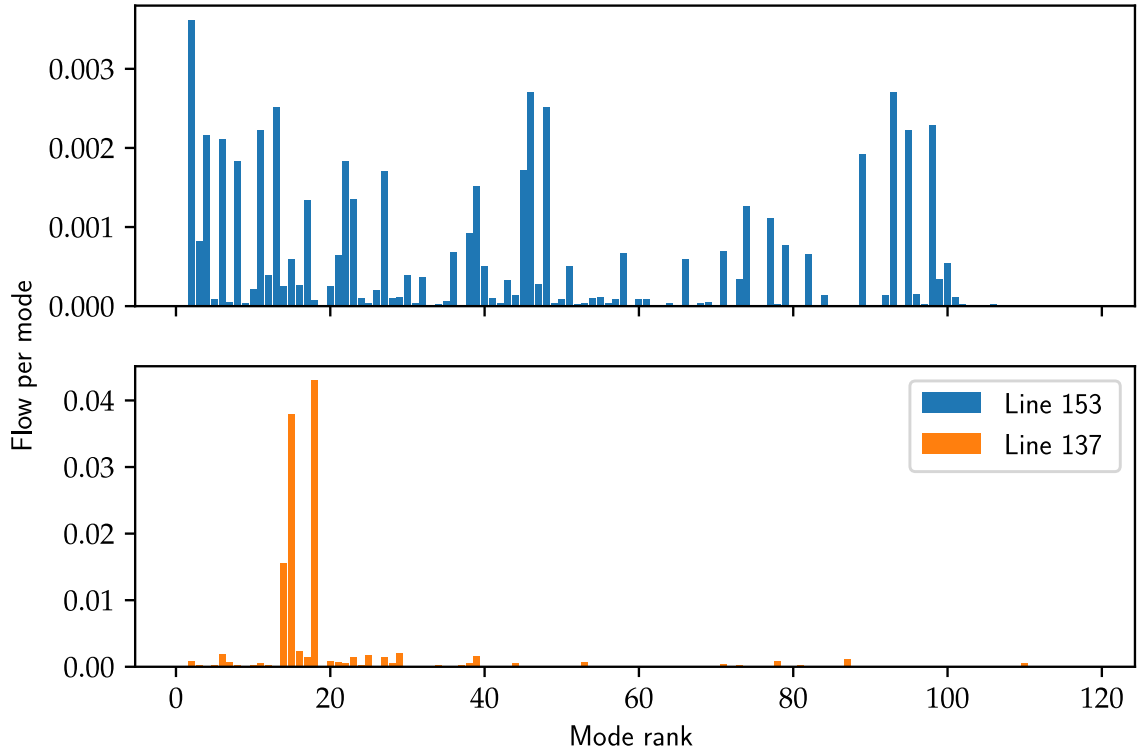

FIGURE 3.8: Decomposed power flow through two different lines in the IEEE 118 test case.

Again, we can also focus on power per line for different modes. In fig. 3.9, the flow per line at three different modes were shown. We choose the examples from fig. 3.7a where the ratio from largest to total flow is the smallest (mode 37) and the two modes with the largest ratio (110 and 117). Here we see that the global behaviour of the system is very different at different modes. For mode 37, many lines have some flows. On the other hand, at mode 110, basically only a single line is active and the remaining flows basically zero.

This behaviour of lines can directly be associated with the eigenvectors. We show two eigenvectors corresponding to the nodes 37 and 117 drawn on the network in fig. 3.10. The edge width corresponds to the flow in the lines at the corresponding mode. We can clearly see that the differences in the eigenvector components are a major factor in the flow in the lines. At mode 117, almost all eigenvector nodal values are zero, except for two. Exactly between these nodes, the flow is relatively large. On the other hand, the eigenvectors of mode 37 are very complex and no large structure or special features can be seen. At the same time, we observe flows all over the network.

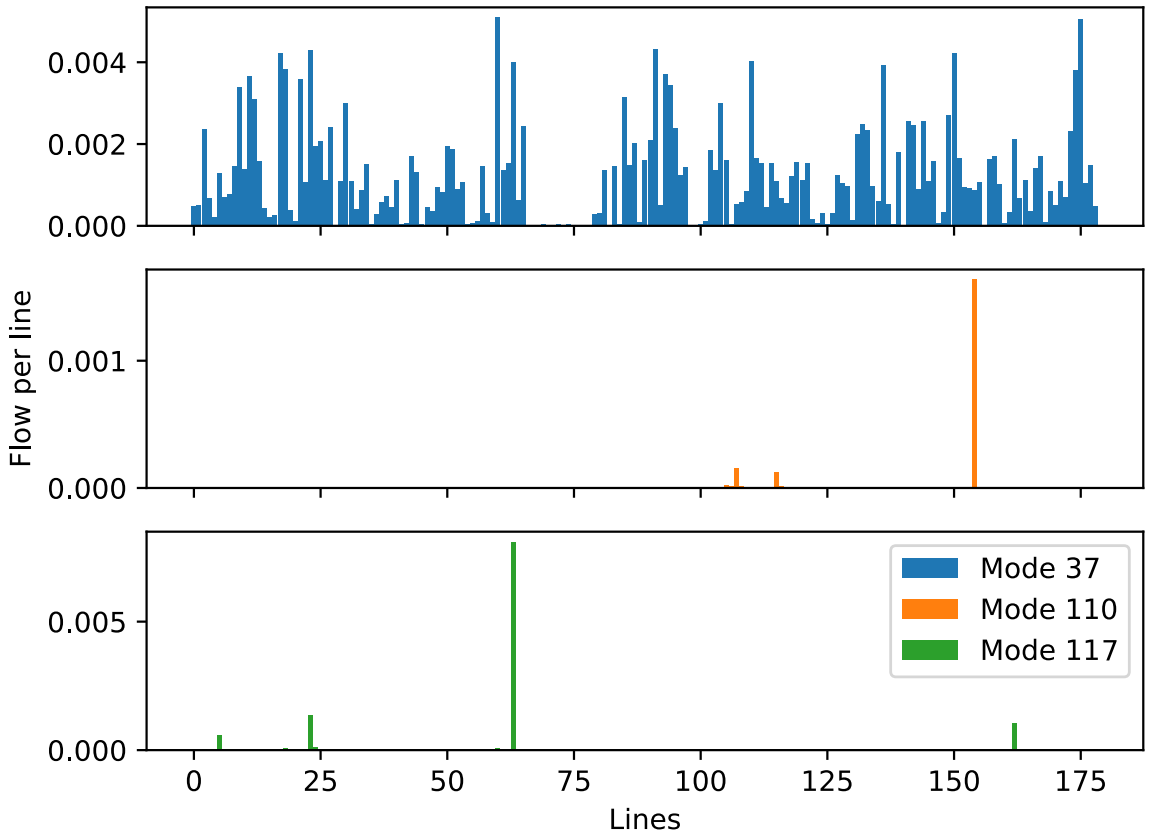

FIGURE 3.9: Flow in line of three different modes of the IEEE 118 test case.

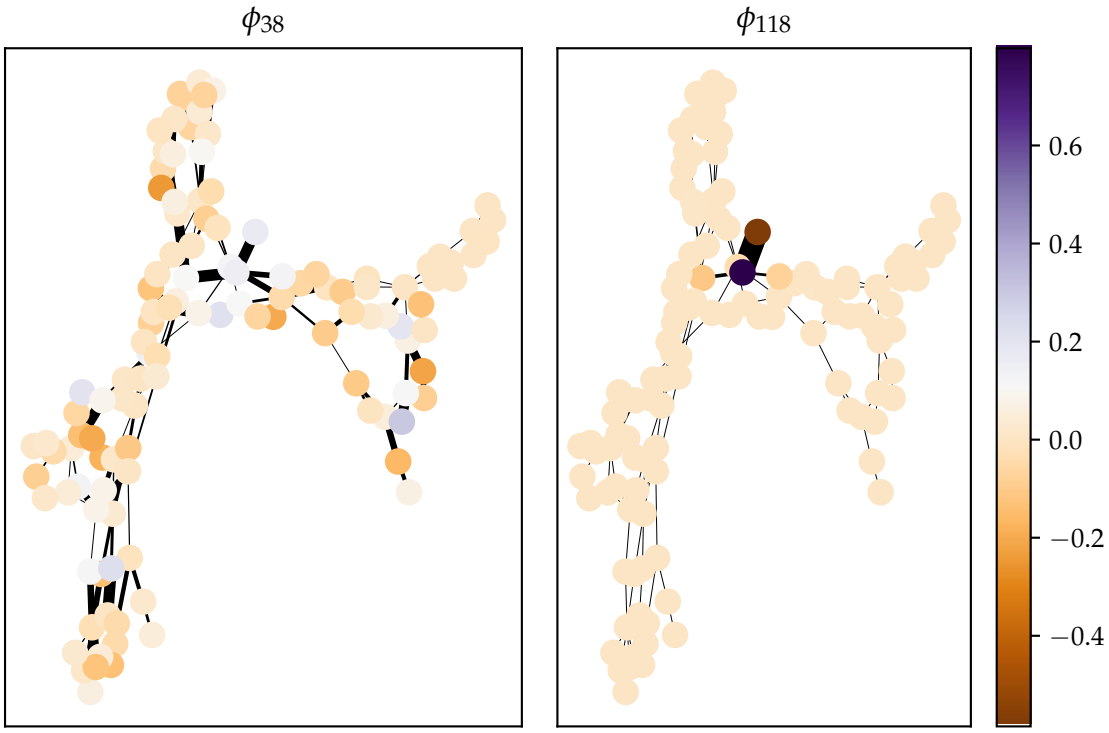

FIGURE 3.10: Eigenvectors and flows corresponding to two nodes of the IEEE 118 test case. The colours of the vertices correspond to the eigenvector components and the width of the edges to the flow at the corresponding mode between the nodes.

3.3 Conclusions

In this chapter, we derived the equations to solve the power flow equations in the spectral domain. We used these equations to deeply investigate the spectral decomposition of the flows in the power system. These flows can be investigated per line or per mode, which results in interesting and different behaviour.

One general observation is that for low modes, the flow is spread over the whole system, with large flows from one to the other side. At the opposite side, we found that the flow in the highest modes is almost completely limited to a single edge. Mathematically, this was linked to the eigenvectors, that were zero almost everywhere, except around this edge. The next issue is now to determine if this noticeable localisation of eigenvectors and the differences of eigenvector geometry with the modes plays also a major role for the dynamic properties on the dynamic properties.

Chapter 4

Spectral Properties of Dynamical Power Systems

4.1 Modelling and Background

In this chapter, we analyse the spectral properties of dynamical power system problems. Building on the previous studies, discussed in section 2.3.1, we aim to do two things:

1. Investigate the small signal properties of a dynamical power system model. We want to know how the model behaves and how the various parameters, the inertia, the damping and the coupling matrix of the network, influence the dynamics of the system.

2. Try to bridge the gap between the studies of the undamped network from [63] and the research on damped systems with identical machine parameters from [65, 21]. We first focus our attention on the role of the damping in the system and later propose a theoretical method to directly link both results.

We use the general power system model explained eq. (1.5), which can models the generators with the swing equations and offers multiple options to model the loads. We want to investigate the small signal stability, which are small perturbations around an operating point $\boldsymbol{\theta}^*$. We can linearise the right hand side of these equations around the operating point, resulting in:

$$\begin{aligned} M_i\ddot{\boldsymbol{\theta}}_i + D_i\dot{\boldsymbol{\theta}}_i &= \boldsymbol{P}_{B,i} - \sum_{j=1}^{n} a_{ij}\cos\Big(\boldsymbol{\theta}_i^* - \boldsymbol{\theta}_j^*\Big)(\boldsymbol{\theta}_i - \boldsymbol{\theta}_j) \quad i \in \mathcal{V}_{\mathcal{P}} \\ D_i\dot{\boldsymbol{\theta}}_i &= \boldsymbol{P}_{B,i} - \sum_{j=1}^{n} a_{ij}\cos\Big(\boldsymbol{\theta}_i^* - \boldsymbol{\theta}_j^*\Big)(\boldsymbol{\theta}_i - \boldsymbol{\theta}_j) \quad i \in \mathcal{V}_{\mathcal{C}} \end{aligned} \tag{4.1}$$

The right hand side of these equations are equal to $\tilde{L}\boldsymbol{\theta}$, with $\tilde{L}$:

$$\tilde{L} = \begin{cases} -a_{ij}\cos\left(\boldsymbol{\theta}_i^* - \boldsymbol{\theta}_j^*\right) & \text{if} \quad i \neq j \\ \sum_{j\neq i}\tilde{L}_{ij} & \text{else} \end{cases} \tag{4.2}$$

Which is the Laplacian matrix for small perturbations around an operating point [63, 65, 81, 21]. As $\tilde{L}$ is a Laplacian matrix, we drop the tilde and call this matrix by L in the remainder of this chapter. The linearised power system model is then given as:

$$M\ddot{\boldsymbol{\theta}} + D\dot{\boldsymbol{\theta}} = \boldsymbol{P}_B - L\boldsymbol{\theta} \tag{4.3}$$

The topological properties of the network are encoded in the Laplacian matrix L. M and D are diagonal matrices which describe the machine parameters at each node in the system. We generally consider the SP model, as described in section 1.2.3. Here, the inertia M is zero at the load nodes. This means that M is a singular diagonal matrix. As we are mostly interested in the influence of the topology and machine parameters, we will focus on the free response system by setting $\boldsymbol{P}_B = 0$. Then, we can use spectral methods to solve the system of ordinary differential equations. From [88], we can express the time evolution of the phases $\boldsymbol{\theta}$ as:

$$\boldsymbol{\theta}(t) = \sum_{k}^{2n} \boldsymbol{\gamma}(k)\boldsymbol{\phi}(k)\exp(\lambda_k t) \tag{4.4}$$

Here, the vector $\boldsymbol{\gamma} = [\gamma_1 \dots \gamma_{2n}]$ is a vector of arbitrary constants related to the initial values of the problem. The factors λ_k and $\boldsymbol{\phi}(k)$ are the eigenpairs of the *quadratic eigenvalue problem* (QEP) of the matrices M, D and L, which is given as:

$$(\lambda^2 M + \lambda D + L)\boldsymbol{\phi} = 0 \tag{4.5}$$

Theoretically, we could transform the quadratic eigenvalue problem in a generalised eigenvalue problem using state-space formalism. This form would have a dimension of $2n$, but would be linear again. The process and results are shown in appendix A.1. The main problem is that the resulting state matrix F does not retain any of the features of the matrices M, D and L. Especially the topological features

of the underlying graph are directly encoded in L but will be lost in F. This is why it can be beneficial to tackle the problem in the quadratic form. The next subsection presents some mathematical properties of the quadratic eigenvalue problem.

4.1.1 Quadratic Eigenvalue Problem

The quadratic eigenvalue problem is directly related to the eigenvalue problem, with the differences being the additional matrices M and D and supplementary quadratic and linear eigenvalue terms. Even when the matrices are $n \times n$ sizes, the quadratic nature results in $2n$ eigenpairs. This can be understood as a result of the positive and negative solutions of a square root. From a theoretical point of view, the following properties can be found in a QEP [88]:

1. M is non singular - $2n$ finite eigenvalues
2. M, D, L are real matrices - eigenvalues are either real or come in complex conjugate pairs
3. M hermitian and positive definite, D and L positive semi definite - The real parts of the eigenvalues are non positive

When M is singular, there will be infinite eigenvalues. As M is a diagonal matrix with zero entries for the $n_{\mathcal{C}}$ load nodes, there are $n_{\mathcal{C}}$ infinite eigenvalues. These infinite eigenvalues correspond to an infintaly fast time response in eq. (4.4) . Infinite eigenvalues correspond to algebraic equations related to passive loads.

Overdamped Behaviour

Under some conditions, an overdamped behaviour is found, named after the phenomena in mechanical systems. Under overdamped conditions, all eigenvalues are real and negative, with a gap between the largest n and smallest n eigenvalues. The eigenvalues can then be separated into two distinct sets. The corresponding eigenvectors then form two separate, linear independent sets. If M and D are symmetric and positive definite, L is positive semi definite, it can be shown that overdamped behaviour is found if damping factor $\gamma(M, D, L)$ is positive [88]. The damping factor is defined as:

$$\gamma(M, D, L) = \min_{\|x\|_2=1} \left((x^* D x)^2 - 4 \left(x^* M x\right) \left(x^* L x\right) \right) \tag{4.6}$$

A simple approximation γ_{up}, which upper bounds the damping factor, can be calculated using the Courant–Fischer Theorem [67]:

$$\gamma_{\text{up}}(M, D, L) = \lambda_{D,\min}^2 - 4\lambda_{M,\max}\lambda_{L,\max} > \gamma(M, D, L) \tag{4.7}$$

Here, $\lambda_{X,\min/\max}$ is the smallest/largest eigenvalue of the matrix X. Overdamped behaviour can be archived by increasing the damping coefficient of the generators or by lowering the inertia or connectivity of the network. The systems relevant for our work are generally not overdamped and the results do not apply here. In [89], we showed that in the IEEE 145 test case, the damping has to be increased by a factor of more than 1000 to reach overdamped behaviour.

Companion Form

The most used method to analyse the quadratic eigenvalue problem results in the companion form of the QEP. The companion form can easily be constructed by using a substitution like $u = \lambda\boldsymbol{\phi}$ inserted in eq. (4.5). Rearranging the QEP with this substitution leads to:

$$\underbrace{\begin{pmatrix} 0_n & \mathrm{I}_n \\ -L & -D \end{pmatrix}}_{=:X} \underbrace{\begin{pmatrix} \boldsymbol{\phi} \\ \boldsymbol{u} \end{pmatrix}}_{=:v} = \lambda \underbrace{\begin{pmatrix} \mathrm{I}_n & 0_n \\ 0_n & M \end{pmatrix}}_{=:Y} \underbrace{\begin{pmatrix} \boldsymbol{\phi} \\ \boldsymbol{u} \end{pmatrix}}_{=:\boldsymbol{v}} \tag{4.8}$$

Which is just a (linear) generalised eigenvalue problem for the $2n \times 2n$ matrices X and Y with the eigenvector $\boldsymbol{v} = (\boldsymbol{\phi} \quad \boldsymbol{u})^T$. In general, other companion forms for the quadratic eigenvalue problem [88] or general polynomial eigenvalue problems [90, 91] can be found. Depending on the properties of the involved matrices, some companion forms might have more desirable properties, but for this work, the companion form described here is sufficient. It should be noted that, while the resulting problem in eq. (4.8) is linear, the companion form is not an approximation and the solutions $\boldsymbol{\phi}$ and λ are identical to the solutions of the quadratic eigenvalue problem. Numerically, solving the $2n \times 2n$ problem might result in increased numerical errors. Methods to reduce or estimate these errors are discussed in [92], but are out of scope for this work. We consider the numerical solution of eq. (4.8) to be accurate enough for our investigations. In all numerical experiments, the solutions from eq. (4.8) are inserted in eq. (4.5) and the equation is checked for equality. Up to rounding errors, all solutions obtained by the companion form have been accurate.

4.1.2 Kron Reduction

In section 1.2.3, the SP-model was introduced either with or without damping of the load nodes. If all load nodes are undamped, the dynamics of the loads are described by purely algebraic equations. The system will have $2n_{\mathcal{C}}$ infinite eigenvalues, where $n_{\mathcal{C}}$ is the number of load nodes in the system. The infinite eigenvalues again correspond to the instantaneous response of the loads. In this case, the system can be simplified by the Kron reduction. The following calculations show the mathematical steps. For simplicity, all generator nodes are considered to be undamped, but the calculations for damped generators is analogous. Partitioning the system in the load $\mathcal{C}$ and generator $\mathcal{P}$ sets leads to:

$$\begin{pmatrix} L_{\mathcal{P}} & L_{\mathcal{PC}} \\ L_{\mathcal{PC}}^T & L_{\mathcal{C}} \end{pmatrix} \begin{pmatrix} \boldsymbol{\phi}_{\mathcal{P}} \\ \boldsymbol{\phi}_{\mathcal{C}} \end{pmatrix} = \lambda^2 \begin{pmatrix} M_{\mathcal{P}} & 0 \\ 0 & 0 \end{pmatrix} \begin{pmatrix} \boldsymbol{\phi}_{\mathcal{P}} \\ \boldsymbol{\phi}_{\mathcal{C}} \end{pmatrix}$$

In this case, the eigenvector of the load nodes can be removed by inserting the second row of the block matrix equation in the first one and calculating:

$$L_{\mathcal{P}}\boldsymbol{\phi}_{\mathcal{P}} + L_{\mathcal{PC}}\boldsymbol{\phi}_{\mathcal{C}} = \underbrace{L_{\mathcal{P}}\boldsymbol{\phi}_{\mathcal{P}} - L_{\mathcal{PC}}L_{\mathcal{C}}^{-1}L_{\mathcal{PC}}^T\boldsymbol{\phi}_{\mathcal{P}}}_{=L_{\text{red}}\boldsymbol{\phi}_{\mathcal{P}}} = \lambda^2 M_{\mathcal{P}}\boldsymbol{\phi}_{\mathcal{P}}$$

The reduced matrix L_{red} is identical to the Schur complement of the Laplacian matrix with respect to the submatrix of the load nodes. This matrix is also a Laplacian matrix [63, 20] with a size of $n_{\mathcal{P}} \times n_{\mathcal{P}}$. The graph corresponding to the reduced Laplacian is a complete, weighted graph. The topological properties of the original graph are encoded into the edge weights of the reduced graph. To solve the QEP, the reduced Laplacian and reduced matrices $M_{\mathcal{P}}$ and $D_{\mathcal{P}}$ can be used. These are now full diagonal matrices. An example for the graph before and after the Kron reduction is shown in fig. 4.1 for the IEEE 57 bus system [93].

4.1.3 Condition Numbers

One important theoretical tool to investigate the properties of eigenvalue problems are the condition numbers. They measure how robust an eigenvalue, and therefore the spectral properties of a systems are regarding to perturbations of the inputs and parameters. Usually, these numbers are defined for matrix perturbations. In [92, 88], the condition number κ of a quadratic eigenvalue problem of the form eq. (4.5) for a given nonzero and finite eigenvalue λ is given as:

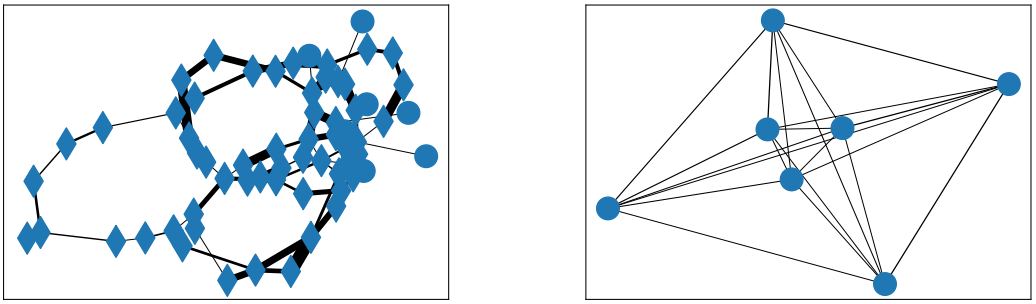

(A) Full Graph (B) Reduced Graph

FIGURE 4.1: Full IEEE 57 test system and graph after Kron reducing all load nodes. Circles depict the generators, diamonds the load nodes.

$$\kappa(\lambda) = \frac{|\lambda|^2 \alpha_M + |\lambda| \alpha_D + \alpha_L}{|\lambda| \left|\boldsymbol{\psi}^* \left(2\lambda M + D\right) \boldsymbol{\phi}\right|} \|\boldsymbol{\psi}\| \|\boldsymbol{\phi}\| \tag{4.9}$$

Where $\boldsymbol{\psi}$ is the left eigenvector of eq. (4.5). The non negative parameters α_i can be used to determine how strong each matrix is perturbed. Each α_i corresponds to one of the matrices M, D or L. If the parameters α_i are set to zero for two matrices, the sensitivity of the quadratic eigenvalue problem in perturbations of the remaining matrix can be assessed. Usually, the perturbations are measured relatively, meaning:

$$\alpha_M = \|M\| \quad \alpha_D = \|D\| \quad \alpha_L = \|L\|$$

So, the perturbation of each matrix corresponds to the *size* of the matrix. The perturbations can also be calculated absolute, for example $\alpha_M = 1$ and $\alpha_D = \alpha_L = 0$. The larger α is chosen, the larger the influence of the corresponding matrix is on the conditioning number. In general, a large condition number means that the eigenvalue is very sensitive to perturbations of the corresponding matrix.

4.1.4 Oscillatory Networks

Oscillatory networks are systems closely related to QEP and have been studied extensively [63]. Good examples for these systems are linear mass spring models or LC circuits. Those systems result in:

$$\lambda^2 M\boldsymbol{\phi} = -L\boldsymbol{\phi} \tag{4.10}$$

For example, in the linear LC circuits, the capacitors represent M, while the connection via inductive cables result in a Laplacian L. This quadratic problem is equivalent to the more simple generalised eigenvalue problem $\mu M\boldsymbol{\phi} = L\boldsymbol{\phi}$ with $\mu = \lambda^2$. The generalised eigenvalue problem can be solved and investigated in many ways. It can be easily transformed to a normal eigenvalue problem by the straightforward calculation of $M^{-1}L$ or investigated directly, as for example shown in [63].

4.2 The Laplacian Spectrum and the QEP

Here, we want to investigate how the spectrum of the quadratic eigenvalue problem behaves with respect to the Laplacian spectrum. We consider the Kron reduced system as discussed previously. This means that M and D are diagonal matrices without any zeros, which corresponds to the absence of any infinite eigenvalues. One main simplification, which is vital for the investigations in [65, 21] is that the inertia and damping parameters are equal for all generators. This means that:

$$M = m_0 \mathrm{I}_n \quad \text{and} \quad D = d_0 \mathrm{I}_n$$

This allows us to significantly simplify the quadratic eigenvalue problem to:

$$\underbrace{\left(\lambda^2 + \lambda\frac{d_0}{m_0}\right)}_{:=-\zeta^2}\boldsymbol{\phi} + \underbrace{\frac{1}{m_0}L}_{\tilde{L}}\boldsymbol{\phi} = 0 \tag{4.11}$$

Where $\tilde{L}$ is a Laplacian matrix, where each edge weight is divided by m_0. The resulting equation is just the eigenvalue problem for the new Laplacian matrix $\tilde{L}$ with the eigenvalue ζ. Using the dissipation factor $a = \frac{d_0}{m_0}$, the eigenvalues λ of the QEP are then calculated as:

$$\lambda_{i,\pm} = -\frac{a}{2} \pm \sqrt{\frac{a^2}{4} - \zeta_i^2} \tag{4.12}$$

For very small dissipation $a \approx 0$, we see that the eigenvalues of the quadratic eigenvalue problems are just the negative square root of the Laplacian eigenvalues. The dynamical properties of the system are then directly linked to the eigenvalues of the Laplacian matrix and thus to the geometric properties of the underlying network.

Dissipation Mode

One interesting consequence of eq. (4.12) is the zero eigenvalue of the Laplacian matrix. As the quadratic eigenvalue problem effectively *doubles* the eigenvalues, it is interesting to find out what happens in this case. For $\zeta = 0$, we find that $\lambda = 0, -a$. This means that one zero eigenvalue is kept, while another eigenvalue becomes a purely real, negative eigenvalue. This eigenvalue has the same eigenvector as the zero eigenvalue, which is the constant vector of all ones[1]. In the power system background, we can interpret this eigenvalue as the dissipation of energy of the whole system.

4.3 Experimental Investigations

In this section, the spectral properties of a dynamical power system are investigated. As in the previous chapter, we focus on the IEEE 118 test system. It should be noted that the IEEE 118 test case has many generators without any active power output [87]. Some of the generators of the IEEE 118 test case do not produce any active power and are treated as loads in the analysis. As load nodes, these generators will be removed by the Kron reduction, as discussed in section 4.1.2 A similar investigation, with the 50 generator dynamical test case [94], has been performed by us previously [89]. The IEEE 118 test case is a usually a static power flow test case, and no dynamical parameters are given. We use the algorithms presented in [21, 24] to find suitable dynamic paramters (M and D) for the IEEE 118 test case. One main challenge in the investigations is that the default parameters of the IEEE 118 test case are not overdamped. This means that all solutions to the eigenvalue problem are generally complex numbers. Using eq. (4.7), we can predict that overdamped behaviour would occur of the damping matrix D is multiplied with a factor of approximately 1100. As condition 1 and 2 from section 4.1.1 are then fulfilled, all eigenvalues have negative real parts and the imaginary parts are zero or come in complex conjugate

[1] Remember that this is only true for the assumption of identical inertia and damping!

pairs. As all the real parts of the eigenvalues are negative (or zero), we also know that the system is always (marginally) stable.

Similar to the behaviour of a mechanical system, the complex eigenvalues result in a damped oscillation. The imaginary part corresponds to the frequency of the oscillations, while the real part is the damping. Comparing and ranking complex numbers is not directly possible, but important for some applications here. In eq. (4.4), a complex eigenvector $\boldsymbol{\phi} = |\boldsymbol{\phi}| e^{\iota\eta}$ results in a phase shift of η, which is the angle of the eigenvector. As we are more interested in the general dynamical properties and not the exact shape of each time evolution, we focus on the magnitude of the eigenvector and ignore the phase shift. While the difference in the imaginary parts and the real parts of the eigenvalues are generally important to describe the oscillations, we will investigate the sensibility of the spectra in the absolute value as well. In some cases, we will use other methods to rank complex numbers (for example their real part).

4.3.1 Time Response and Oscillations

As mentioned, the time response of the normal IEEE 118 system is a damped oscillation. We plot the time response, calculated with eq. (4.4) for all nodes of the reduced system in fig. 4.2a. While all nodes show a damped oscillations, the individual behaviour of the nodes is very different. In figs. 4.2b to 4.2d, the same curves are plotted with different colours. The colour (and opaqueness) of each curve corresponds to the eigenvector component of a certain mode. This allows us to investigate the influence on single modes on the complete time response.

In fig. 4.2b, we observe multiple nodes which have a very similar time response for most of the time. They all seem to oscillate with roughly the same frequency and a similar amplitude. This corresponds to coherent behaviour of these generators. On the other hand, fig. 4.2c shows a single node which oscillates with a very high frequency. Especially the fast oscillation also seems to decay very fast. These high frequency oscillations are not observed in any other nodes. The single node in fig. 4.2d also oscillates with an individual frequency, this time a much lower frequency though.

These examples show the complex dynamics which can be found even in a linearized system. Especially interesting is the difference between behaviour which is similar in multiple nodes, as in fig. 4.2b in contrast to some oscillations only observed in individual nodes, for example the fast oscillations in fig. 4.2c or the single slowly oscillating node fig. 4.2d. The different behaviour of the nodes can be explained by the eigenvectors of the system, which is presented in the next section.

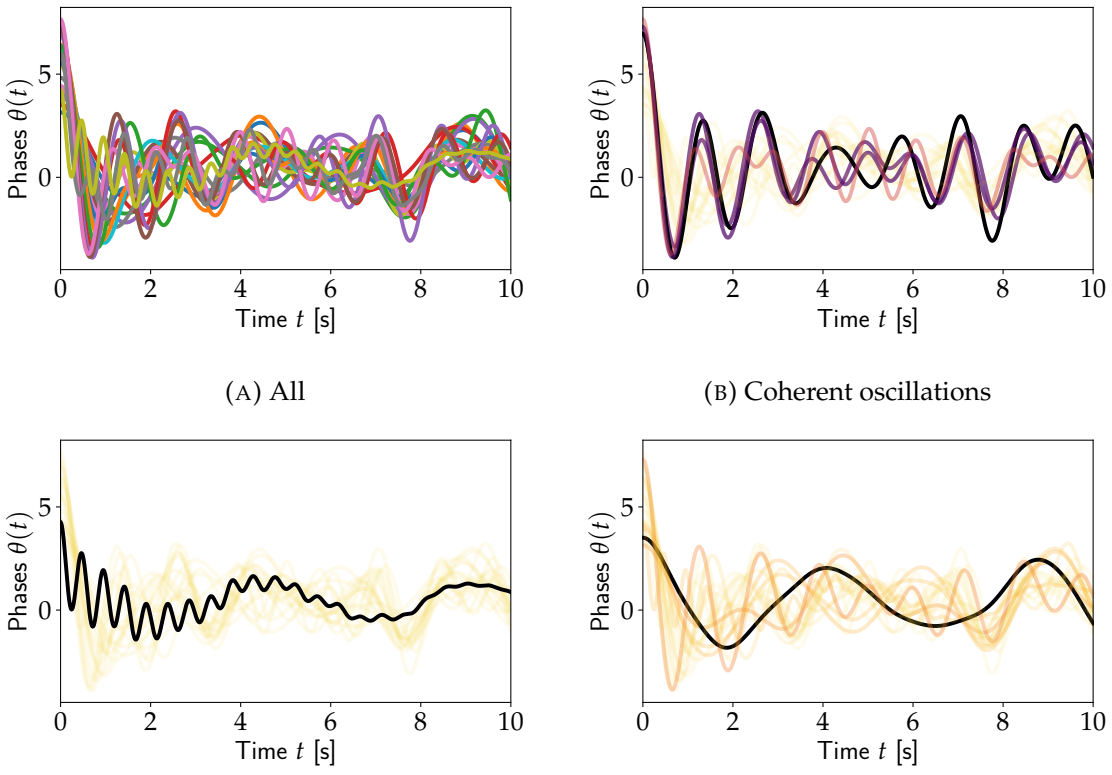

(A) All

(B) Coherent oscillations

(C) Fast oscillations

(D) Slow oscillations

FIGURE 4.2: Time response of the linearized IEEE 118 test case. In (B) to (D), the colour and opaqueness corresponds to the eigenvector components at different modes.

4.3.2 Eigenvectors

In fig. 4.3a, the absolute value of the eigenvector components from the QEP are shown. The eigenvectors are sorted by the real part of the eigenvalues. As the eigenvalues come in complex conjugate pairs, all eigenvectors are doubled. We can also observe that generally that the eigenvectors with high rank are more localised, while the lower ranked eigenvalues are distributed over many nodes. This means that the eigenvalues corresponding to the high ranked eigenvalues are only observed in the time response of a few single nodes, while the lower ranked eigenvalues correspond to long ranging interactions possibly observed in the whole system. We also show two eigenvectors drawn on the reduced network in fig. 4.3b. Those two examples can be used to explain some behaviour observed before in fig. 4.2. For $k = 30$, multiple nodes are active. For $k = 30$, four nodes have a relatively large eigenvector components(13,14,15,16). Those node are exactly the ones showing a coherent oscillation in fig. 4.2b. On the other hand, at $k = 37$, only node 18 has nonzero eigenvector components. This node corresponds to the fast oscillating time response highlighted in

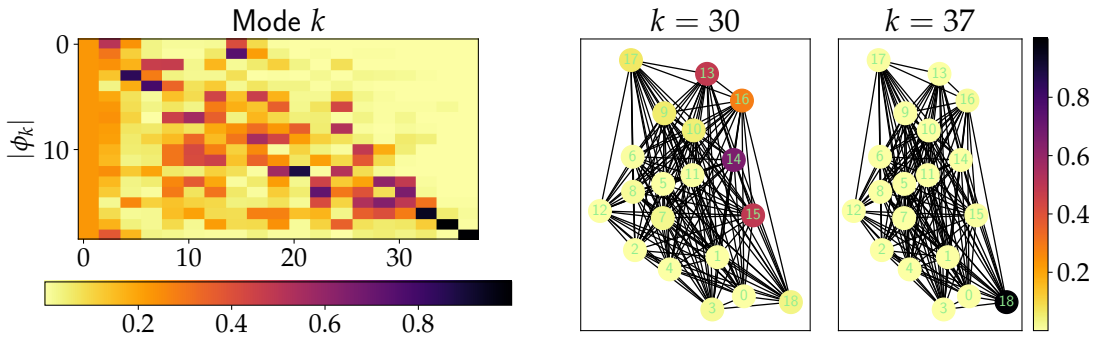

(A) Eigenvector components (B) Reduced network

FIGURE 4.3: Eigenvector components of reduced IEEE model for all modes and drawn on a network for two different modes.

fig. 4.2c.

4.3.3 Spectrum of the Reduced Power System Laplacian

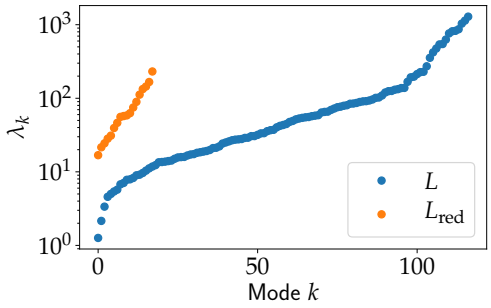

FIGURE 4.4: Spectra of Laplacian and reduced Laplacian matrix.

Section 4.3.3 shows the spectra of the full Laplacian matrix of the IEEE 118 test case and the Laplacian matrix after removing the inertialess nodes. Obviously, the reduced system is much smaller, which corresponds to less eigenvalues. The similar ranked eigenvalues of the reduced system are larger than those of the normal Laplacian, which corresponds to a higher *connectivity* in the reduced system. Especially the algebraic connectivity in the reduced system is much larger than in the full network. As the graph of the reduced system is a complete graph, this system is maximally connected. In both spectra, we see a large increase of the eigenvalues in the highest modes. As the number of eigenvalues is much lower for the reduced system, this system is less complex than the full system.

4.3.4 Parameter Influence

The previous examples and theoretical approaches show the basic behaviour of a linearised power system. We now focus our attention on the influence of the parameters of the machines (M and D) and the Laplacian L. We want to know how these parameters influence the spectrum, which in turns influences the time behaviour observed in fig. 4.2. We are interested how sensitive the spectrum is to changes of the parameters and especially how the damping influences the system.

Bifurcation Diagrams

At first, we investigate possible bifurcations in the eigenvalues of the quadratic eigenvalue problem. We consider a bifurcation diagram and investigate the real and imaginary parts of λ, under the influence of changes in the damping and the inertia. In both cases, the relevant matrix is multiplied with a scalar m_i or d_i, respectively.

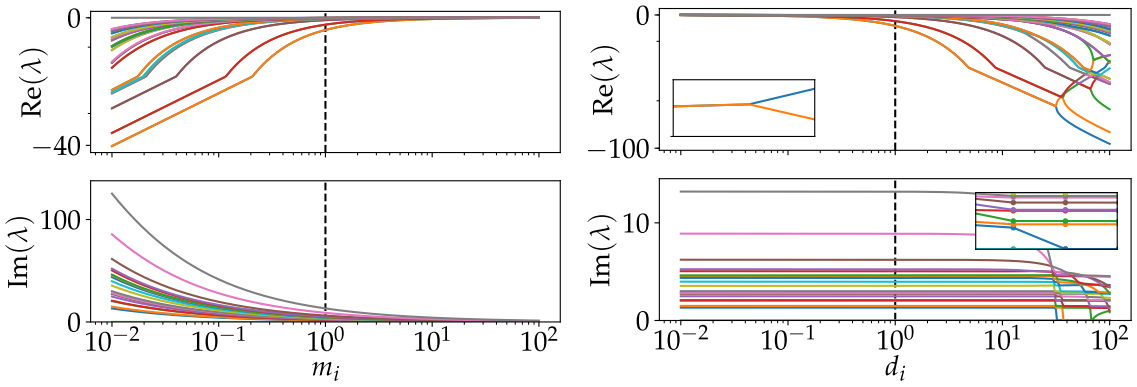

(A) Inertia (B) Damping

FIGURE 4.5: Bifurcations of the real and (positive) imaginary parts for constant change of inertia or damping coefficients. The literature value is indicated by the black vertical line.

The results are shown in fig. 4.5. We see relative regular behaviour when the inertia is changed. Decreasing the inertia increases the imaginary parts and results in larger negative real parts. Generally, the real parts correspond to the damping. When the inertia decreases, the damping is thus more influential. Increase of the imaginary parts is similar to the behaviour of a damped oscillator, where the natural frequency, which is the imaginary part of the eigenvalue, is inversely proportional to the mass of the oscillator. Thus, decreasing the inertia increases the imaginary parts. It should be noted that only the positive imaginary parts are shown, as all eigenvalues come in complex conjugate pairs. Changing the damping shows very different behaviour on both sides. Decreasing the damping results in real parts

which converge to zero. The imaginary parts are almost constant and correspond to the imaginary values of the undamped case. When the damping is increased, we see more complex behaviour for large damping. The real parts increase with damping, as expected. For very high values, we can observe bifurcations, as highlighted in the inserted zoom. At these bifurcations, the imaginary parts of one complex pair become zero and the real parts split up to two different real parts. This is the transition to overdamped behaviour. As discussed in the theoretical background, at under damped conditions we observe complex conjugate eigenvalue pairs. Under overdamped conditions, we observe only real eigenvalues with a gap between the highest and lowest eigenvalues. We observe this transition here, when the imaginary parts of a eigenvalue pair becomes zero but the real parts splits up.

It should be noted that the rate of parameter change is generally larger in the bifurcation diagrams for the inertia than for the damping. The imaginary parts are bounded to a narrow range when the damping is changed. Also, the negative real parts reach higher values for very low inertia than for high damping.

Randomly Perturbed Matrices

More insight in the influence of the matrices can be found with a simple Monte Carlo simulation. We calculate the spectra after slightly perturbing the relevant matrices. Comparing the resulting spectra can be used to answer two questions. First, how sensitive is the spectra to perturbations of a matrix. Secondly, are some modes more sensitive than other modes? The randomly perturbed matrices M_i are calculated with:

$$M_i = M \cdot \mathrm{diag}(\mathrm{uni}(0.5, 1.5))$$

Where $\mathrm{uni}(a, b)$ are uniformly distributed random numbers supported on the interval (a, b). The same procedure can be done to find perturbed damping matrices D_i. In both cases, 200 perturbed matrices were calculated and the results are shown in fig. 4.6. In fig. 4.6a, the inertia is randomly perturbed. We can observe a band of perturbed eigenvalues in grey around the original eigenvalues. For small eigenvalues, this band is relatively narrow and the eigenvalues will not divert far from the original value. For the highest ranked eigenvalues, this band grows much larger and the influence of M is much bigger on those eigenvalues.

Similarly, the spectra for perturbed damping matrices is shown in fig. 4.6b. This time, the eigenvalues are basically not changed by the matrix perturbations. Even

with a increased range of random value (the figure actually used random values uni$(0.1, 1.9)$), the damping almost does not influence the behaviour. This is similar to the observation from fig. 4.5, where small changes around the original value of D has very little influence.

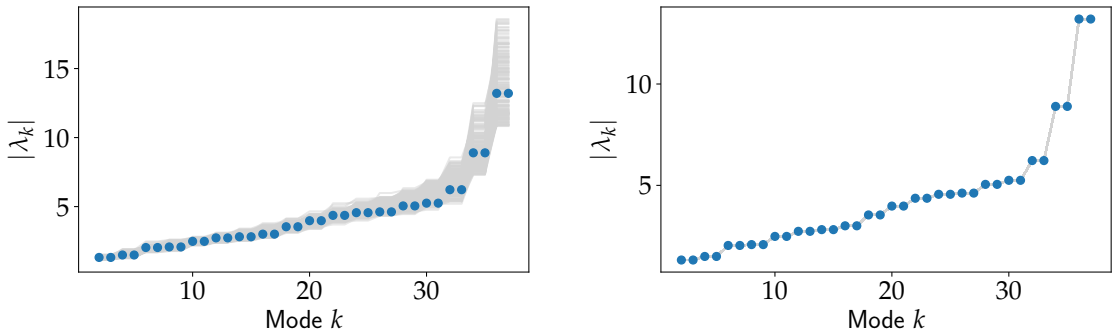

(A) Changing inertia

(B) Changing damping

FIGURE 4.6: Spectra of the IEEE 118 test case with randomly changed inertia M and damping parameter D.

We can also change the weights of the Laplacian matrix L as shown in fig. 4.7a. This calculation was done by randomly changing all weights of the underlying graph related to L and then creating a new Laplacian matrix L_i. This matrix has different weights than L, but similar mathematical properties, like symmetry and zero column sum. The behaviour observed here resembles that of the inertia M. High eigenvalues are sensitive to changes of the matrix, while lower ranked eigenvalues are almost constant. In general, the band around the Laplacian matrix is more tight than that around the inertia matrix.

To investigate the difference between changing D and M in more detail, the variance of the grey values from fig. 4.6 for each mode is shown in fig. 4.7b. Also, additional data where M and D are perturbed at the same time is included. As observed before, changing the inertia has a much larger influence on the spectrum. The variance differs by multiple orders of magnitude. We can also observe that the variance increases with higher ranked eigenvalues, for all cases.

In general, these results show multiple important features. The matrices M and L mostly influence the higher ranked eigenvalues. In the eigenvectors, we observed that these eigenvalues correspond to the more localised dynamics. When the eigenvalue only corresponds to a single node, changing a machine parameter like the inertia results in a large change of the dynamics at this mode. We can also observe again that the system seems less sensitive for changes in the damping parameter

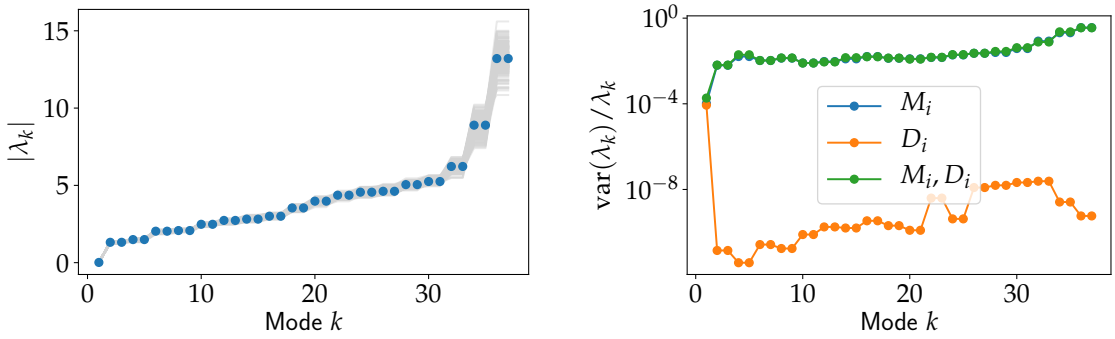

(A) Changing weights (B) Variance

FIGURE 4.7: Spectra of the IEEE 118 test case with randomly changed Laplacian L and relativle changes between M and D.

than the inertia and the coupling matrix. Still, the random perturbations observed here show that the spectrum seem relatively stable to small perturbations.

4.3.5 Pseudo Spectra

A powerful tool to investigate the sensitivity of the spectra of an eigenvalue problem are the the so called pseudo spectra. It allows to measure to global sensitivity of the eigenvalues depending on perturbations of the matrices. The pseudo spectra displays the region where eigenvalues will change after a relative perturbation of a certain strength [88]. While pseudo spectra are usually used for normal eigenvalue problems, they can be extended to quadratic eigenvalue problems. To do this, we calculate the scaled resolvent norm [95] $r(z)$ for a grid of complex numbers. The values of r are calculated as:

$$r(z) = \left(\left(|z|^2 \alpha_M + |z| \alpha_D + \alpha_L \right) \left\| \left(z^2 M + zD + L \right)^{-1} \right\| \right)^{-1}$$

Where the parameters α_i are defined as for the condition numbers in section 4.1.3. At each point z, the resolvent norm measures how strong perturbations of the original matrices of the QEP have to be to make z a solution of the perturbed problem. From the definition above, it is clear that the pseudo spectra are related to the condition numbers and can work together to explain the sensitivity of the system.

In fig. 4.8 the pseudo spectra for the IEEE 118 system are shown. In total, four spectra for the influence of different matrices are pictured. The colour indicates r on the grid of complex numbers while the crosses are the unperturbed eigenvalues.

We can observe a region with identical colour around each eigenvector. This region indicates the possible values for the eigenvalue, after matrix perturbation with the strength corresponding to the colour. Stronger perturbations can make the eigenvalues leave the area with equal colour and the necessary perturbation strength is also indicated by r.

At first in figs. 4.8a to 4.8c, the matrices M, D and L are perturbed individually and finally all matrices are perturbed together in fig. 4.8d. We can make the following observations about the perturbations of the various matrices:

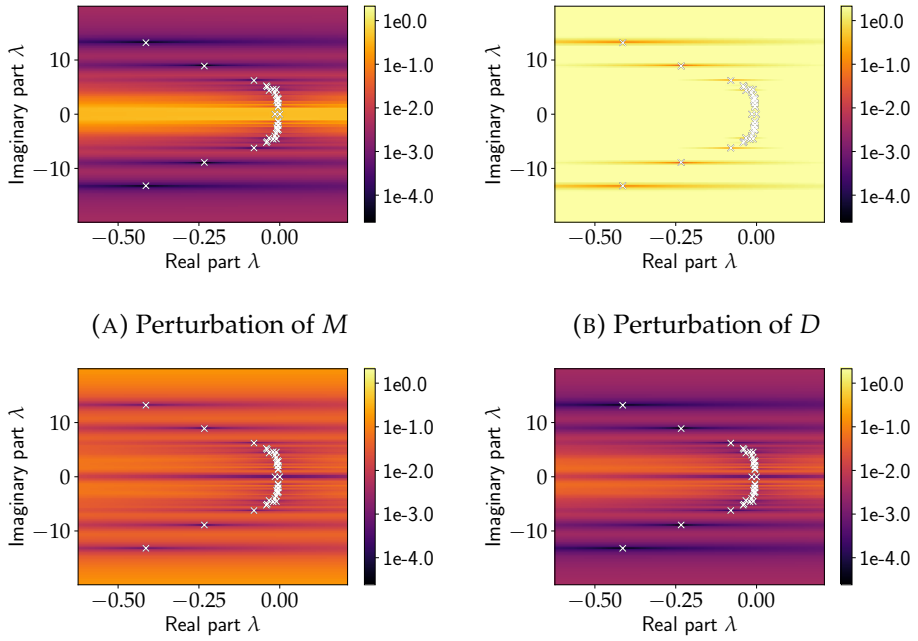

(A) Perturbation of M

(B) Perturbation of D

(C) Perturbation of L

(D) Perturbation of M, D, L

FIGURE 4.8: Pseudo spectra after perturbation of different matrices of the QEP. The crosses are the eigenvalues of the unperturbed system.

- Perturbing M: The spectrum is relatively sensitive to perturbations, especially in the real direction. The eigenvalues with a small imaginary parts are less sensitive, especially the eigenvalues with zero imaginary part.
- Perturbing D: The spectrum is less sensitive in general. Only the eigenvalues with large imaginary parts can be perturbed in the real direction. Also, perturbing the eigenvalues to positive real parts requires very strong perturbations.
- Perturbing L: Again, the system is easier perturbed in the real direction. One main difference is that the eigenvalues with zero imaginary parts are very sensitive, even to small changes. This is very different for perturbing the inertia or

the damping. The imaginary parts are also less sensitive as for perturbations of M.

- Perturbing all: The smallest perturbations of M dominate the pseudo spectra. The main difference are the zero imaginary eigenvalues, which resemble the perturbation of the Laplacian matrix.

Some of these observations are easily explained by the properties of the matrices M, D and L. The zero eigenvalues are a direct consequence of the Laplacian matrix. So, perturbing this matrix might influence these eigenvalues directly. If L is constant, these eigenvalues are basically independent of those matrices. This explains why the zero eigenvalues are very insensitive, especially when M is perturbed.

4.3.6 Condition Numbers

As explained in section 4.1.3, an important tool in the theoretical studies of eigenvalue sensitivity are the condition numbers. We investigate the influence of absolute and relative perturbations for each individual matrix M, D and L and the results are shown in fig. 4.9.

If absolute perturbations are considered, the system is most sensitive when the inertia M is perturbed, as seen in fig. 4.9a. Higher ranked modes are more sensitive than lower ranked modes in this case. In absolute perturbations, the Laplacian matrix is the least sensitive with damping in the middle. One exception is the zero eigenvalue, which is very sensitive to changes of the Laplacian matrix. As discussed in the pseudo spectra, this is a result of the zero eigenvalue being a direct result of the Laplacian matrix.

When relative perturbations are considered, the condition numbers are almost identical for M and L, except for the zero eigenvalue, as before. The eigenvalues are less sensitive to relative perturbations of the damping matrix.

4.3.7 Eigenvector Sensitivity

Calculating the sensitivity of the eigenvectors can be more complex. The different normalisation and the sheer amount of values to compare make a good investigation difficult. The best way, also used in many perturbation and sensitivity analysis studies, for example [96], are the complex angle between vectors. The larger the angle between two vectors is, the more different these vectors are. As before, we will use the absolute values of the eigenvectors to calculate the difference. For complex vectors, different methods to calculate angles exist [97]. Again, in this analysis, only

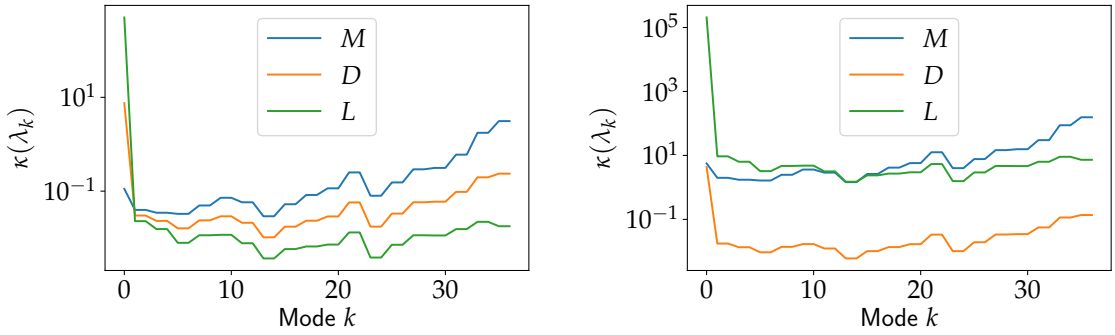

(A) Absolute perturbations (B) Relative perturbations

FIGURE 4.9: Conditioning numbers for the IEEE 118 test case. In each plot, the perturbations parameters are chosen so that one of the three matrices are perturbed. Absolute and relative perturbation strength are investigated.

the absolute value of the eigenvector matters, which is why we restrict our investigations to this case.

If the angle between the original and perturbed value is very small, the perturbation has almost no effect. The maximum angle of $\pi/2$ means that the vector is changed almost completely. Values in between mean that the vector is changed to some extend, but some structure of the original value can still be observed. Examples for all three behaviours are found in appendix B.1.2.

We can investigate the influence of the damping and the inertia on the eigenvector with a similar investigation as for the eigenvalues. We concentrate here on the method of using randomly perturbed matrices. As before, we solve the quadratic eigenvalue problem for 200 randomly perturbed matrices. Now, we compare the eigenvectors with the original eigenvectors. The results for randomly perturbed inertia and damping are shown in fig. 4.10.

For the inertia, we observe that except for the smallest mode, the angles are distributed over the whole range of possible values. Only for the smallest modes, we see a clustering of values around small angles. This means that even these small perturbations have a strong influence on the eigenvectors. On the other hand, the damping perturbations shown in fig. 4.10b have much less influence. For the first ten modes, the angles are almost zero, which means that both eigenvectors are the same. For higher modes, we see many eigenvectors still around zero, but some individual eigenvectors being perturbed. This can be explained by the localised nature of higher modes. Even if the damping has little influence on the eigenvectors, if the vector is relatively localised, the local changes of D might be able to influence the vector. As mentioned previously, we observe that the highly ranked modes have

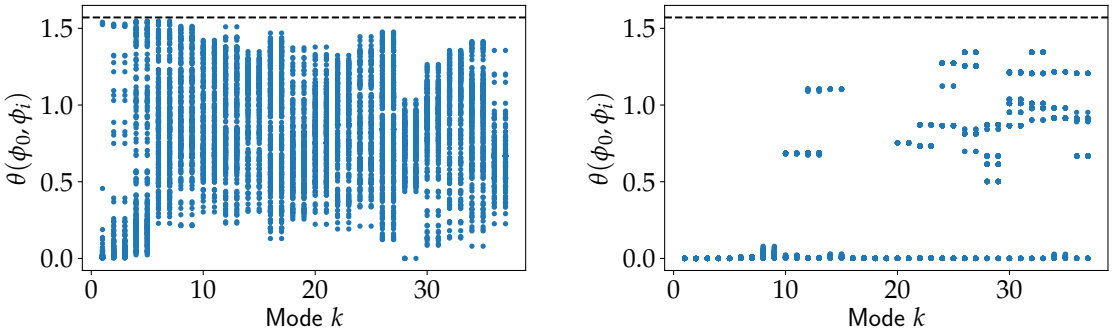

(A) Changing inertia

(B) Changing damping

FIGURE 4.10: Euclidean angles between the original eigenvectors $\boldsymbol{\phi}_0$ and perturbed eigenvector $\boldsymbol{\phi}_i$.

a more local, while the lower ranked modes a more global behaviour. The local change of parameters in M and D thus generally influence the eigenvectors, which determine the interactions, stronger at higher modes. This is exactly what is observed here. At low modes, the eigenvectors are often almost identical (sometimes pointing in the other way), while the higher ranked eigenvectors are changed completely.

4.3.8 Damped and Undamped Oscillations

As seen in the previous sections, the damping parameter is less influential than the inertia or the Laplacian matrix of the system. Also the bifurcation diagrams from section 4.3.4 show that especially for very low values of the damping parameters, the spectrum is almost constant. In this section, we want to explore the differences between the damped and the undamped system in more detail.

At first, fig. 4.11 shows the time series, calculated from eq. (4.4) of a damped and an undamped system. We highlight two nodes (this time nodes 0 and 1). We observe many similarities between the damped and undamped system. Especially the two highlighted nodes have very similar behaviour for both systems. We can observe that the oscillations decay slightly for the damped case. The frequencies of Node 1 and Node 2 are almost identical in the damped and undamped case.

The different eigenvalues are shown in fig. 4.12. At first, the absolute value of the eigenvalues are compared in fig. 4.12a. The absolute value of the eigenvalues are almost identical over all ranks. The difference can only be observed in fig. 4.12b, where it is clear that the damped eigenvalues have a small negative real part, while the undamped values are purely imaginary. The imaginary parts of the damped and undamped eigenvalues are almost identical.

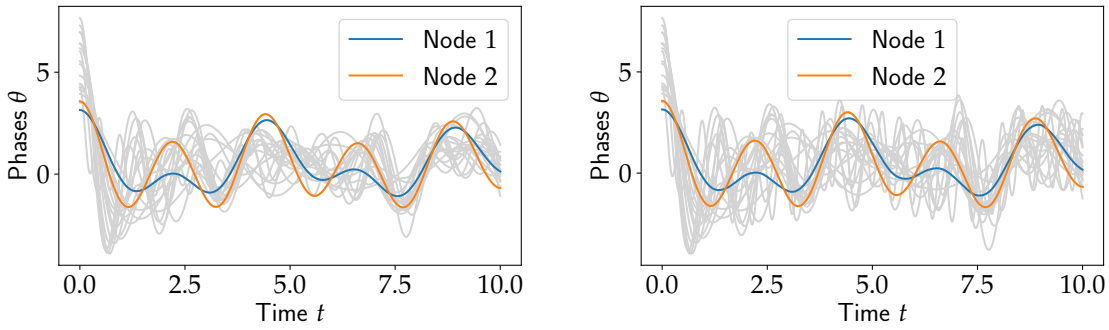

(A) Damped (B) Undamped

FIGURE 4.11: Time series of the phases for the undamped and the damped system.

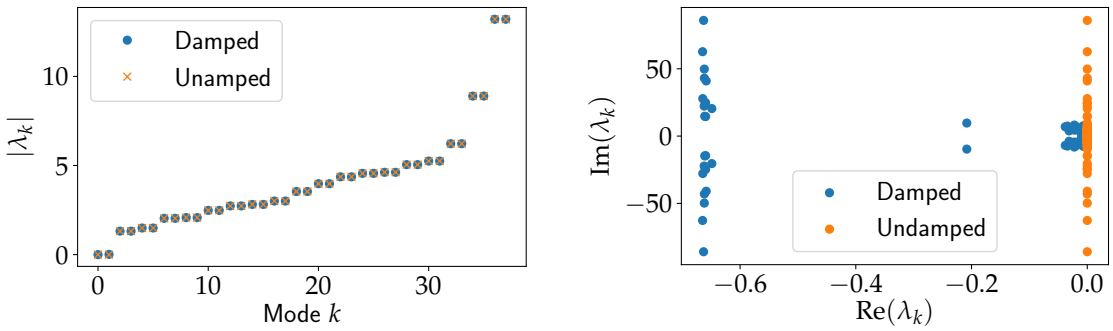

(A) Spectrum (B) Complex spectrum

FIGURE 4.12: Eigenvalues of the damped and undamped quadratic eigenvalue problem. Magnitude of the eigenvalues and real and imaginary parts are shown.

The eigenvectors, which are responsible for the similarities in the time series of the nodes 0 and 1 are shown in fig. 4.13. This time, the eigenvectors are sorted by the absolute value of the corresponding eigenvalues, similar to fig. 4.12a. There is no observable difference in the absolute parts of the eigenvectors, similar to the results for the absolute part of the spectrum. As before, the main difference is that the eigenvectors for the damped case are complex numbers, while they are purely real for the undamped system. Especially for the eigenvectors, we are mostly interested in the absolute value, as the complex phase only results in a phase shift of the oscillations, which are not as interesting as the frequencies and decay of the oscillations.

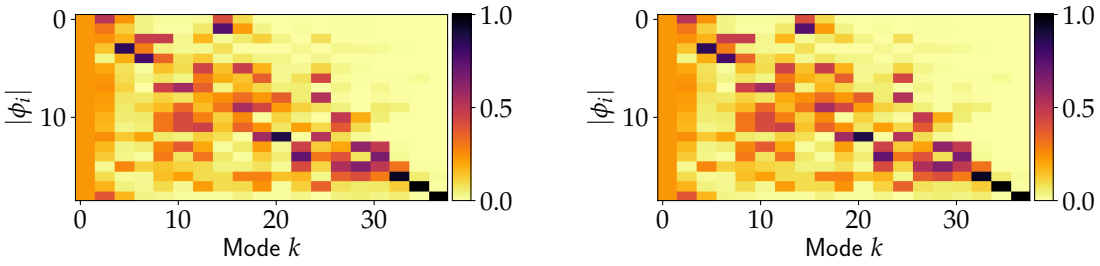

(A) Damped system (B) Undamped system

FIGURE 4.13: Magnitude of eigenvector components of the dynamical IEEE 118 test case with and without damping.

In this section, we have seen that the damped and undamped system of the IEEE 118 behave almost identical. The damping of the literature value is very low and the damping parameter has very little influence on the frequencies of the system.

As the influence of D is almost negligible, it seems plausible that it is sufficient to investigate the undamped system, as has been done in [63]. As discussed previously, the undamped case is much easier to investigate. In the next section, we therefore propose a method to use eigenvalue perturbation to assess the spectral properties of the damped system using the results from the undamped case.

4.4 Proposal - Perturbations of the Undamped System

As we have seen in the previous sections, the damping parameter is not very influential on the spectral properties of a dynamical power system. The system was always less sensitive to perturbations of D and the damped and the undamped systems often behaved very similarly.

The damping values observed in Literature are also far from over damped behaviour and it is reasonable to assume that the systems investigated here are only slightly damped.

Thus, we propose to extend the results of the undamped system, especially those which are found in [63] by introducing small perturbations on the zero damping value.

4.4.1 Small Damping Perturbation

In this section, we want to explore the possibility to use eigenvalue perturbation to relate the results of the undamped system, which is a generalised eigenvalue problem, to the damped, full quadratic eigenvalue problem. The unperturbed system is identical to eq. (4.10). The solutions of the unperturbed system λ_0 and $\boldsymbol{\phi}_0$ (as well as the left eigenvector $\boldsymbol{\psi}_0$) are supposed to be known. We then introduce a small damping $D = \partial D$, which leads to eq. (4.5). As L and M are positive semi definite, we know that λ_0 is purely imaginary. Introducing a damping results in a complex number with nonzero real part (similar to the damped oscillator in classical mechanics). While eigenvalue perturbation has been studied extensively [98], perturbation theory in the quadratic eigenvalue problem remains a more niche field in mathematics. The strongest results are usually found for the overdamped case [99]. The sensitivity of perturbations is for example investigated in [92], with extensions for higher order polynomial eigenvalue problems. The most complete treatment of perturbations in the quadratic eigenvalue problem known to the authors is probably given in [96]. This theory is not applicable to the problem described here, as the Laplacian matrix L is not invertible, which is required in the method presented in this publication. In general, no directly applicable eigenvalue perturbation methods for the problem here were found in literature. Mathematically, the following main problems for the eigenvalue perturbations are:

1. The Laplacian matrix L is singular.
2. The unperturbed matrix $D_0 = 0$ is singular as well.
3. If the unperturbed system is undamped, even small perturbations ∂D have a very large relative perturbation strength. This means that the assumption of linearity is less valid.

The first problem makes companion forms except the one described by eq. (4.8) hard to work with, as they become singular as well. The second problem means

that relative perturbation bounds cannot be used directly, as all perturbations are large compared to D_0. Keeping these problems in mind, we propose an eigenvalue perturbation method in the next section.

4.4.2 Companion Form Method

Here, we use the companion form as eq. (4.8). We can transform the generalised eigenvalue problem in a simple eigenvalue problem by inverting the matrix Y. As M is a diagonal matrix, the inverse of Y is just another diagonal matrix with the inverse diagonal entries. Using the rules of block matrix multiplication then leads to the following eigenvalue problem:

$$C\boldsymbol{\phi} =: \left(Y^{-1}X\right)\boldsymbol{\phi} = \begin{pmatrix} 0_n & \mathrm{I}_n \\ -M^{-1}L & -M^{-1}D \end{pmatrix}\boldsymbol{\phi} = \lambda\boldsymbol{\phi} \tag{4.13}$$

The perturbation in C can be expressed by the unperturbed matrix C_0 and ∂C. Those matrices are defined, using eq. (4.13), as:

$$C_0 = \begin{pmatrix} 0_n & \mathrm{I}_n \\ -M^{-1}L & 0_n \end{pmatrix} \quad \text{and} \quad \partial C = \begin{pmatrix} 0_n & 0_n \\ 0_n & M^{-1}\partial D \end{pmatrix} \tag{4.14}$$

Obviously, C_0 has the same eigenvalues λ_0 and (left and right) eigenvectors $\boldsymbol{\phi}_0$ and $\boldsymbol{\psi}_0$ as the unperturbed system eq. (4.8), while C has the eigenvalues of the quadratic eigenvalue problem eq. (4.5). As C is an analytical matrix function of ∂D, we can use the eigenvalue perturbation methods presented in [100, Theorem 1]. For eigenvectors which are normalised so that $\boldsymbol{\psi}_0^*\boldsymbol{\phi}_0 = 1$ and small perturbations ∂C, the perturbed eigenvalues $\tilde{\lambda}$ are given as:

$$\tilde{\lambda} = \lambda_0 + \boldsymbol{\psi}_0^*\partial C\boldsymbol{\phi}_0 + \mathcal{O}(\|\partial C\|_2^2) \tag{4.15}$$

This eigenvalue perturbation is identical to the results presented in [69, pp. 15–2]. As M and ∂D are diagonal matrices, ∂C is just a diagonal matrix and all non-zero entries are the generators damping divided by the inertia. The magnitude of the error of eq. (4.15) can be estimated in this simple case, using $\|\partial C\|_2^2 = \max(\frac{\partial D_i}{M_i})^2$.

Validation of Eigenvalue Perturbation

We want to test the accuracy of this perturbation approach on a simple system. The inertia M, damping D and Laplacian L are given in eq. (4.16):

$$L = \begin{pmatrix} 1 & 0 & 0 & -1 & 0 \\ 0 & 3 & -1 & -1 & -1 \\ 0 & -1 & 2 & 0 & -1 \\ -1 & -1 & 0 & 2 & 0 \\ 0 & -1 & -1 & 0 & 2 \end{pmatrix}$$
$$M = \begin{pmatrix} 2 & & & & \\ & 3 & & & \\ & & 1 & & \\ & & & 2 & \\ & & & & 4 \end{pmatrix} \quad D = 0.1 \cdot \begin{pmatrix} 4 & & & & \\ & 5 & & & \\ & & 3 & & \\ & & & 1 & \\ & & & & 2 \end{pmatrix} \tag{4.16}$$

The solutions for the unperturbed system, the solution of the QEP and the perturbed eigenvalues are shown in table 4.1. We can see that the perturbation mostly changes the real part of the eigenvalues and the imaginary part is almost identical. The real parts of the perturbed eigenvalues are very close to the true solutions, except for the dissipation mode. As the real parts of the undamped systems are zero, we see that the perturbation approach is good in predicting the real part of the damped system.

λ_0	$0 + \imath 1.533$	$0 + \imath 1.225$	$0 + \imath 0.959$	$0 + \imath 0.481$	$0 + \imath 0$
λ	$-0.134 + \imath 1.524$	$-0.055 + \imath 1.222$	$-0.062 + \imath 0.954$	$-0.069 + \imath 0.477$	$-0.126 + \imath 0$
$\tilde{\lambda}$	$-0.134 + \imath 1.533$	$-0.055 + \imath 1.225$	$-0.063 + \imath 0.959$	$-0.069 + \imath 0.481$	$-0.062 + \imath 0$

TABLE 4.1: Eigenvalues of the example system eq. (4.16), calculated with eq. (4.15). Only the positive imaginary parts are shown and the zero eigenvalue is omitted.

For illustration, we also show the perturbed eigenvalues and the damped eigenvalues in fig. 4.14a. Now, we want to investigate how the damping matrix influences the perturbation error. We do predict that the error increases with increasing damping. To investigate this behaviour, we calculate the distance of the perturbed solution with the real solution for different values of d_i, which is the scalar factor applied to the damping matrix in eq. (4.16). The original choice was $d_i = 0.1$. We can investigate the difference in the real part, the imaginary part or the magnitude of the complex number and the results are shown in fig. 4.14b. The error in the

real part dominates the error of the perturbation, as it is more than two magnitudes larger than the error in the imaginary part. We can also observe that for large damping values, the error in the imaginary part flattens out and is not dependent on d_i anymore. This appears to be around the case of overdamped behaviour, when the imaginary parts of the full solutions become zero and not change with d_i anymore. For very small damping values, the levelling out of the error for the imaginary part is probably due to numerical accuracy. Apart from that, we see that this method is able to predict the eigenvalues of a small damped system with decent accuracy.

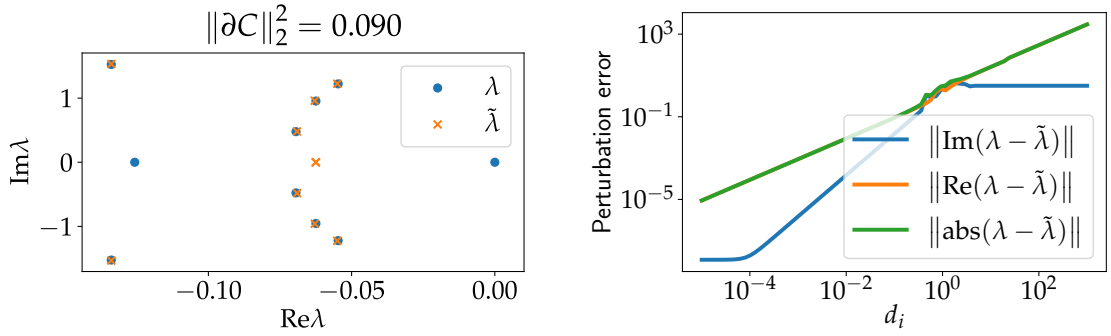

(A) Eigenvalues (B) Perturbation error

FIGURE 4.14: Eigenvalues and perturbed solutions of system eq. (4.16) and perturbation error depending on the damping coefficient.

4.4.3 Eigenvector Perturbations

Calculating eigenvector perturbations can be more complicated. Eigenvectors can be very sensitive, so even small changes in the matrices can have a large impact. Also, the choice of normalisation of the eigenvectors can influence how to calculate the eigenvector perturbations. A method to calculate first order perturbations is found in [100, Theorem 2]. This method depends on the so called *group-inverse* (or reduced resolvent) of the matrix C for the unperturbed eigenvalue λ_0. The group inverse is defined in [101] to be the only matrix S for any matrix K which solves:

$$KS = SK \quad \text{and} \quad SKS = S \quad \text{and} \quad KSK = K \tag{4.17}$$

Here, we search S which solves eq. (4.17) for $K = C_0 - \lambda_0 \mathrm{I}_n$. A algorithm to find a solution is given in [100]. For each eigenvector perturbation, this matrix has to be calculated with the corresponding unperturbed eigenvalue λ_0. The perturbations for the left and right eigenvalues $\tilde{\boldsymbol{\phi}}$ and $\tilde{\boldsymbol{\psi}}$, respectively, are then calculated as:

$$\tilde{\boldsymbol{\phi}} = \boldsymbol{\phi}_0 - S\left(\partial C \boldsymbol{\phi}_0\right) \tag{4.18}$$

$$\tilde{\boldsymbol{\psi}}^* = \boldsymbol{\psi}_0^* - \boldsymbol{\psi}_0^*\left(\partial C S\right) \tag{4.19}$$

The perturbed eigenvectors can be normalised together with $\tilde{\boldsymbol{\psi}}^* \tilde{\boldsymbol{\phi}} = 1$. Applying this theory to calculate perturbations of weakly damped oscillators showed that the perturbation error is much larger than for the eigenvalues. The eigenvector components of all nodes and all modes for the example system are shown in fig. 4.15. In this figure, all eigenvectors components for each mode are shown. The index l first counts the eigenvector components for $k = 0$, then for $k = 1$ and so on. The perturbed eigenvector is only sometimes closer to the *real* solution than the unperturbed solution. This shows that the eigenvector perturbation is not directly successful. Other perturbation methods were tested (for example, based on [102]). None of the methods resulted in better perturbation results. Eigenvector perturbation from the undamped to the damped system might not be directly possible, but further investigations are needed.

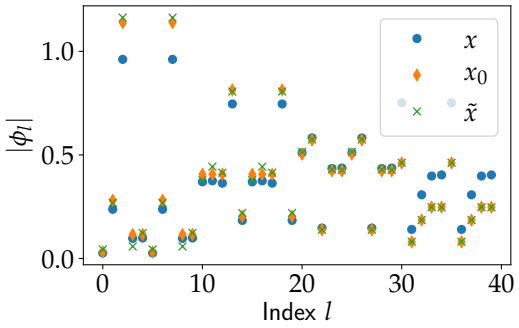

FIGURE 4.15: Absolute part of damped, undamped and perturbed eigenvector components for all modes and nodes from the example system described in eq. (4.16).

4.5 Conclusions

In this section, the spectral properties of a dynamical power model were investigated. The linearized equations result in a quadratic eigenvalue problem, which features many unique properties which explain the dynamical properties of the system. This quadratic eigenvalue problem was introduced and the most important properties were explained. Numerical analysis for the IEEE 118 test case was then

carried out. We investigated the sensitivity of the eigenvalues and eigenvectors of the system. The main results were:

1. The inertia and the Laplacian matrix greatly influence the spectral properties of the system. The damping parameter has a much lesser impact on the dynamical properties. In fact, the undamped and the damped system behave very similar.

2. The higher ranked eigenvalues and eigenvectors are more sensitive to perturbations of the machine parameters, especially of M. The zero eigenvalues of the QEP are directly linked with the Laplacian matrix and those are very sensitive to perturbation of corresponding matrix.

The observation that the damping is less influential than the inertia has been previously reported by us [89] using the 50 generator 145 bus test system [94]. While the conclusion that the damping is less influential than the inertia is valid in both systems, the observed differences are smaller. One possibility is that with the parameters we found, the 50 generator test case is more damped than the IEEE 118 test case. For example, the system was much closer to overdamped behaviour. Similar results to the IEEE 118 test case have been found using the IEEE 300 test case [93]. A subset of the results presented here are shown for the IEEE 300 system in appendix B.1.1.

In the time response, we have identified some localised, very high frequency oscillations (plant mode oscillations). These oscillations are very sensitive to the systems parameter. Those oscillations have to be identified and sufficiently damped, to prevent a local collapse of the associated generator [84]. In the following chapter, we will investigate the problem of mode localisation from a theoretical point of view.

Lastly, we tried to use eigenvalue perturbations to relate the behaviour of the undamped to the damped system. While the eigenvalue perturbation worked well in the proposed method, perturbing the eigenvectors was much more difficult and did not lead to desirable results. We believe that the method to perturb the quadratic eigenvalue problem might be the best approach to successfully perturb the undamped system to the damped system, further investigations about the sensitivity and the shape of the group inverse K are necessary to conclude this method.

Chapter 5

Localisation of Modes

As we have seen in the previous chapters, one of the phenomena found in the spectral analysis of power systems is the localisation of modes. Here, the eigenvectors corresponding to a given frequency are zero in most nodes, but non zero (and thus relatively large) in the remaining nodes. This indicates a short range interaction at this frequency, in contrast to the often long range interactions found for example in nodal domains. For example, localised oscillations in fig. 4.2c dominates the behaviour of the relevant node. In a complex network, the interplay between short and long range interactions are complicated and important for the understanding, control and design of the system. Localised modes are directly linked to those short range interaction and have to be considered for applications in the system.

This chapter gives a comprehensive investigation of localisation of Laplacian eigenvectors of a network. At first, two simple examples for systems with localisation are given and investigated analytically. We then proceed to give the formal definitions and explanations of localisation. In the second section, two eigenvector bounds are derived which are able to help in predicting and explaining localisation. In the third section, these bounds are tested numerically on the example systems from before and more extensively on a power system test case..

5.1 Background, Definitions and Simple Examples

In the remainder of the chapter, we are interested in the eigenvectors $\boldsymbol{\phi}$, corresponding to the eigenvalues λ of a Laplacian matrix L, as defined in eq. (2.5).

To illustrate the existence and properties of localisation, two simple examples are investigated. Both examples can be seen as building blocks of a real network. A larger, realistic graph, especially in power system applications, might include one or both of these parts and features some of the localisation properties. The investigated graphs are drawn in fig. 5.1, where the orange nodes correspond to the nodes of interest, where localisation appears.

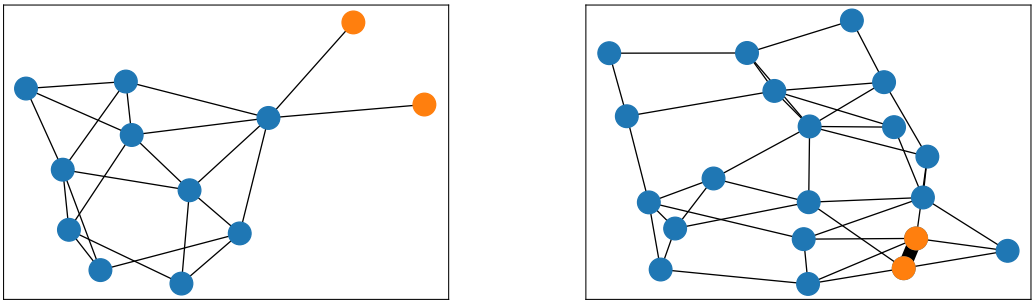

(A) Fork (B) High impedance line

FIGURE 5.1: Examples for the two motives which exhibit localisation. The important nodes are highlighted in orange.

5.1.1 Fork

This section investigates the fork, shown in fig. 5.1a as an unweighted graph. A more general investigation is found in [103], where it was shown that the same results are valid for the weighted graph, as long as the branches of the fork have the same weight.

We assume that the orange nodes are labelled 1 and 2 and the connecting node number 3. The first two rows of the eigenvalue equation for a Laplacian matrix (as in eq. (2.5)) are:

$$(1-\lambda)\,\boldsymbol{\phi}_1 - \boldsymbol{\phi}_3 = 0$$
$$(1-\lambda)\,\boldsymbol{\phi}_2 - \boldsymbol{\phi}_3 = 0$$

From which directly follows that either $\boldsymbol{\phi}_1 = \boldsymbol{\phi}_2$ or $\lambda = 1$ and $\boldsymbol{\phi}_3 = 0$. For $\lambda = 1$, we can now easily construct a valid solution to the eigenvalue problem. Letting all eigenvector components $\boldsymbol{\phi}_j$ for each $j > 3$ be zero solves all rows in the eigenvalue problem for $j > 3$, as the nodes 1 and 2 are not connected to any of the nodes. Then, the third row of the eigenvalue problem is:

$$-\boldsymbol{\phi}_1 - \boldsymbol{\phi}_2 + \left(1 + \sum_{j>3}^{n} L_{3,j}\right)\boldsymbol{\phi}_3 - \sum_{j>3}^{n} L_{3,j}\boldsymbol{\phi}_j = \lambda\boldsymbol{\phi}_3$$

As all $\boldsymbol{\phi}_j$ for $j \geq 3$ are zero, it follows that $\boldsymbol{\phi}_1 = -\boldsymbol{\phi}_2$. So, the eigenvalue problem of the fork graph has a solution where the mode is totally localised in the fork,

at the eigenvalue 1. For all other eigenvalues, we also know that the eigenvector components of the fork are identical to each other.

5.1.2 High Impedance Line

Another simple example for localisation is a high impedance line, as shown in fig. 5.1b. Here, we consider a weighted graph with all but one edge weights set to a very low value of order $\mathcal{O}(\epsilon)$. The remaining line (called the high impedance line) has an edge weight of order $\mathcal{O}(1)$. Calculating the eigenvectors of the resulting Laplacian matrix, we observe localisation around the high impedance line for the largest eigenvalue. For all lower modes, the eigenvector components around this line will be (almost) identical. We can mathematically show this behaviour using the analytical results for coherency described in section 2.2.4 and some simple calculations:

1. The high impedance line can be seen as a single, strongly connected cluster. All other edges are the connecting edges of lower order. From this follows that the system has a single eigenvalue of order $\mathcal{O}(1)$, while all other eigenvalues are of order $\mathcal{O}(\epsilon)$.

2. For all eigenvalues of order $\mathcal{O}(\epsilon)$, coherency is observed around the high impedance line.

3. To show localisation in the largest eigenvalue, some calculations are necessary. We define the largest eigenvalue of order $\mathcal{O}(1)$ as λ_s. May the high impedance line be located between the nodes i and j with a edge weight of b, while the link strength between the remaining nodes is called a_{lm}. Consider a node m which is not connected to the high impedance line, so $m \neq i, j$:

$$\sum_{l=1}^{n} a_{lm} \boldsymbol{\phi}_l = \lambda_s \boldsymbol{\phi}_m$$

   As no eigenvector component can be larger than $\mathcal{O}(1)$ (due to the normalisation of the eigenvector) and all edge weights a_{lm} are of order $\mathcal{O}(\epsilon)$, the left hand side is of order $\mathcal{O}(\epsilon)$. As λ_s is of order $\mathcal{O}(1)$, $\boldsymbol{\phi}_m$ must be of order $\mathcal{O}(\epsilon)$ for all $m \neq i, j$.

4. Now, calculate the sum of the i-th and j-th row of the eigenvalue problem, which correspond to the nodes around the high impedance line. When we calculate the rows, we observe that the terms with the factor b cancel each

other out. The sum of these rows is then given as:

$$\underbrace{\sum_{l\neq i}^{n} a_{il}\boldsymbol{\phi}_l + \sum_{l\neq j}^{n} a_{jl}\boldsymbol{\phi}_l}_{\mathcal{O}(\epsilon)} = \lambda_s\left(\boldsymbol{\phi}_i + \boldsymbol{\phi}_j\right)$$

From which follows that $\boldsymbol{\phi}_i \approx -\boldsymbol{\phi}_j$. As all eigenvector components outside of i, j are of order ϵ, the normalisation requires the eigenvector components around the impedance line to be of order $\mathcal{O}(1)$.

Together, this shows that we can expect localisation in a graph around a high impedance line. This is also compatible to the results found in [104], as a graph with a single high impedance line will have a large (weighted) degree heterogeneity.

Case	$\max \mathcal{E}$	$\min \mathcal{E}$	$\text{mean}(\mathcal{E})$
IEEE 30	384.6	16.0	82.8
IEEE 118	247.0	2.4	19.8
IEEE 300	2156.2	0.2	50.1
Poland test case	10000.0	2.2	607.6

TABLE 5.1: Largest, smallest and average connection weight in different IEEE test systems.

To see that this situation is actually realistic in a power system setting, table 5.1 shows the largest, smallest and average edge weight for IEEE test systems. In the larger systems, the largest edge weight are more than a magnitude larger than the smallest edge weights. So, in a system with a line which has a very large edge weight, localisation should appear in the highest modes around this line. For example, the line with the largest edge weight in the IEEE 118 test case corresponds to the localised flow in mode 117 observed in fig. 3.9.

5.1.3 Exact Localisation

To investigate localisation in a more general way, we partition the graph into the subgraph $\mathcal{S}$, the boundary $\partial\mathcal{S}$ around $\mathcal{S}$ and the complement $\overline{S}$. We can then partition the eigenvalue problem eq. (5.1) as:

$$L\boldsymbol{\phi} = \begin{pmatrix} L_{\overline{\mathcal{S}}} & L_{\overline{\mathcal{S}}\partial\mathcal{S}} & L_{\overline{\mathcal{S}}\mathcal{S}} \\ L_{\partial\mathcal{S}V} & L_{\partial\mathcal{S}} & L_{\partial\mathcal{S}\mathcal{S}} \\ L_{\mathcal{S}\overline{\mathcal{S}}} & L_{\mathcal{S}\partial\mathcal{S}} & L_{\mathcal{S}} \end{pmatrix} \begin{pmatrix} \boldsymbol{\phi}_{\overline{\mathcal{S}}} \\ \boldsymbol{\phi}_{\partial\mathcal{S}} \\ \boldsymbol{\phi}_{\mathcal{S}} \end{pmatrix} = \lambda \begin{pmatrix} \boldsymbol{\phi}_{\overline{\mathcal{S}}} \\ \boldsymbol{\phi}_{\partial\mathcal{S}} \\ \boldsymbol{\phi}_{\mathcal{S}} \end{pmatrix} = \lambda\boldsymbol{\phi} \tag{5.1}$$

Of certain interest are the so called *Dirichlet eigenvectors* of L on $\mathcal{S}$. Dirichlet vectors are all vectors which are zero for all indices of $\overline{\mathcal{S}}$. If and only if these vectors are eigenvectors of the submatrix $L_{\mathcal{S}}$, they are called Dirichlet eigenvectors [66, 62]. Dirichlet vectors can be eigenvectors of L, but not all of them are [62, Example 4].

Exact localisation to $\mathcal{S}$ means that the corresponding eigenvector $\boldsymbol{\phi}$ of L is exactly zero on all nodes $\overline{\mathcal{S}}$ (to simplify notation, we set $\partial\mathcal{S} = \varnothing$ here). Obviously, this means that $\boldsymbol{\phi}$ is a Dirichlet eigenvector of $\mathcal{S}$ and an eigenvector of L. For a Dirichlet eigenvalue, we know that the components belonging to $\mathcal{S}$ of $L\boldsymbol{\phi}$ are given as [62, Lemma I.4]:

$$(L\boldsymbol{\phi})_{\mathcal{S}} = L_{\mathcal{S}}\boldsymbol{\phi}_{\mathcal{S}}$$

To examine exact localisation, we can use eq. (5.1) for $\boldsymbol{\phi}_{\overline{\mathcal{S}}} = 0$, which leads to:

$$\begin{aligned} L_{\overline{\mathcal{S}}\mathcal{S}}\boldsymbol{\phi}_{\mathcal{S}} &= 0 \\ L_{\mathcal{S}}\boldsymbol{\phi}_{\mathcal{S}} &= \lambda\boldsymbol{\phi}_{\mathcal{S}} \end{aligned}$$

For every subgraph $\mathcal{S}$, we know that $L_{\mathcal{S}}$ is an invertible matrix [63, Theorem 3.16]. Combining the two equations for a nonzero eigenvalue yields:

$$L_{\overline{\mathcal{S}}\mathcal{S}}L_{\mathcal{S}}^{-1}\boldsymbol{\phi}_{\mathcal{S}} = 0 \tag{5.2}$$

So, all exact localised eigenvectors lie in the null space of $L_{\overline{\mathcal{S}}\mathcal{S}}L_{\mathcal{S}}^{-1}$. This is a necessary condition: all exact localised eigenvalues are part of the null space of $L_{\overline{\mathcal{S}}\mathcal{S}}L_{\mathcal{S}}^{-1}$, but not all vectors of this null space are necessarily eigenvectors of L. Showing that $L_{\overline{\mathcal{S}}\mathcal{S}}L_{\mathcal{S}}^{-1}$ has an empty null space thus proves that no exact localisation for the vector $\boldsymbol{\phi}_{\mathcal{S}}$ exists. For example, from the graph shown in fig. 5.1a (the corresponding Laplacian matrix is shown in eq. (B.1) in the appendix), using the nodes of the fork to span the subgraph $\mathcal{S}$, we find that:

$$L_{\overline{\mathcal{S}}\mathcal{S}}L_{\mathcal{S}}^{-1} = \begin{pmatrix} -1 & 0 & 0 & 0 & 0 & 0 & 0 & 0 & 0 & 0 \\ -1 & 0 & 0 & 0 & 0 & 0 & 0 & 0 & 0 & 0 \end{pmatrix}^T$$

Calculating the null space shows that the non zero vector $\boldsymbol{\phi}_{\mathcal{S}} = (-1, 1)^T$ is a solution to eq. (5.2). This means that exact localisation can be observed in the subgraph, where both modes have eigenvector components with opposite signs, as we

have seen in the analytical investigation.

On the other hand, for the high impedance line graph shown in fig. 5.1b, using the nodes around the high impedance line as $\mathcal{S}$, we find the following (the data for L is again shown in the Appendix eq. (B.2)):

$$L_{\overline{\mathcal{S}}\mathcal{S}}L_{\mathcal{S}}^{-1} = \begin{pmatrix} -0.29 & 0 & 0 & -0.14 & 0 & 0 & 0 & 0 & 0 & 0 & 0 & -0.14 & 0 & 0 & 0 & 0 & -0.14 & -0.29 \\ -0.29 & 0 & 0 & -0.14 & 0 & 0 & 0 & 0 & 0 & 0 & 0 & -0.14 & 0 & 0 & 0 & 0 & -0.14 & -0.29 \end{pmatrix}^T$$

Which has an empty null space. Thus, this graph does not have exact localisation and the eigenvector components for $\mathcal{S}$ are only small. We consider this to be an example of *approximate localisation*, as discussed in the next section.

5.1.4 Approximate Localisation

Another possibility, which is observed in many real world graphs, is approximate localisation of a mode. We speak of approximate localisation if the eigenvector components not included in $\mathcal{S}$ are *small* in comparison with the values included in $\mathcal{S}$. For example, we search for a eigenvector $\boldsymbol{\phi}$ with:

$$\boldsymbol{\phi}_i = \begin{cases} \mathcal{O}(1) & \text{if} \quad i \in \mathcal{S} \\ \mathcal{O}(\epsilon) & \text{else} \end{cases}$$

From the previous examples, the fork shows exact localisation, while the high impedance line shows approximate localisation. Of course, exact localisation can be seen as a *subset* of approximate localisation. In the following sections, we mostly focus on approximate localisation, as this is what we mostly observed in real world graphs.

5.2 Localisation Bounds

In this section, we derive two eigenvector bounds which we can use to predict and explain localisation. The analysis is based on the investigations presented in [105], where localisation in vibrating systems was investigated. Vibrating systems are continuous and with boundary conditions (for example, Dirichlet boundary conditions were considered). In contrast, the graph theoretical analysis is discrete without any

boundary conditions. Arguably, the bounds presented here are structurally similar to those in [105], but the transfer to discrete systems in graphs is non trivial. The first bound consist of a *landscape* which the Laplacian matrix imposes on the eigenvectors. This landscape bounds the individual eigenvector components and can be used to predict the behaviour of individual nodes and to find clusters which might exhibit localisation. The second bound relates the eigenvalues of a subgraph with those of the main graph. The eigenvector norm on the subgraph will depend on the distance of the eigenvalues between graph and subgraph. This bound can be used to predict at which eigenvalue localisation occurs.

5.2.1 Localisation of Modes

The landscapes of a graph are a powerful tool to predict localisation in a graph. Mathematically, the landscapes bound the eigenvector components by the following theorem:

Theorem 1 *The eigenvector components $\boldsymbol{\phi}_i$ corresponding to the solution of eigenvalue problem of the Laplacian L (2.5) with the corresponding eigenvalue λ are bounded by the two landscapes h and l:*

$$\frac{|\boldsymbol{\phi}_i|}{|\boldsymbol{\phi}|_{max}} \leq \begin{cases} h_i \\ l_i \end{cases} \tag{5.3}$$

Where $|\boldsymbol{\phi}|_{max}$ is the largest component of $\boldsymbol{\phi}$. The landscapes are defined as:

$$h_i = \left|\frac{1}{\lambda}\right| \sum_{j=1}^{n} \left|L_{ij}\right| \tag{5.4}$$

$$l_i = |\lambda| \sum_{j=1}^{n} \left|L^{\dagger}_{ij}\right| \tag{5.5}$$

PROOF This proof starts with a special property of pseudo inverses of Laplacian matrices L, which was previously shown in eq. (2.8). To repeat, the product of a Laplacian L and its pseudo inverse $L^{\dagger}$ is given as:

$$LL^{\dagger} = L^{\dagger}L = \mathrm{I}_n - \frac{1}{n}\mathrm{J}_n$$

Where I_n is the $n \times n$ identity matrix, J_n the $n \times n$ matrix of all ones and n is the number of rows/columns of L. eq. (2.8) directly implies that $\boldsymbol{\phi} = LL^\dagger\boldsymbol{\phi} + \frac{1}{n}\mathrm{J}\boldsymbol{\phi}$. The i-th component of $\boldsymbol{\phi}$ is then given as:

$$|\boldsymbol{\phi}_i| = \left|\left(LL^\dagger\boldsymbol{\phi} + \frac{1}{n}\mathrm{J}_n\boldsymbol{\phi}\right)_i\right| = \left|\left(LL^\dagger\boldsymbol{\phi}\right)_i\right| = \left|\frac{1}{\lambda}\left(L\boldsymbol{\phi}\right)_i\right|$$

The second equality depends on the fact that $\mathrm{J}_n\boldsymbol{\phi}$ is zero for all eigenvectors of a Laplacian matrix. This can be easily shown by multiplying the eigenvalue problem eq. (2.5) with J_n and using that the Laplacian matrix has zero column and row sum. The second equality is shown in [65, Section 2.3.1] for the pseudo inverse of a Laplacian matrix. The i-th element of the matrix product $L\boldsymbol{\phi}$ is $\sum_{j=1}^{n} L_{ij}\boldsymbol{\phi}_j$, which leads to:

$$|\boldsymbol{\phi}_i| = \left|\frac{1}{\lambda}\sum_{j=1}^{n} L_{ij}\boldsymbol{\phi}_j\right| \leq \left|\frac{1}{\lambda}\right| \sum_{j=1}^{n} \left|L_{ij}\boldsymbol{\phi}_j\right| \leq \left|\frac{1}{\lambda}\right| \sum_{j=1}^{n} \left|L_{ij}\right| \left|\boldsymbol{\phi}_j\right| \leq \left|\frac{1}{\lambda}\right| \sum_{j=1}^{n} \left|L_{ij}\right| |\boldsymbol{\phi}|_{\max}$$

Which leads to the desired result of the landscape h_i:

$$\frac{|\boldsymbol{\phi}_i|}{|\boldsymbol{\phi}|_{\max}} \leq \left|\frac{1}{\lambda}\right| \sum_{j=1}^{n} \left|L_{ij}\right| =: h_i$$

The proof for the other landscape is analogous, by replacing $LL^\dagger$ with $L^\dagger L$ and repeating the same steps. For Laplacian matrices, we know that $\lambda \geq 0$, so we can drop the absolute value around the eigenvalue factor ($|\lambda| = \lambda$).

The landscapes are easy to calculate and only depend on the edge weights and the spectrum of the graph. Obviously, $\frac{|\boldsymbol{\phi}_i|}{|\boldsymbol{\phi}|_{\max}} \leq 1$. Because of this, both landscapes only bound the eigenvector components if they are smaller than one. If any of the landscapes is very low for many nodes, the mode will be localised in the remaining nodes. Obviously, the *strength* of the landscapes depends on λ. Landscape h is stronger at high eigenvalues, while landscape l is stronger at low eigenvalues (hence the names).

This behaviour of the landscapes indicate a possible phenomenon reported for localisation in random graphs previously, for example in [106]. It has been reported that localisation mostly appears for larger and smaller eigenvalues. For large or small λ, one of the landscapes is bounding the nodes stronger, which might explain

localisation at this mode inside the weaker bounded nodes. As the two landscapes and their dependency on the eigenvalue can get very complicated, we make the following corollary:

Corollary 1 *Consider the both landscapes h_i and l_i for the same eigenvalue λ from Theorem 1. The eigenvector components $\boldsymbol{\phi}_i$ are also bounded by the combined landscape $u_{i,\lambda}$:*

$$\frac{|\boldsymbol{\phi}_i|}{|\boldsymbol{\phi}|_{max}} \leq u_i$$

Where $u_{i,\lambda} = \min(h_i, l_i)$.

PROOF As both landscapes bound $\boldsymbol{\phi}_i$ individually and are true at the same time, we only need to consider the smaller bound, as the other one is more conservative. Thus, we can just replace both landscapes by the composite landscape made by the smaller one.

In the remainder, we will focus on the landscape $u_{i,\lambda}$. Of special interest are the two extreme cases for the largest and smallest eigenvalue. Those will be called the algebraic landscape u_a for the second smallest eigenvalue (or the algebraic connectivity) and the spectral landscape u_s for the largest eigenvalue (the spectral radius).

5.2.2 Localisation in Subgraphs

To accurately predict if and at which mode localisation appears in a given subgraph, we find a bound for the eigenvector components of a connected subgraph $\mathcal{S}$. This bound can be used to calculate or predict localisation, or the absence of localisation, for a connected subgraph of arbitrary size.

Theorem 2 *The components of an eigenvector $\boldsymbol{\phi}$ of the eigenvalue problem* (2.5) *belonging to a subgraph $\mathcal{S}$ are bounded by:*

$$\|\boldsymbol{\phi}\|_{\mathcal{S}} \leq \left(1 + \max_{\lambda_{\mathcal{S}}} \left|\frac{\lambda}{\lambda - \lambda_{\mathcal{S}}}\right|\right) \|\boldsymbol{v}\|_{\mathcal{S}} \tag{5.6}$$

Where $\lambda_{\mathcal{S}}$ are the eigenvalues of the Laplacian matrix restricted to the nodes of $\mathcal{S}$ and $\boldsymbol{v}_{\overline{\mathcal{S}}}$ is a vector which solves the Laplace equation on $\mathcal{S}$ and coincides with $\boldsymbol{\phi}$ on the boundary $\partial\mathcal{S}$.

PROOF For this proof, we need to define a vector $v_{\overline{\mathcal{S}}}$, which solves the Laplace equation on $\mathcal{S}$ and which coincides with the eigenvector $\boldsymbol{\phi}$ of the Laplacian matrix L outside of $\mathcal{S}$:

$$(Lv)_{\mathcal{S}} = 0 \quad \text{with} \quad v_{\overline{\mathcal{S}}\cup\partial\mathcal{S}} = \boldsymbol{\phi}_{\overline{\mathcal{S}}\cup\partial\mathcal{S}} \tag{5.7}$$

In [7], it was shown that a solution exists for all connected graphs and a construction for this vector is given. The exact solution is not necessary for the remainder of this proof, but the details necessary to calculate the vector are described in more detail in Appendix A.2. The main calculations are carried out by a supporting vector $\boldsymbol{w}$, which is defined as $\boldsymbol{w} = \boldsymbol{\phi} - \boldsymbol{v}$. With the definition of $\boldsymbol{v}$, this leads to:

$$\boldsymbol{w}_i = \begin{cases} \boldsymbol{\phi}_i - \boldsymbol{v}_i & \text{if} \quad i \in \mathcal{S} \\ 0 & \text{else} \end{cases}$$

This vector is used to calculate:

$$((L-\lambda)\,\boldsymbol{w})_{\mathcal{S}} = \underbrace{L_{\mathcal{S}\overline{\mathcal{S}}}\boldsymbol{w}_{\overline{\mathcal{S}}} + L_{\mathcal{S}\partial\mathcal{S}}\boldsymbol{w}_{\partial\mathcal{S}}}_{=0} + L_{\mathcal{S}}\boldsymbol{w}_{\mathcal{S}} - \lambda\boldsymbol{w}_{\mathcal{S}} = (L_{\mathcal{S}} - \lambda)\,\boldsymbol{w}_{\mathcal{S}}$$

As the submatrix $L_{\mathcal{S}}$ is symmetrical and real, we can find a basis of orthonormal eigenvectors [67, Chapter 7]. We denote the eigenvectors of $L_{\mathcal{S}}$ as $\boldsymbol{\phi}^{\mathcal{S}}$, with the eigenvalues $\lambda_{\mathcal{S}}$, as before. We can use this basis to express $\boldsymbol{w}_{\mathcal{S}}$ with the coefficients of the projection a_i onto the basis of $\boldsymbol{\phi}^{\mathcal{S}}$. Inserted in the previous equation, we find that:

$$\begin{aligned} ((L-\lambda)\,\boldsymbol{w})_{\mathcal{S}} &= (L_{\mathcal{S}} - \lambda)\,\boldsymbol{w}_{\mathcal{S}} = (L_{\mathcal{S}} - \lambda)\sum_{i=1}^{n} a_i \boldsymbol{\phi}_i^{\mathcal{S}} \\ &= \sum_{i=1}^{n} a_i \left(L_{\mathcal{S}}\boldsymbol{\phi}_i^{\mathcal{S}} - \lambda\boldsymbol{\phi}_i^{\mathcal{S}}\right) = \sum_{i=1}^{n} a_i \left(\lambda_{\mathcal{S},i} - \lambda\right)\boldsymbol{\phi}_i^{\mathcal{S}} \\ &\geq \min_{\lambda_{\mathcal{S}}} (\lambda_{\mathcal{S}} - \lambda) \sum_{i=1}^{n} a_i \boldsymbol{\phi}_i^{\mathcal{S}} = \min_{\lambda_{\mathcal{S}}} (\lambda_{\mathcal{S}} - \lambda)\,\boldsymbol{w}_{\mathcal{S}} \end{aligned}$$

The left hand side can also be simplified using the definition of the vector $\boldsymbol{v}$, resulting in:

$$((L-\lambda)\,\boldsymbol{w})_{\mathcal{S}} = \left(\underbrace{L\boldsymbol{\phi}-\lambda\boldsymbol{\phi}}_{=0} - Lv + \lambda v\right)_{\mathcal{S}} = -\underbrace{(Lv)_{\mathcal{S}}}_{=0} + \lambda v_{\mathcal{S}} = \lambda v_{\mathcal{S}}$$

Taking the norm over $\mathcal{S}$, we find that:

$$\|\boldsymbol{w}\|_{\mathcal{S}} \leq \max_{\lambda_{\mathcal{S}}} \left(\left|1-\frac{\lambda_{\mathcal{S}}}{\lambda}\right|^{-1}\right) \|\boldsymbol{\phi}\|_{\mathcal{S}} \tag{5.8}$$

With $\|\boldsymbol{w}\|_{\mathcal{S}} \leq \|\boldsymbol{\phi}\|_{\mathcal{S}} + \|v\|_{\mathcal{S}}$, we finally arrive at the desired condition:

$$\|\boldsymbol{\phi}\|_{\mathcal{S}} \leq \left(1+\max_{\lambda_{\mathcal{S}}}\left|\frac{\lambda}{\lambda-\lambda_{\mathcal{S}}}\right|\right) \|\boldsymbol{v}\|_{\mathcal{S}}$$

To simplify notation, we define the leading factor of eq. (5.6) as ξ:

$$\xi(\lambda_{\mathcal{S}}) := \left(1+\max_{\lambda_{\mathcal{S}}}\left|\frac{\lambda}{\lambda-\lambda_{\mathcal{S}}}\right|\right)$$

The advantage of this bound in comparison to the previous landscape approach is that this bound works with subgraphs, instead of single nodes. Often, localisation happens on a few connected nodes. This bound depends on the choice of the subgraph and can thus help to predict which subgraphs might be localised. Also, while the landscape can find candidates localisation, it cannot predict at which modes localisation appears. In contrast, this mode predicts that localisation appears at certain eigenvalues. To use the bound eq. (5.6), we need the vector $\boldsymbol{v}$ and the factor ξ. To calculate the vector $\boldsymbol{v}$, we need to know the solutions of the eigenvalue problem on the boundary $\partial\mathcal{S}$. This leads to some circular reasoning, as the bound of the eigenvector can only be calculated when the eigenvector is already known. In [105], which is the inspiration for this bound, the landscape was able to bound $\boldsymbol{v}$ to a very small value, when the subgraph $\mathcal{S}$ was chosen correctly. We will show that the bound also works when only ξ is considered because it is reasonable to assume that $\boldsymbol{v}$ is not very large, so that the leading factor can dominate the bound.

5.3 Empirical Studies of Landscape Properties

In this section we are going to investigate the properties of the two bounds derived in the last section. At first, both bounds are tested on the simple examples discussed in the introduction. As we already know that both systems show localisation, we can see whether the bounds are able to predict this behaviour and not. After this, we perform statistical analysis on the landscapes. We want to know which landscapes performs better and which modes can be investigated by the landscapes. Then, we propose a method to investigate localisation in a complex network using the two different landscapes. For all this analysis, we again focus on the IEEE 118 test system. As seen in the previous chapters, we can observe localisation in the IEEE 118 test system.

5.3.1 Simple Systems

We now focus on the two simple test systems from section 5.1. The localisation properties are already calculated in the previous section, so we can use those to benchmark the two new bounds.

Fork Graph

As seen before, the fork graph exhibits exact localisation for the eigenvalue $\lambda = 1$. Another observation is that the eigenvector components of the fork are very small for larger frequencies. Calculating the landscapes from section 5.2.1 shows that the landscapes indicate this behaviour, as seen in fig. 5.2. The spectral landscape u_s is very small at the fork and we predict small eigenvector components. On the other hand, the algebraic landscape is much larger at the fork, but smaller at all other nodes. This means that the landscapes would predict possible localisation for small eigenvalues at the fork, but small eigenvector components for larger modes.

Also, the localisation bound for subgraphs from section 5.2.2 can be used for the fork graph. The submatrix for the fork is given as:

$$L_{\mathcal{S}} = \begin{pmatrix} 1 & 0 \\ 0 & 1 \end{pmatrix}$$

Which obviously has the double eigenvalue 1. From the previous analysis, we also know that the matrix L also has the eigenvalue 1 and we observe exact localisation at this eigenvalue in $\mathcal{S}$. As $\lambda_{\mathcal{S}}$ in this case is perfectly identical to λ, ξ grows to

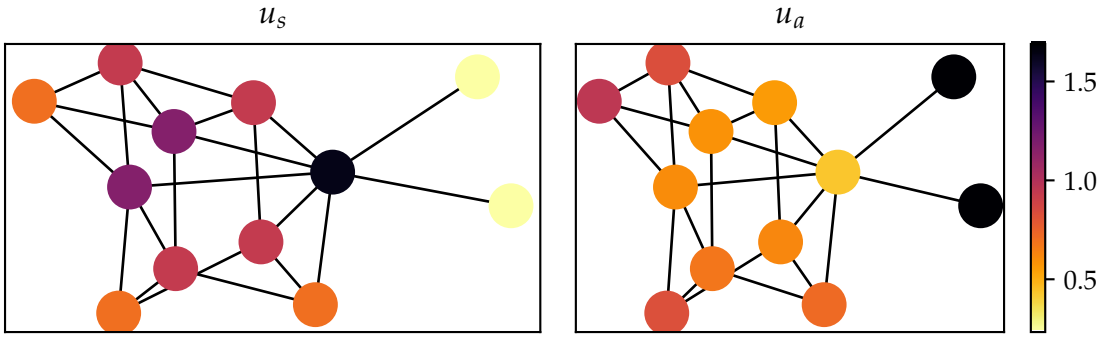

FIGURE 5.2: Landscapes u_s and u_a, calculated with the largest and smallest eigenvalue of L for the fork graph.

infinity, which means that the eigenvalues are totally unbounded on $\mathcal{S}$. For all other eigenvalues λ, the bound is smaller for $\mathcal{S}$. While this indicates possible localisation on the subgraph $\mathcal{S}$, it is important to mention that a large eigenvector bound is a necessary, but not sufficient condition to find the localised subgraph. For example, other subgraphs with the eigenvalue one (which then corresponds to an unbounded eigenvector) can be found. All of those subgraphs will include one or both of the fork nodes[1].

High Impedance Line

Doing the same calculations on the high impedance line graph, we see that the spectral landscape is completely dominated by the nodes around the line, see fig. 5.3. This corresponds to what was theoretically calculated and observed, that the nodes around the high impedance line are localised in the highest mode. For the algebraic, we do not observe anything specific around the high impedance line. The algebraic landscape used the pseudo inverse of the Laplacian, which *averages* out the impact of the high impedance line. As the eigenvector components at lower eigenvalues were not very small either way, the landscapes again work really well in predicting the behaviour of the eigenvectors.

Looking at the second bound, we can calculate that the largest eigenvalue of the matrix is close to two times the edge weight of the high impedance line. If this edge weight is set to 1, while all other edge weights are set to ϵ, the submatrix $L_{\mathcal{S}}$ for the subgraph $\mathcal{S}$ of the nodes around the high impedance line is given as:

[1] All these subgraphs are not connected and thus diagonal matrices. These matrices only have the one eigenvalue if the degree of at least one of the nodes is one, which is limited to the fork nodes.

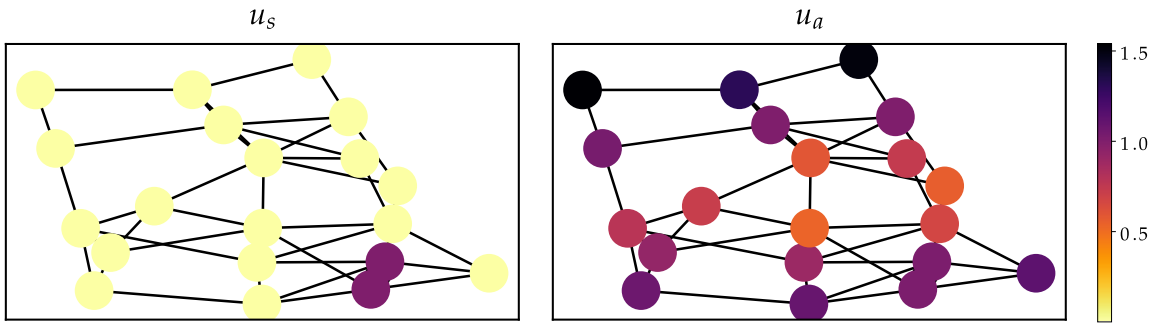

FIGURE 5.3: Landscapes u_s and u_a, calculated with the largest and smallest eigenvalue of L for the high impedance graph.

$$L_{\mathcal{S}} = \begin{pmatrix} 1+\epsilon & -1 \\ -1 & 1+\epsilon \end{pmatrix}$$

The eigenvalues of this matrix are $\epsilon, 2+\epsilon$. The second eigenvalue is very close to the spectral radius of the full matrix and thus ξ grows very large, which predicts the observed localisation. For any subgraph not consisting of the nodes around the high impedance line, Gershgorins circle theorem [67, Chapter 7] tells us that the eigenvalues can only be of order $1+\epsilon$, but is smaller than two. This means that for this mode, the subgraph bound will never be as large for subgraphs without the high impedance line.

5.3.2 Landscape Statistics of the IEEE 118 Test System

Now, we want to analyse the properties of the landscapes. We first investigate the general properties of the landscapes h and l as defined in theorem 1. Both landscapes bound, for each eigenvalue, the corresponding eigenvector component. All bounds depend on the mode λ. Depending on the eigenvalue, the bound u will consist more of l or h. Figure 5.4a shows at how many nodes l is smaller (and larger) than h for each mode. This indicates which bound is stronger at this eigenvalue. It is clear that h is generally smaller for larger eigenvalues, while the opposite is true for large eigenvalues. Obviously, if one landscape is smaller for all nodes at a given frequency, the combined landscape u is identical to that landscape. Especially, the spectral landscape is identical to h at the largest eigenvalue, while the algebraic landscape is identical to l at the algebraic connectivity.

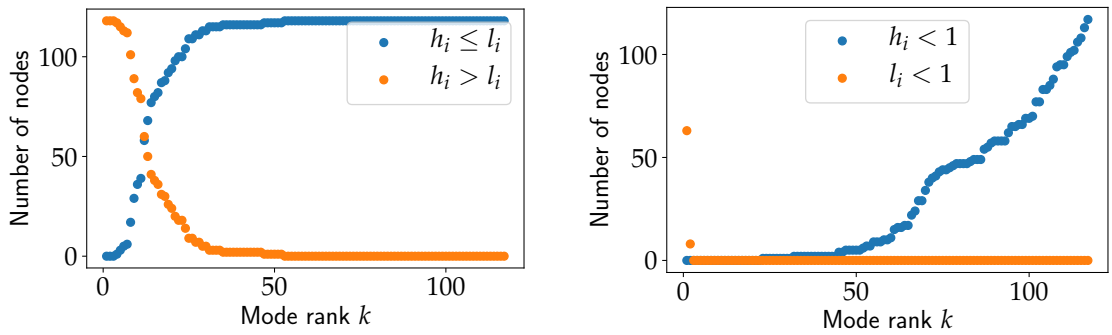

(A) Smaller landscapes (B) Landscapes smaller than one

FIGURE 5.4: Number of nodes where h or l is the smaller landscape and number of nodes where each landscape is smaller than one with respect to the eigenvalue.

The amount of nodes bounded for a given mode is shown in fig. 5.4b. Here, it is clear that l only bounds the first two modes, while h is effective for many higher modes, but with varying strength. For low modes, a region without any effective bounds exists, from mode three to about 50. For these frequencies, the bound is essentially useless for all nodes. The interesting cross section observed in fig. 5.4a completely lies in this region. It should be noted that the bound itself is too conservative in the intermediate area. While this bound cannot give any concrete information about the individual eigenvector component, we can see later that these values can still be used to partition the graphs, which help the analysis of localisation.

In section 5.3.2, the (sorted) values of the spectral and algebraic landscape are given. The difference between those landscapes is interesting. The spectral landscape increases very slowly, but suddenly rises strongly, while the other landscape shows a more gradual increase. It should be noted that u_s is identical to two times the weighted degree of each node[2] divided by the largest eigenvalue. The graph considered here has a large degree heterogeneity, which can be observed in the large increase of the spectral landscape values as well. In contrast, the algebraic landscape depends on the pseudo inverse of the Laplacian matrix. The more steady increase indicates a more *global* behaviour. The pseudo inverse does not just depend on the values of a single node, but also on connected nodes. This results in an effective smoothing of the heterogeneity and thus the heterogeneity of the landscape. The lowest values of the spectral landscape are much smaller the those of the algebraic landscape. This means that in general, u_s is a stronger bound than u_a. More than half of the nodes are bounded to a value less than 0.25 from the spectral radius.

[2]The weighted degree, introduced in section 2.1.5, is identical to the diagonal value of the Laplacian or the absolute value of the row sum of all non diagonal values.

The algebraic landscape is way more conservative and even the lowest eigenvector bounds are still around 0.4.

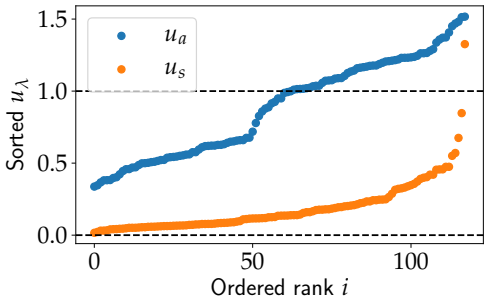

FIGURE 5.5: The sorted values of the spectral and algebraic landscapes of the IEEE 118 test case.

This statistical analysis will become helpful in the next section, where the landscapes are used to cluster the graph and find possible candidates for localisation.

5.4 Localisation Candidates

Having understood the statistical properties, we can now use the landscapes to find *candidates* for localisation. One way is to use the landscapes to remove nodes which are bounded strongly from the graph. The landscapes tells us that those nodes will not have a large eigenvector component and can thus not exhibit localisation. So, a threshold is chosen in the range of values of the corresponding landscape. All nodes which landscape value is lower than the threshold will be removed from the graph. The remaining nodes will then have a more conservative bound and we predict that localisation will mostly happen in these nodes. For a suitable large threshold, the remaining graph will not be connected anymore. The connected components (CCs) of this graph are candidate subgraphs for localisation. This method is applied to large eigenvalues first and for low eigenvalues later.

5.4.1 Node removal - High Frequencies

At first, the spectral landscape u_s is used. For the IEEE 118 test case, the statistical influence of removing nodes with a varying threshold is shown in in fig. 5.6. Figure 5.6a shows the number of connected components and the number of remaining nodes for each threshold. The number of connected components reach a maximum for a threshold of around 0.3. The number of remaining nodes is relatively small. To investigate the structure of the reduced graph, fig. 5.6b shows the number of nodes

of each connected component. For smaller thresholds, only some outer nodes are removed, but the main structure keeps intact. Just at a threshold of around 0.15, the *main* graph seems to break apart and multiple, intermediate sized subgraphs emerge.

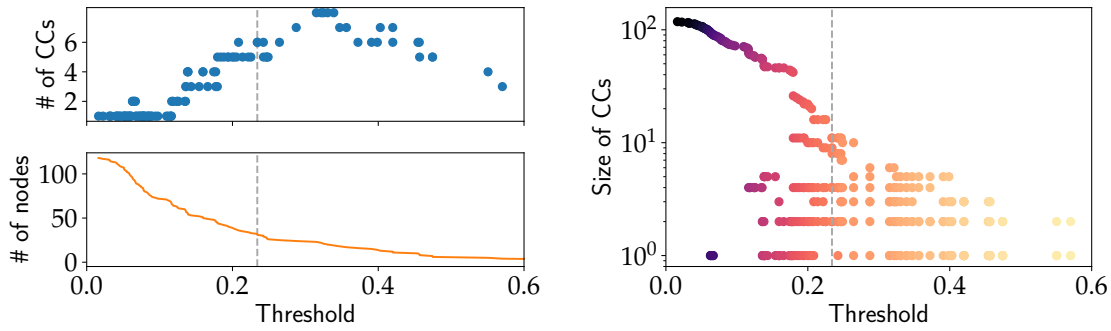

(A) Number of CC (B) Size of CC

FIGURE 5.6: Removal of nodes by the spectral landscape and a varying threshold in the IEEE 118 test system. The number of connected components (CC) the number of remaining nodes and the number of nodes in all connected components are shown. The landscape u_s is calculated for the largest eigenvalue of the Laplacian L.

As an example, fig. 5.7 shows the IEEE 118 system before and after removing nodes with a threshold of approximately 0.23. This threshold corresponds to the smallest threshold where the most connected components with at least two nodes are found (in total, six connected components are found). The vertical dotted lines in fig. 5.6 indicate this threshold. The node colour in fig. 5.7a shows the values of the spectral landscape at each node. The connected components of the reduced graph fig. 5.7b are the candidates for localisation.

The nodes corresponding to each connected components, the largest eigenvector components and the node rank of the largest eigenvector component is shown in table 5.2. We can see that every connected component, except $\mathcal{S}_2$, exhibits localisation at a high frequency. Some of these subgraphs exhibit localisation at multiple frequencies, as shown in fig. 5.8a. There, the largest eigenvector components of all subgraphs $\mathcal{S}_j$ from table 5.2 for all mode ranks between 105 and 117 (the spectral radius). All modes in this figure show localisation in at least one of the candidate subgraphs. If we zoom out of this picture, as in fig. 5.8b, we see that the connected components which do not exhibit localisation have landscape components very close to zero.

An interesting outlier is $\mathcal{S}_2$, where no localisation is observed. In fig. 5.8b, the eigenvector components corresponding to $\mathcal{S}_2$ is almost identical to zero everywhere.

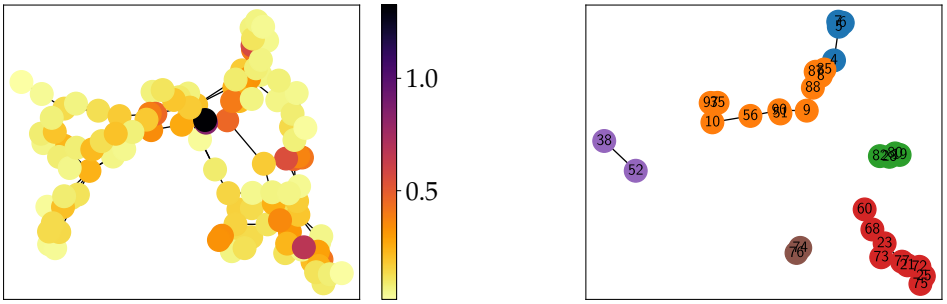

(A) Full graph (B) Reduced graph

FIGURE 5.7: Full graph of the IEEE 118 test system and graph after removing nodes by minimal landscape.

j	$\|\boldsymbol{\phi}\|_{\mathcal{S}_j,\max}$	$k(\|\boldsymbol{\phi}\|_{\mathcal{S}_j,\max})$	Node indices
$\mathcal{S}_1$	0.9977	116	1, 20, 21, 73, 75, 95, 101, 106, 111
$\mathcal{S}_2$	0.7486	100	3, 26
$\mathcal{S}_3$	0.9973	111	17, 22, 64, 69
$\mathcal{S}_4$	0.9988	114	29, 40, 41, 42
$\mathcal{S}_5$	0.9990	117	37, 39, 43, 50, 52, 80, 82, 85, 86, 113, 114
$\mathcal{S}_6$	0.9946	110	98, 99

TABLE 5.2: Connected components, maximum eigenvector components and corresponding mode rank k of IEEE 118 test case after removing nodes with the spectral landscape with a threshold of 0.23.

A slight increase in the threshold would remove both nodes, as they are two of the three nodes with the lowest landscape values.

Investigating the values of table 5.2, we can also make a direct connection with the flows over a line found in fig. 3.9. We see that the flows at mode 110 and mode 117 are almost only found in a single line. These lines are just the lines between the localised nodes from table 5.2. At mode 110, the most overloaded line is in fact the line connecting the nodes 98 and 99, while at mode 117, the largest flow is between nodes 113 and 114.

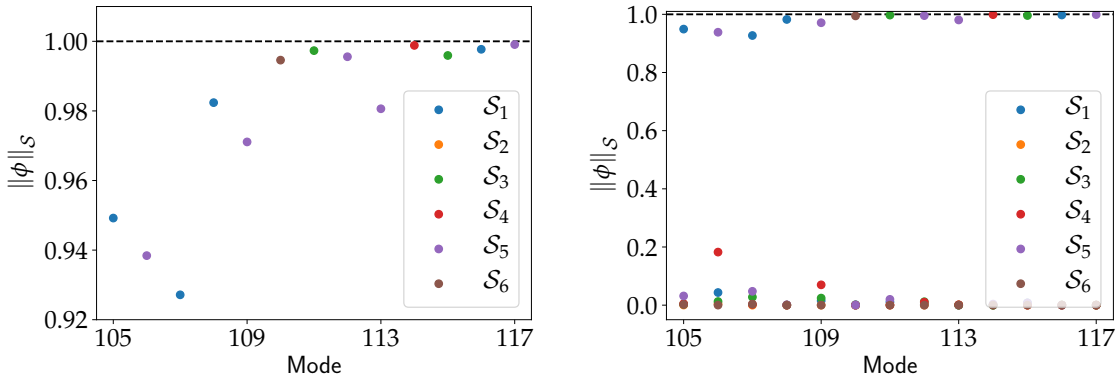

(A) Largest eigenvector components

(B) Full picture

FIGURE 5.8: Eigenvector components of largest eigenvalues of connected components found after removing nodes with small spectral landscape.

5.4.2 Node Removal - Low Frequencies

Now, we present a similar analysis as before, this time using the algebraic landscape. This landscape is calculated with the second smallest eigenvalue of the Laplacian matrix. As for the spectral landscape, we first look at the number of connected components and the size of those components for varying thresholds, shown in fig. 5.9. The behaviour here is very different from what was observed for the spectral landscape. From a threshold of about 0.4, which is indicated by the light blue line the graph splits in two large subgraphs. These subgraphs stay mostly constant until a threshold of about 1.0, when one subgraphs breaks up, as indicated by the grey line. It should be noted again that the thresholds here are generally larger than for the spectral landscapes, as was seen previously in section 5.3.2.

The graphs after removing nodes with four different thresholds are shown in fig. 5.10. Because of the more complicated shape of the number of connected components, multiple thresholds r are shown here. The first threshold is just after the

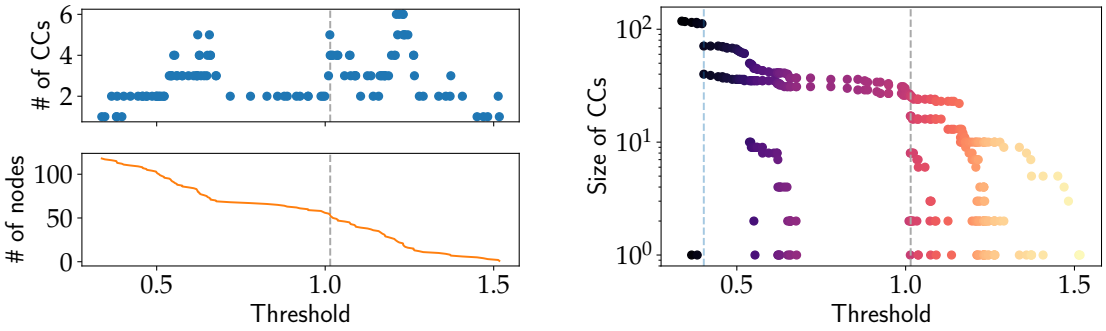

(A) Number of CC (B) Size of CC

FIGURE 5.9: Removal of nodes by the algebraic landscape and a varying threshold in the IEEE 118 test system. The number of connected components (CC) and the number of nodes in all connected components are shown. The landscape u_a is calculated for the algebraic connectivity of the Laplacian L.

graph brakes up in two large subgraphs. The second threshold is chosen when one of the larger subgraphs breaks up into two, while the third threshold is shows the total breakup of this subgraph. The largest threshold shown indicates the largest number of connected components with at least two nodes, which is five (with six connected components in total).

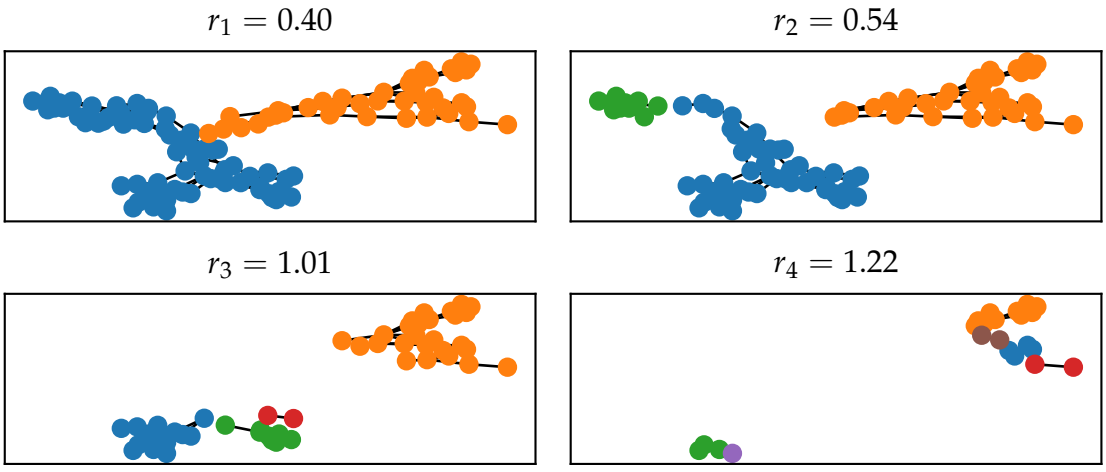

FIGURE 5.10: IEEE 118 graph after removing nodes with four different thresholds on the algebraic landscape.

In a similar fashion as before, we calculate the connected components and their eigenvectors. For a threshold of $r_3 = 1.015$, the results are shown in table 5.3. This threshold is chosen as this is the lowest threshold without any single nodes subgraphs and a maximum number of subgraphs. Many interesting properties are

directly clear. To distinguish these sets from the sets of the previous section, the sets calculated with the second smallest eigenvalue (the algebraic connectivity) are called $\mathcal{A}_i$ here. Of course, there is no intrinsic difference between those sets and all general remarks about any sets $\mathcal{S}$ are valid for all $\mathcal{A}_i$.

j	$\|\boldsymbol{\phi}\|_{\mathcal{A}_j,\max}$	$k(\|\boldsymbol{\phi}\|_{\mathcal{A}_j,\max})$	Node indices
$\mathcal{A}_1$	0.9999	108	1, 16, 19, 20, 21, 25, 30, 58, 72, 93, 95, 97, 100, 101, 106, 111, 117
$\mathcal{A}_2$	0.9999	60	2, 3, 4, 5, 6, 7, 14, 26, 27, 28, 44, 45, 46, 47, 49, 55, 56, 60, 92, 94, 102, 104, 105, 107, 108, 109
$\mathcal{A}_3$	0.9999	110	11, 15, 18, 48, 84, 87, 98, 99
$\mathcal{A}_4$	0.8703	63	76, 77

TABLE 5.3: Connected components of IEEE 118 test case for algebraic landscape, maximum eigenvector components and corresponding mode k.

The following observation can be made:

1. $\mathcal{A}_1$ shows localisation at mode 108. We can also see that $\mathcal{A}_1$ has many similar nodes as $\mathcal{S}_1$ from the previous section.

2. $\mathcal{A}_2$ is localised at mode 60.

3. $\mathcal{A}_3$ shows localisation at mode 110. We can see that $\mathcal{A}_3$ is a superset of $\mathcal{S}_6$, which also exhibited localisation at mode 110. This time, the localisation at mode 110 was almost complete in $\mathcal{S}_6$, which means that some eigenvector components of $\mathcal{A}_3$ must be relatively small.

4. $\mathcal{A}_4$ does not show localised behaviour, similar to $\mathcal{S}_2$ from before. Again, the two nodes of $\mathcal{A}_4$ have the lowest bounds of all remaining nodes and would be removed with a slightly larger threshold.

Interestingly, we can see that some nodes are predicted as localisation candidates from both the algebraic and the spectral landscapes. It seems like the two bounds complement each other, as they are able to predict localisation in similar nodes, but the resulting sets are not completely.

It should be noted that the subgraphs here, especially $\mathcal{A}_1$ and $\mathcal{A}_2$, are very large. In some contexts, the large eigenvector components in this subgraphs are referred to as mode confinement [63]. While the physical interpretation of this mode confinement different, the tools and techniques developed here are generally applicable in both cases.

5.4.3 Mode Prediction

In the last sections, it was shown how the landscapes can be used to partition the graph and find possible candidates for localisation. While this method is successful in this task, one main question cannot be answered: at which mode is localisation observed? Here, the second bound derived in section 5.2.2 can be used to investigate this question. As calculating the vector v required for the bound from eq. (5.6) is difficult and requires knowledge about the eigenvectors, we concentrate on the factor $\xi(\lambda_{\mathcal{S}})$. We predict that large eigenvector components on a subgraph $\mathcal{S}$ correspond to a large $\xi(\mathcal{S})$. To test this hypothesis and try to predict the right modes for localisation, we use all subgraphs from tables 5.2 and 5.3 and calculate ξ for all modes λ. In table 5.4, the four mode ranks k_{ξ} for which $\xi(\lambda_{\mathcal{S}})$ is the largest are shown, as well as the four ranks with the largest eigenvector components $k_{|\boldsymbol{\phi}|}$. Similar colours indicates where the same values are found k_{ξ} and $k_{|\boldsymbol{\phi}|}$ among the four maxima.

j	$k_{\xi,1}$	$k_{\xi,2}$	$k_{\xi,3}$	$k_{\xi,4}$	$k_{\lvert\boldsymbol{\phi}\rvert,1}$	$k_{\lvert\boldsymbol{\phi}\rvert,2}$	$k_{\lvert\boldsymbol{\phi}\rvert,3}$	$k_{\lvert\boldsymbol{\phi}\rvert,4}$
$\mathcal{S}_1$	116	103	45	46	116	108	105	107
$\mathcal{S}_2$	86	85	89	84	100	99	76	85
$\mathcal{S}_3$	111	115	23	22	111	115	91	6
$\mathcal{S}_4$	35	114	34	99	114	101	103	33
$\mathcal{S}_5$	117	46	108	112	117	112	113	109
$\mathcal{S}_6$	32	110	31	33	110	22	23	69
$\mathcal{A}_1$	108	34	52	116	108	116	102	52
$\mathcal{A}_2$	60	100	29	72	60	100	72	29
$\mathcal{A}_3$	110	22	86	85	110	86	48	69
$\mathcal{A}_4$	20	60	19	59	63	8	37	46

TABLE 5.4: Localisation candidates, modes for the four largest ξ and modes with maximum activation in subgraph in IEEE 118 test system. The coloured numbers correspond to the mode ranks where identical modes are found.

Obviously, for all subgraphs where localisation is observed (so all except $\mathcal{S}_2$ and $\mathcal{A}_4$), either the largest or second smallest ξ corresponds to the mode where localisation was observed. In some cases (e.g. $\mathcal{S}_4$), some kind of *false positives* can be observed, where a very large ξ does not correspond to localisation. Obviously, the bound in eq. (5.6) only bounds the eigenvalue components to be smaller than a value and does not indicate how tight this bound is at all. In the values presented here, the false positives happen mostly for intermediate modes. We expect localisation mostly at very large or low modes, as shown in the examples for the fork and high impedance graph or discussed in [104, 106]. Also, the candidates for localisation were found by the algebraic and spectral landscape, which are bounding the largest

and smallest eigenvector. Thus, it might be reasonable in practice to discard the intermediate values, for example from mode 20 to mode 80. If those values are discarded, the large values of ξ in table 5.4 directly correspond to large eigenvector components.

5.4.4 Bounds on the Relative Complement Subgraph

Instead of investigating $\mathcal{S}$, where we predict localisation, we can use the eigenvalue bound to investigate the relative complement subgraph $\overline{\mathcal{S}}$. This graph is obtained by removing $\mathcal{S}$ from $\mathcal{G}$ and thus has the complement vertex set of $\mathcal{S}$[3]. The relative complement subgraph is not necessarily connected. We would expect that the bound on the eigenvectors is very large, except at the modes where localisation is observed in $\mathcal{S}$. As for those values, the eigenvector components of $\overline{\mathcal{S}}$ should be very small and the bound from eq. (5.6) should predict this small values.

We can use this behaviour to further discriminate the false positives from the previous section. Focusing on $\mathcal{S}_4$ and $\mathcal{S}_5$ from table 5.2, we can calculate ξ with eq. (5.6) for the subgraphs and the complement. We focus on the two modes with the largest factor ξ. The results are shown in table 5.5. We can see that at the false positives (35 and 32), ξ is very large at the complement. For the second value of k_ξ, where localisation is observed, this factor is much larger at the subgraph. Using this discrepancy hints that the false positive modes can be removed when the complement graph in this cases, as the bounding factor is much larger.

k_ξ	35	114	k_ξ	32	110
$\xi(\mathcal{S}_4)$	2896	469	$\xi(\mathcal{S}_6)$	164	134
$\xi(\overline{\mathcal{S}}_4)$	30202	14	$\xi(\overline{\mathcal{S}}_6)$	3839	17

TABLE 5.5: Factors ξ for the false positives of table 5.2 for the subgraph and the complement subgraph.

This can be verified in a general way if we look at all eigenvector components and all ξ for each complement subgraph. In fig. 5.11, those values are plotted against each other. Clearly, for the smallest factors ξ, the eigenvectors are small as well. When the eigenvalues of the complement subgraphs are small, it necessarily follows that the subgraph of the candidate subgraphs $\mathcal{S}_i$ and $\mathcal{A}_i$ are large and the mode is localised in those.

[3]This graph is not the complement graph!

At the other hand, for very large values of ξ in the complement subgraphs, the eigenvector components are basically one. This means that no localisation in the candidates can be found at those modes.

The orange points for the spectral and red points for the algebraic landscape correspond to $\mathcal{S}_2$ and $\mathcal{A}_4$ from table 5.4. Those two subgraph did not show localisation, thus the relative component graph will not have very low eigenvector components.

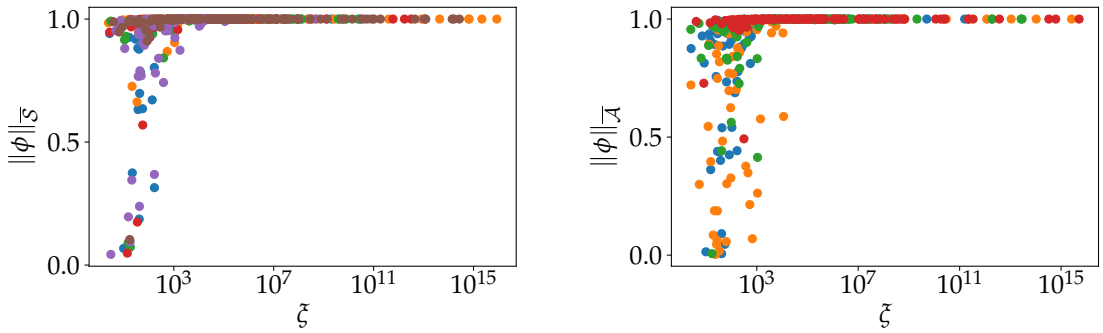

(A) Spectral landscape

(B) Algebraic landscape

FIGURE 5.11: Eigenvector components and factor ξ for the relative complement graphs $\overline{\mathcal{S}}$ of the subgraphs from table 5.4. The different colours indicate the different complement graphs.

5.5 Localisation and Resonance

As seen in the previous section, the landscapes are a powerful tool to find possible subgraphs for localisation These candidates can be used with the second bound to predict at which eigenvalue the localisation takes place, which usually was when ξ was very large. These very large ξ are found when one eigenvector of the subgraph $\lambda_{\mathcal{S}}$ is very close to the eigenvector λ of the graph at the given mode. In this section, we focus on this situation, namely that:

$$\lambda_{\mathcal{S}} \approx \lambda$$

Under this condition, we say that the subgraph $\mathcal{S}$ *resonates* with the the graph $\mathcal{G}$. In this section, we want to test the condition from section 5.2.2 without the knowledge of the subgraphs from the landscape calculations and see how this resonance can be used to explain localisation.

5.5.1 Small Subgraphs

One possibility to show the direct relationship between localisation and resonance is to investigate whether resonance and localisation always happen in conjunction. For this, we explore all possible subgraphs of a given length ($l = 2, 3, 4, 5$) in the graph. Using these large sets of subgraphs allows us to perform statistical investigations to test the condition. Finding all subgraphs has been performed with a simple brute force algorithm, which has a complexity of $\mathcal{O}(n^l)$. More sophisticated algorithms have been proposed in literature (see [107, 108]), but no implementation of those algorithms has been found. The brute force algorithm was fast enough to find all subgraphs in the IEEE 118 test case up to $l = 5$. For larger networks or search for larger subgraphs, better algorithms should be used. The number of connected subgraphs of the IEEE 118 test system of size l from 2 to 5 is shown in table 5.6.

l	2	3	4	5
$N_{\mathcal{S}_l}$	179	463	1429	4701

TABLE 5.6: Number of subgraphs of size l in the IEEE 118 test case.

To see the relationship between localisation and ξ, we calculate ξ and $\|\boldsymbol{\phi}_k\|_{\mathcal{S}}$ for all subgraphs $\mathcal{S}$ and all modes k (which are in total $4701 \cdot 118 = 554718$ data points for $l = 5$). For each mode k, we then search the subgraph with the largest eigenvector component (the vertex set is called $\mathcal{S}_{\max,k}$) and the subgraph with the largest value ξ. If both subgraphs are identical, the bound ξ successfully predicts the right subgraphs for localisation. The number of modes n_{E} for which the found subgraphs are identical for a given length l is shown in table 5.7. We also include an analysis for all lengths $l = 2, 3, 4, 5$, where a total of 6772 subgraphs are investigated. For all lengths l, this number is relatively small. When looking at the modes which are predicted correctly k_{E}, especially the largest frequencies are predicted well, for every length. These are exactly the frequencies which can also be found in table 5.4.

We can investigate those modes further, leading to the following observations and comparisons with the sets found in table 5.4:

- Mode 117: For all length l, the same subgraphs was found for maximal ξ and maximal eigenvector component. For $l = 5$, this subgraph is given by the nodes $\mathcal{S}_{\max,117} = (82, 43, 37, 114, 0)$. This set is very similar to $\mathcal{S}_5$, found by the spectral landscape. Interestingly though, node 0 is not part of $\mathcal{S}_5$, but has been observed as part of the best match.

- Mode 116: The most localised subgraphs were found again, and the nodes are $\mathcal{S}_{\max,116} = (101, 20, 1, 25, 100)$. This subgraph is a subset of $\mathcal{S}_1$ and $\mathcal{A}_1$. While node 25 is not in the former, it is in the latter subgraph.

- Mode 115 and 111: In both cases, the set with the largest eigenvector components is given as $\mathcal{S}_{\max,115} = (17, 22, 57, 64, 69, 74)$. This set has been predicted correctly for mode 115 at all l, but for mode 111, only for length $l = 4, 5$. This nodes are also identified as a localisation candidate with the landscape as $\mathcal{S}_3$, except for node 74.

- Mode 114: The largest set is given as $\mathcal{S}_{\max,114} = (40, 29, 41, 62, 115)$, which is almost identical to $\mathcal{S}_4$, except for node 115. For $l = 3$ and $l = 4$, the largest eigenvector component corresponds to the largest ξ, but not for $l = 4$. For $l = 4$, we have observed that the largest ξ is observed for $(29, 40, 41, 62)$, but the largest eigenvector is reached for $(29, 40, 41, 115)$.

l	n_E	k_E
2	10	3, 5, 7, 14, 17, 26, 110, 115, 116, 117
3	9	3, 5, 7, 29, 110, 114, 115, 116, 117
4	7	3, 7, 110, 111, 115, 116, 117
5	10	3, 47, 55, 86, 110, 111, 114, 115, 116, 117
2,3,4,5	10	3, 47, 55, 86, 110, 111, 114, 115, 116, 117

TABLE 5.7: Modes and number of modes in which the largest eigenvector component subgraph is identical to the subgraph of largest ξ.

It should be noted that if a mode is localised in a subgraph with for example three nodes, it will also be localised in the subgraph with five nodes, but not vice versa. We do now that increasing the size l of the landscape always increases the size of $\|\boldsymbol{\phi}\|_{\mathcal{S}}$, while not necessarily the size of ξ.

We can see that the resonance alone is able to predict localisation at the highest modes. We also observe very similar results for the subgraphs found by the resonance and the subgraphs found by the landscapes.

5.5.2 Statistical Properties

To investigate the cases in which the largest ξ does not correspond to the most localised subgraph, we plot the largest eigenvector components against the eigenvector component of the subgraphs with the largest ξ. Now, we are interested in the

situation where the largest ξ does not directly correspond to the largest eigenvector components. For every mode, we search the subgraph with the largest eigenvalue component and the subgraph with the largest ξ. We then plot the eigenvector components of these two subgraphs against each other. The results are shown in fig. 5.12. All points on the main diagonal correspond to the exact matches, as listed in table 5.7. While the *perfect* matches are rare, we can clearly see that most data is close to the main diagonal. This indicates that for every mode, a largest ξ corresponds to a large eigenvalue component. Also, we can see that for increasing l, the outliers seem to decrease and more data points are close to the main diagonal. We can repeat the investigation with the subgraphs of all sizes together. In fig. 5.12e, a similar plot is shown, calculating the maximum values of $\|\boldsymbol{\phi}\|_{\mathcal{S}}$ and ξ for subgraphs of all lengths l. The graph is very similar to fig. 5.12d, calculated with the largest subgraphs, except for some outliers further away from the main diagonal. As discussed before, larger size of the subgraph increases the norm of the eigenvector components restricted to this subgraph, but not necessarily the factor ξ. Because of this, all largest eigenvector components are found for $l = 5$, but the largest values of ξ can be found at other lengths. This is why the results of $l = 5$ are not identical to the ones found for all lengths l.

The analysis in this section shows that we can use the resonance to find localised subgraphs, without using the landscapes. Especially for the very localised modes ($k = 115, 116, 117$), we see that eigenvalue resonance and localisation are directly linked to each other.

5.6 Conclusion

In this section, localisation was defined and investigated for very simple test cases. In these simple examples, we were able to prove the existence of localisation in certain modes. To generalise the investigations of localisation, two different bounds which are able to predict at which nodes and for which eigenvalue localisation might appear were derived. These bounds are able to predict the eigenvector components of a graph and are thus able to predict localisation in the system. Both bounds have been tested in the simple test cases and in various ways on a large real world network, especially the IEEE 118 test case. It was shown that in combination, the bounds are a powerful tool to predict and explain localisation.

One main result useful for power system research is the equivalence of localisation and resonance. We have found that localisation in a subgraph usually appears when an eigenvalue of the subgraph is identical to an eigenvalue of the full graph.

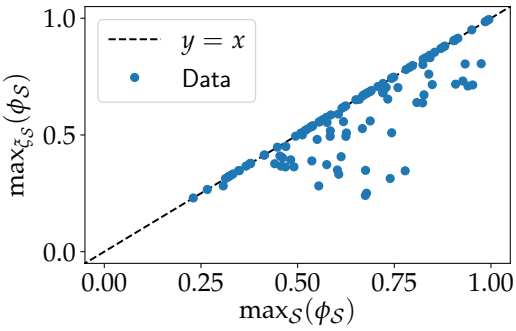

(A) $l = 2$

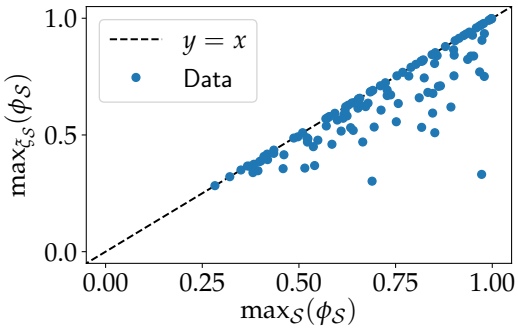

(B) $l = 3$

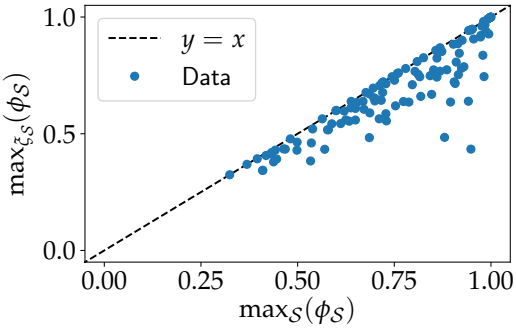

(C) $l = 4$

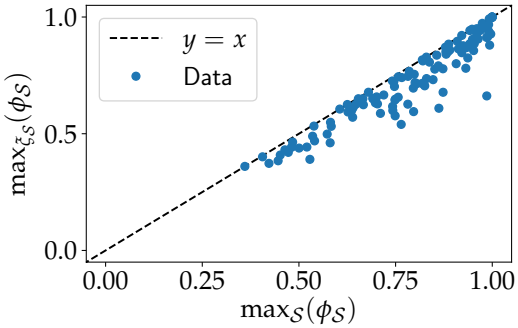

(D) $l = 5$

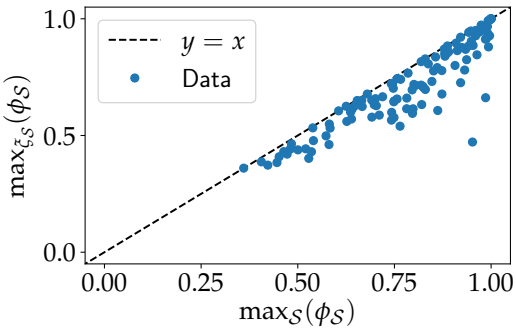

(E) $l = 2, 3, 4, 5$

FIGURE 5.12: Investigations on the IEEE 118 test case network. Showing the maximum eigenvector components of all connected subgraphs of size l against the eigenvector components of the subgraph with the largest ξ.

With this condition, we can relate localisation to the geometry of the subgraph and the full graph which describes the system.

While the experimental validation in this system only showed the results for the IEEE 118 test case, we have tested the method on the IEEE 300 test case as well. To streamline the presentation, the data has not been included in detail here. Some results can be found in appendix B.1.1. Generally, the method appears to work as good in the IEEE 300 test case.

Chapter 6

Conclusions and Outlook

6.1 Conclusions

This work investigated the spectral graph properties in power systems, especially dynamical power systems. One of the main problems in power system research is the complexity of the system, due to its many components and many different scales, both length and time wise. Spectral methods were shown to be a powerful tool to investigate this complexity and is thus useful to approach many problems arising in power system research.

Spectral graph methods in power system research mainly investigates the eigenvalues and eigenvectors of the Laplacian matrix of the underlying network. While often the eigenvalues are the focus of the research, we have shown that the eigenvectors are of main importance to understand the system. The eigenvectors play a fundamental role in both static and dynamic analysis. In spectral power flow analysis, the eigenvectors are responsible for the shape of the Voltages. Also, the flow over each line per mode is proportional to the gradient of the eigenvector components adjacent to the line. In dynamical systems, the eigenvectors describe the participation of each node to the oscillations in the systems and are thus responsible for important effects like local plant modes or coherent generator.

For dynamical power systems we showed how network with generators behave similarly to networks with damped generators. We also found that the system is more sensitive to parameter changes, especially of the inertia, at the high ranked eigenvalues. These eigenvalues correspond to short range interactions in the system. The large range interactions at lower ranked eigenvalues are more influenced by the underlying geometry of the system.

One main problem is to relate the structure of the eigenvectors with the structure of the network. Of the many interesting properties of eigenvectors, we further investigated localisation, which means that only a subset of nodes have a non zero (or non small) eigenvector component at a given mode. These localised dynamics

have some important impact on the power system. In power flow, localised eigenvectors correspond to localised flows at a given mode, as only the lines around the localisation have any flow in them. As seen earlier, the localised modes in the dynamical power systems are more sensitive to parameter changes. These modes are also important for stability studies, as they correspond to local plant modes.

To investigate localisation, we propose and derived two bounds for the eigenvectors. These bounds can be used to explain and predict localisation of the eigenvectors of a Laplacian matrix of a graph. We believe that both bounds are useful tools to investigate localisation, in power system research and related fields, where the spectral properties of graphs are important. We have shown that the bounds are able to predict localisation in simple example systems, where the localisation properties can be calculated theoretically. Then, we have used the bounds to show that the localisation properties of a real power system test case can be predicted successfully.

While this work was motivated by and focused on properties of power systems, the results from chapter 5 might have greater appeal. The method to find and describe localisation in graphs can be applied to all graphs. Localisation of eigenvectors is, as far as we know, not yet used a lot in spectral graph theory, but applications might arise in the future. More generally, only few results show the relationship between Laplacian eigenvectors and the properties of the graph. This localisation results might be a step in finding a comprehensive explanation of these eigenvectors.

6.2 Outlook

As usual, a thesis like this poses as many (if not more) questions than it answers. This is not a weakness, but a strength of science, the eternal search for more knowledge and wisdom. As an outlook, we want to highlight some research directions and possible extensions.

6.2.1 Localisation Bounds

The eigenvector bounds in section 5.2 have been proven a powerful tool to investigate and predict localisation in graphs. Still, some shortcoming are obvious. First of all, both bounds are only valid for the eigenvectors of the eigenvalue problem of a Laplacian matrix. Ideally, we would like to extend these bounds for general matrices or the generalised eigenvalue problem, which would allow us to investigate oscillatory networks. Together with the results of the chapter on spectral properties

of dynamical power systems, this would allow to investigate the dynamical localisation properties of the system in great detail. The landscapes presented in theorem 1 are also valid for all invertible matrices. The extension to general matrix problems is not trivial, as the pseudo inverse matrices generally do not have the same eigenvalues as the normal matrix.

Another question would be whether it is possible to tighten any of the bounds presented here. Especially for the landscapes, some modifications of the bounds seem possible. One different approach is presented in appendix A.3, but the drawbacks of this bound are also obvious and explained therein. Circumventing these drawbacks would result in an improved landscape.

The bound for the subgraphs presented in section 5.2.2 might be investigated further. The bound depends on a factor ξ and the norm of a vector $\|v\|_{\mathcal{S}}$. In the analysis presented in chapter 5, we focused on the factor ξ. The vector v can be calculated by:

$$v = \sum_{i \in \mathcal{S}} \left(\frac{1}{\lambda_i^{\mathcal{S}}} \sum_{x \in \mathcal{S}, x \sim y \in \partial \mathcal{S}} \phi_{i,x}^{\mathcal{S}} \sigma_y e_{x,y} \right) \phi_i^{\mathcal{S}} \tag{6.1}$$

Which is discussed in appendix A.2. As we can see, the calculation of this bound required the eigenvector $\boldsymbol{\phi}$. This means that this method fails to predict eigenvector components, as we need to know the values beforehand. A similar problem was observed in the continuous system in [105]. There, the landscapes were able to sufficiently bound the eigenvector components, so that it was clear that $\|v\|_{\mathcal{S}}$ is small. This is not possible on the discrete problems on graphs discussed here, as the landscapes are much more conservative. We hope that in the future, further analysis of eq. (6.1) or tighter landscapes can be used to approximate the vector v, which would improve the localisation bounds.

6.2.2 Spectral Properties of Dynamical Power Systems

The first challenge is to continue the combination of the theoretical results for the undamped oscillatory networks with the power system network. While the effect of the damping in the analysis appears to be almost negligible, a theoretical foundation of this result and a possible quantification of the impact of damping would be a great step forward.

One first outlook is coherency. When the damping can be neglected, we believe that more theoretical results on the geometry of the eigenvectors are possible. We believe that the geometry of the eigenvectors can be understood further, which might result in better methods to predict important properties such as coherency.

In many fundamental studies on small signal stability, the inertia of the system is simplified to uniform values. We have shown in this work how important the inertia is for the spectral properties and believe that this has to be taken under consideration. We also found that in some cases, generalised eigenvalue problem found in oscillatory networks might be further simplified to separate eigenvalue problems of the inertia and the Laplacian matrix. This method is proposed in appendix A.4. Continuing these investigations might make it possible to use even more theoretical results, for example the localisation studies presented in this work or the investigations popular in mathematics.

Another interesting outlook, related to the synchronisation metrics and fixed point equations discussed in section 2.3.2. In both equations, the product of the pseudo inverse $L^\dagger$ on the bus power $\boldsymbol{P}_B$ is of interest. As in chapter 3, we can express the vector $\boldsymbol{P}_B$ in the eigenbasis of L and link the synchronisation property and values of the synchronised phases to the flows in a line. The synchronisation properties developed in [33] and spectral solution of the DC power flow problem are thus related problems. A promising research direction might be to use the results of spectral power flow investigations to explore more details about the synchronisation property in electrical networks.

6.2.3 Nodal Domains and Localisation Bounds

While not the objective of the landscape method, we observed another interesting property in the connected components after removing nodes with a low threshold of the algebraic connectivity. Looking at the low ranked eigenvectors, we observed some patterns in the remaining eigenvector components. The results are shown in fig. 6.1. For the smallest threshold r_1 at $k = 1$, we see that the eigenvectors are almost partitioned in positive and negative values. This means that the method could maybe help in finding the nodal domains of the graph. For the larger thresholds $r_{3/4}$, we can observe similarity in the eigenvector components for many subgraphs, indicating possible sets with coherent behaviour.

This shows that the landscapes of the graph might be used not just to investigate localisation, but might be used to hint nodal domains or coherent clusters. How to extend those domains to the full graph is a open question which should be investigated in more detail as well.

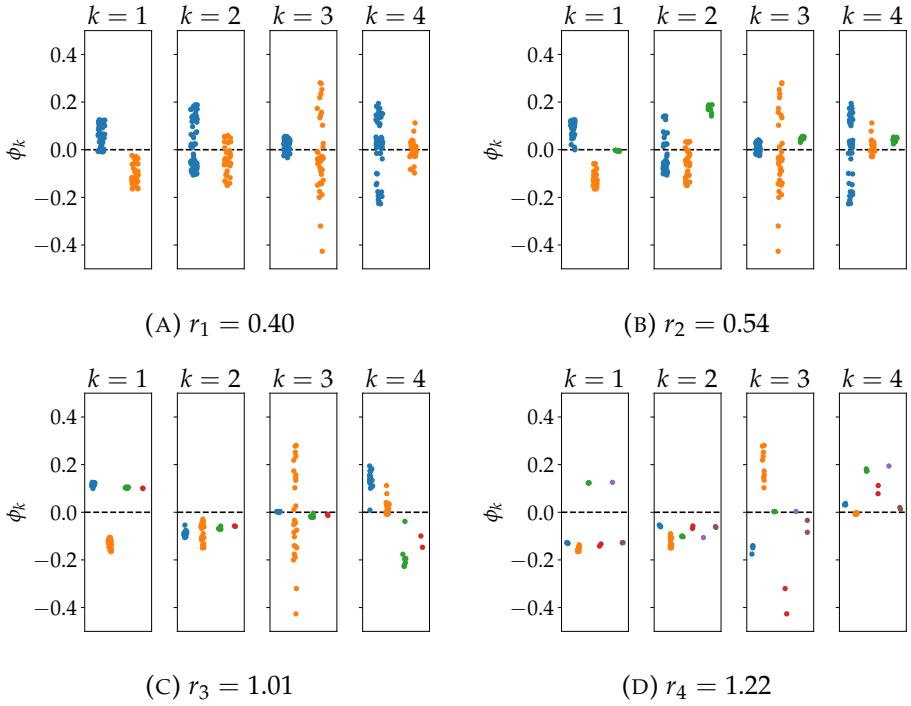

(A) $r_1 = 0.40$ (B) $r_2 = 0.54$

(C) $r_3 = 1.01$ (D) $r_4 = 1.22$

FIGURE 6.1: Eigenvector patterns for connected components after removing low algebraic landscape nodes in the IEEE 118 test case. The different colours indicate the different connected components found at the given threshold.

6.2.4 Eigenvectors from Eigenvalues

One of the main problems we need to understand is how the eigenvectors of a graph correspond to the topology of the graph. The extensive research on nodal domains and some results on coherency are one step. We believe that understanding the localisation is another step to understand this interplay better. In a very recent mathematical publication[1], a new method to calculate eigenvectors from eigenvalues in hermitian matrices was presented [109]. Here, we denote $\phi_{i,j}$ to be the j-th entry of the eigenvector corresponding the the i-th eigenvalue $\lambda_i(L)$. For any hermitian matrix L with the principal submatrix L_j, where the j-th row and column were deleted, the eigenvector components are given as:

$$|\phi_{i,j}|^2 \prod_{k=1;k\neq i}^{n} (\lambda_i(L) - \lambda_k(L)) = \prod_{j=1}^{n-1} (\lambda_i(L) - \lambda_k(L_j)) \tag{6.2}$$

From this, it directly follows that if any $\phi_{i,j} = 0$, one eigenvalue of L_j must be identical to $\lambda_i(L)$. This can be used to predict exact localisation. For example, the

[1]The article was published during the writing period of this work.

exact localisation in section 5.1.1 can be predicted. For each node not in the fork (where exact localisation appears), the principal submatrix has at least one identical eigenvalue to the full graph. If this condition could be extended to a subgraph, it might be possible to investigate exact localisation with this technique. It might also be interesting to investigate whether eq. (6.2) can be used to predict nodal domains or coherent clusters.

6.2.5 Application to realistic power system cases

The analysis presented in this work was applied to very simplified systems, both in modelling and in size. To improve the application and compare the system to more realistic test cases, we have to investigate how to apply the theory to

To apply the localisation bounds and theory developed in this work to realistic systems, the computational complexity for large systems has to be taken to account at first. Realistic transmission system models for the European transmission system have over 16000 buses [110]. The solution of the eigenvalue equations and applications of the methods presented here might be impossible for system of this size. It might still be possible to use the spectral landscape to find possible candidates for localisation. While the spectral radius might not be available, the relative strength of the bound at individual nodes can highlight possible nodes which might exhibit localised behaviour. For the landscape investigations, approximations of the largest and the smallest eigenvalues (for example [72, 111, 112, 113]) might be used in combination with the landscapes to investigate bound the eigenvectors without solving the whole system. Approximations of the spectral radius might also be used to find the most localised subgraph of length 2, as finding subgraphs with this length is computationally easy (all subgraphs are given by the edges of the graph).

6.2.6 Beyond AC systems

All the results were presented for AC systems. With integration of renewable energy sources, more HVDC connections will be included in the power system. An interesting and ongoing research direction is to apply the results and methods obtained here to the HVDC system ans especially a incorporated systems, consisting of AC and DC parts. Our ongoing research shows that the equations of the incorporated system have similarities with the equations discussed in chapter 4. The connection of the AC and the DC system require more complex control schemes, which have to be included in the simplified equations.

This thesis offer many perspectives for either applied mathematicians or power engineers for power systems and maybe other field of applications. We hope that the methods and ideas presented here can help engineers to design and operate a stable power system but also motivate further scientific studies in the field of power system research and complex networks.

Appendix A

Additional Theoretical Results

A.1 State Space Formalism

In [21, 65], the linearization of the system eq. (1.5) has been performed in state space form. We define the state vector $x = (\omega_{\mathcal{P}}, \theta_{\mathcal{P}}, \theta_{\mathcal{C}})^T$, where $\mathcal{P}$ are the producers (generators), $\mathcal{C}$ the consumers (loads) and $\omega_{\mathcal{P}} = \dot{\theta}_{\mathcal{P}}$. The resulting state space formalism of the linearised power systems equation is then:

$$\dot{x} = \underbrace{\begin{pmatrix} M_{\mathcal{P}}^{-1} D_{\mathcal{P}} & -M_{\mathcal{P}}^{-1} L_{\mathcal{P}} & 0 \\ 1_{n_{\mathcal{P}}} & 0 & 0 \\ 0 & 0 & -D_{\mathcal{C}} L_{\mathcal{C}} \end{pmatrix}}_{=:F} x + \begin{pmatrix} M_{\mathcal{P}}^{-1} P_{\mathcal{P}} \\ 0 \\ D_{\mathcal{P}}^{-1} P_{\mathcal{C}} \end{pmatrix} \tag{A.1}$$

The properties of the matrix F and the role of the Laplacian matrix L are not at all clear in this formalism, even though it is theoretically equivalent to the quadratic eigenvalue problem from (4.5). The aforementioned studies only investigate generator networks without any consumers. The resulting state space formalism is much easier in this case. Using the simplified vector $\tilde{x} = (\omega_{\mathcal{P}}, \theta_{\mathcal{P}})^T$, one finds:

$$\dot{x} = \underbrace{\begin{pmatrix} M_{\mathcal{P}}^{-1} D_{\mathcal{P}} & -M_{\mathcal{P}}^{-1} L \\ 1_{n_{\mathcal{P}}} & 0 \end{pmatrix}}_{=:\tilde{F}} \tilde{x} + \begin{pmatrix} M_{\mathcal{P}}^{-1} P_{\mathcal{P}} \\ 0 \end{pmatrix}$$

The spectral properties of this matrix has been extensively studied in [21, 65].

A.2 Solution to the Laplace Equation on Graphs

For the proof of theorem 2, we require a vector v statisfying the Laplace equation on a subgraph. In technical terms, we search a solution v inside a region $\mathcal{S}$, given Dirichlet boundary conditions σ on $\partial\mathcal{S}$, of the following equation:

$$(Lv)_{\mathcal{S}} = 0 \quad \text{and} \quad v_{\partial\mathcal{S}} = \sigma \tag{A.2}$$

A similar problem has been solved for the discrete Laplacian operator $\Delta = D^{-1}L$ in [7, Theorem 1].

$$v = \sum_{i \in \mathcal{S}} \left(\frac{1}{\tau_i^{\mathcal{S}}} \sum_{x \in \mathcal{S}, x \sim y \in \partial\mathcal{S}} d_x^{1/2} \psi_{i,x}^{\mathcal{S}} \sigma_y \right) \frac{1}{\sqrt{d_{\mathcal{S}}}} \psi_i^{\mathcal{S}} \tag{A.3}$$

Where $\tau^{\mathcal{S}}$ and $\psi^{\mathcal{S}}$ are the solutions of the eigenvalue problem of $\mathcal{L}_{\mathcal{S}}$, which is defined in [114] as $\mathcal{L} = D^{-1/2}LD^{-1/2}$. It should be noted that the proof of [7, Theorem 1] is only valid for unweighted graphs. Including weighted graphs is possible by introducing the edge weight e_{ij} between edges i and j in the proof, leading to:

$$v = \sum_{i \in \mathcal{S}} \left(\frac{1}{\tau_i^{\mathcal{S}}} \sum_{x \in \mathcal{S}, x \sim y \in \partial\mathcal{S}} d_x^{1/2} \psi_{i,x}^{\mathcal{S}} e_{x,y} \sigma_y \right) \frac{1}{\sqrt{d_{\mathcal{S}}}} \psi_i^{\mathcal{S}} \tag{A.4}$$

While this solution generally only solves the Laplace equation for the discrete Laplace operator, it is easy to show that this also solves the equation for the combinatorial Laplacian as stated in eq. (A.2):

$$\begin{aligned} (\Delta v)_{\mathcal{S}} &= \left(D^{-1} L v \right)_{\mathcal{S}} = 0 \\ (Lv)_{\mathcal{S}} &= D^{-1} 0 = 0 \end{aligned}$$

Experimentally, we were able to verify that the eigenpairs of $\mathcal{L}_{\mathcal{S}}$ can be replaced by the eigenpairs of $L_{\mathcal{S}}$, using the following, simplified equation, which also solves eq. (A.2):

$$\overline{v} = \sum_{i \in \mathcal{S}} \left(\frac{1}{\lambda_i^{\mathcal{S}}} \sum_{x \in \mathcal{S}, x \sim y \in \partial \mathcal{S}} \phi_{i,x}^{\mathcal{S}} \sigma_y e_{x,y} \right) \phi_i^{\mathcal{S}} \tag{A.5}$$

The solution of the Laplace equation thus depends on the topological structure of the subgraph (which is also responsible for the eigenpairs) and the boundary values σ. Outside of S, where eq. (A.5) defines v and the boundary $\partial\mathcal{S}$, where the values are defined, v can be defined freely.

A.3 Improved Landscape Bounds

A possible improvement of the landscape bounds derived in section 5.2 are discussed here. Following a similar argument as before, we can improve the bounds using the fact that the sum of the landscapes sums over $(\boldsymbol{\phi})_i$:

$$\begin{aligned} |(\boldsymbol{\phi})_i| \leq \frac{1}{\lambda} \sum_{j=1}^{n} \left|L_{ij}\right| \left|(\boldsymbol{\phi})_j\right| &= \frac{1}{\lambda} \left(\sum_{j \neq i} \left|L_{ij}\right| \left|(\boldsymbol{\phi})_j\right| + \left|L_{ii}\right| \left|(\boldsymbol{\phi})_i\right| \right) \\ &\leq \frac{1}{\lambda} \left(\sum_{j \neq i} \left|L_{ij}\right| |\boldsymbol{\phi}|_{\max} + \left|L_{ii}\right| \left|(\boldsymbol{\phi})_i\right| \right) \end{aligned}$$

Which results in the *improved landscape*:

$$\frac{|(\boldsymbol{\phi})_i|}{|\boldsymbol{\phi}|_{\max}} \left(1 - \frac{|L_{ii}|}{\lambda}\right) \leq \frac{1}{\lambda} \sum_{j \neq i} \left|L_{ij}\right| =: \tilde{h}_i$$

In similar fashion, the landscape $\tilde{l}$ can be defined using the pseudo inverse $L^{\dagger}$. One of the main problem with both landscapes is the factor $1 - \frac{|L_{ii}|}{\lambda} =: \nu$. For example, if this factor is negative, the whole interpretation of the bound changes, as this bound turn to a *lower* bound then.

For a unweighted, complete graph of size N we know that $\frac{L_{ii}}{\lambda} = \frac{N-1}{N} = 1 - \frac{1}{N}$. Thus, the factor ν is always positive and this bound can be used without any problems. On the other hand, ν is smaller than zero for roughly half of the possible cases of the Florentine family graph discussed in chapter 2. Obviously, the chance of ν being negative is higher for smaller eigenvalues. In fact, all observed graphs have completely positive factors for the spectral radius[1].

[1] For regular graphs, this can be easily proven using the bound presented in [113, Theorem 2].

This improvement of the bounds might be useful for further studies. In this work, only the original landscapes were used, as they already produced desirable results. To use the improved bounds, finding provable estimations for the values of ν would be needed.

A.4 Proposal - from the GEP to the Eigenvalue Problem

As we have seen in chapter 4, it might be possible to transform the quadratic eigenvalue problem to a generalised eigenvalue problem, which has been discussed in [63]. In this section, we want to note that in some cases, the generalised eigenvalue problem can be further simplified to a normal eigenvalue problem. If M is a diagonal matrix, this is directly obvious and has already been discussed in section 4.2.

Following the arguments in section 4.1.4, we can use the GEP, given in eq. (4.10), for the investigation of spectral properties of dynamical power systems. An interesting result can be found if M and L are simultaneously diagonalisable. Then, a unitary matrix S exists, for which $S^{-1}MS = \Lambda_M$ and $S^{-1}LS = \Lambda_L$ with λ_M and Λ_L being diagonal matrices. Left- and right multiplying eq. (4.10) with S^{-1} and S, respectively, results in:

$$\lambda \left(S^{-1}MS\right) v = \lambda \left(\Lambda_M\right) v = \left(S^{-1}LS\right) v = \Lambda_L v$$
$$\lambda = \Lambda_M^{-1}\Lambda_L$$

A necessary condition for simultaneous diagonalisation is that the matrices M and L commute [67, Ex. 7.2.16]. A diagonal matrix (like M) on commutes with another matrix (and thus, is simultaneously diagonalisable), iff all entries m_i are identical. For the systems investigated in this work, this is not generally the case[2]. Writing down the products LM and ML makes it clear why the matrices do not commute:

[2] In many simplifying investigations, equal machine parameters are assumed. Then, this is possible.

$$LM = \begin{pmatrix} (N-1)\,m_1 & -m_1 & -m_1 & \dots & -m_1 \\ -m_2 & (N-1)\,m_2 & -m_2 & \dots & -m_2 \\ \vdots & \vdots & \vdots & \ddots & \vdots \\ -m_N & -m_N & -m_N & \dots & (N-1)\,m_N \end{pmatrix}$$

$$ML = \begin{pmatrix} (N-1)\,m_1 & -m_2 & -m_3 & \dots & -m_N \\ -m_1 & (N-1)\,m_2 & -m_3 & \dots & -m_N \\ \vdots & \vdots & \vdots & \ddots & \vdots \\ -m_1 & -m_2 & -m_3 & \dots & (N-1)\,m_N \end{pmatrix}$$

From this, it is also clear that $ML = (LM)^T$. We can see though that both products will be approximately identical if for each i, j, $(N-1)\,m_i \gg m_j$. With this, we can argue that the system is almost diagonalisable if:

$$N \gg N_{\min} = \frac{m_{\max}}{m_{\min}} + 1 \tag{A.6}$$

Another interesting result on the diagonalisation of non-commuting matrices is found in [115]. There, it was shown that for two hermitian $N \times N$ matrices X and Y, the sum of the squares of all off-diagonal elements $K(X, Y)$ of the *almost* diagonalisation $U^{-1}XU$ and $U^{-1}YU$ is bounded by the commutators $[X, Y] = XY - YX$ as:

$$\frac{1}{4}\left\|[X, Y]\right\|_F^2 \leq K(X, Y) \leq N\epsilon\left(\left\|[X, Y]\right\|_F\right)$$

With some function $\epsilon(x) \overset{x\to 0}{=} 0$ and the Frobenius norm $\|X\|_F = \sqrt{\sum_{ij}\left|x_{ij}\right|^2}$. Here, the matrices X and Y are normalised ($\|X\|_F = 1$). This means that the error of the diagonalisation decreases when the commutator decreases, as the upper and lower bounds of the error K decrease. The norm of the commutator depends on the differences of the inertia over each connected line. The larger the difference, the larger the commutator. As the matrices have to be normalised for this equation, the interpretation can difficult. We observed though that more meshed systems have a smaller commutator, which mostly follows from the impact of the normalisation of the Laplacian matrix.

While the approximation for the generalised eigenvalue problem is not valid in general, it would be very useful in the study of the dynamic properties of the general

eigenvalue problem. The eigenvalues of M are, as M is diagonal, directly obvious. The spectral properties of L have been intensively studied as part of spectral graph theory. Examples for this approximations are shown in fig. A.1. There, the real eigenvalues of the GEP $\lambda(M, L)$ are plotted against the approximation $\tilde{\lambda}(M, L) = \frac{\lambda(L)}{\lambda(M)}$. In fig. A.1a, three regular networks with an random inertia taken form a uniform distribution uni$(0.5, 1.5)$ are used. The networks are a complete network, a ring network and a ring connected to its sixteen nearest neighbours are shown. Obviously, for the complete graph, the approximation is very accurate, but the accuracy decreased with the less connected networks. The values for the commutator are 0.007 for the complete graph, 0.024 for the ring and 0.012 for the sixteen nearest neighbour graph. We also test the IEEE 118 test case, with values identical to those investigated in section 4.3. The approximation is not very accurate, which probably depends on the large range of inertia in the system. The different values of m vary by a factor of 151, which is too large for this approximation.

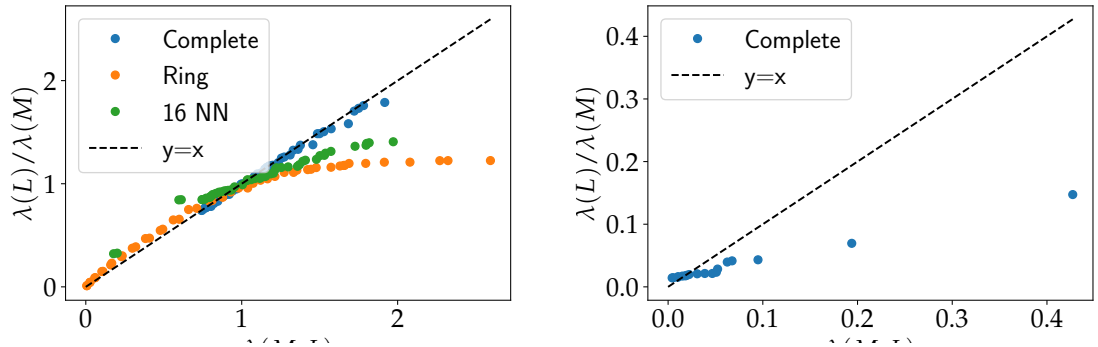

(A) Example graphs (B) IEEE 118

FIGURE A.1: Examples for the approximation of the generalised eigenvalue problem by the eigenvalues of the corresponding eigenvalue problems.

Appendix B

Additional Data and Figures

B.1 Additional Information for Chapter 4

B.1.1 Dynamical properties of the IEEE 300 test case

The complete analysis of section section 4.3 has also been performed with the IEEE 300 test case [93]. While this system obviously behaves different, only a few major differences were observed.

The eigenvectors in fig. B.1a show a similar behaviour to the IEEE 118 test case, some features are just more obvious. We especially observe a strong localisation in the highest modes, while more coherent and long range dynamics are observed for the low ranked eigenvalues. Figure B.1b shows the sensitivity of the spectrum after perturbations of M and D and we again observe that the inertia perturbations are much more influential than perturbations of the damping parameter. The bifurcation diagram shown in fig. B.1c closely resemble those of the IEEE 118 test case. Especially decreasing the damping parameter has little effect on the eigenvalues of the system. The biggest difference between the IEEE 118 test case and the IEEE 300 test case is probably found in fig. B.1d, where the real and imaginary parts of the eigenvalues are shown. The eigenvalues here can be grouped into two main groups. One group has a small negative real part and small imaginary parts. The other group has much larger negative real parts and the imaginary parts are also much larger. This groups might correspond to the different behaviour of the eigenvectors observed in fig. B.1a, where the higher ranked eigenvalues (which are the eigenvalues with the larger negative real part) correspond to the localised eigenvectors. The divide in the eigenvalues might also be observed in the eigenvectors, where two different behaviours can be observed.

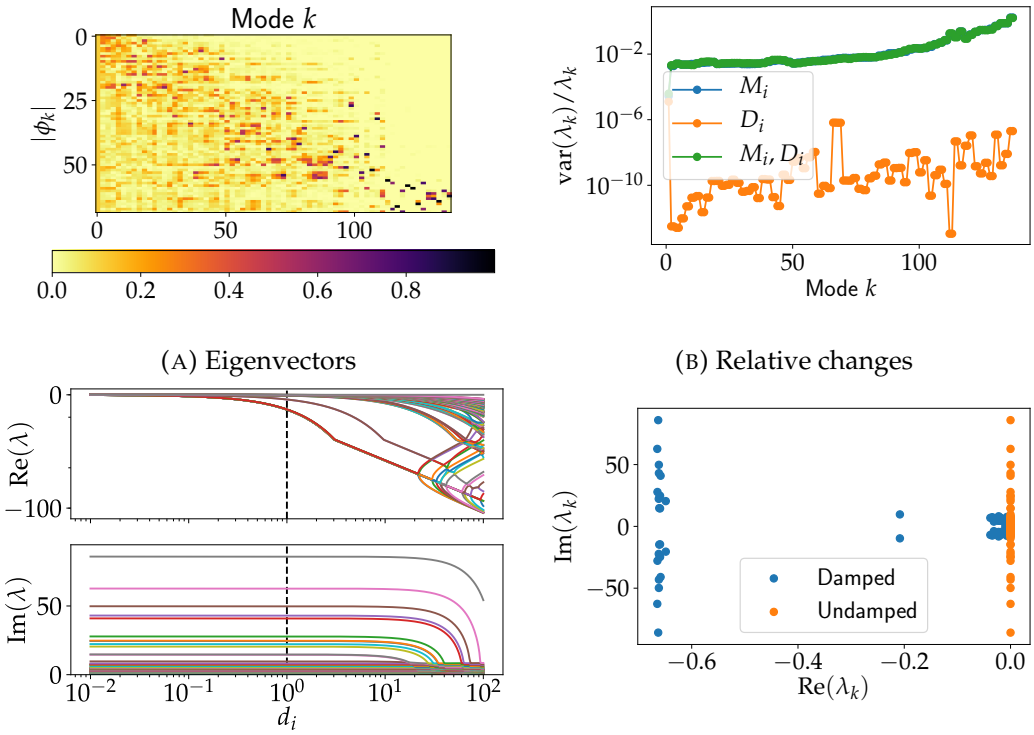

(A) Eigenvectors

(B) Relative changes

(C) Bifurcation diagram

(D) Eigenvalues

FIGURE B.1: Examples for the investigations of the IEEE 300 test case. The eigenvector components, the relative changes of the eigenvalues, the bifurcation diagram with respect to the damping parameters and the eigenvalues of the damped and the undamped system are shown.

B.1.2 Angles Between Eigenvector Examples

To illustrate what the angles between eigenvectors mean, we show three typical examples for angles found in figure fig. 4.10. The illustrations are shown in fig. B.2. Figure B.2a shows a small angle between the vector. We can see that all modes of $\boldsymbol{\phi}$ and $\boldsymbol{\phi}_0$ are almost identical. So, the vectors are almost identical and the angle is small. In fig. B.2b, the difference between the nodes is more obvious and the angles are not similar anymore. This corresponds to a much larger angle. Lastly, the largest angle observable is shown in fig. B.2c. Here, the original eigenvector is very localised at one node. The perturbed eigenvector is also normalised, but at another node. This corresponds to a angle of $\pi/2$.

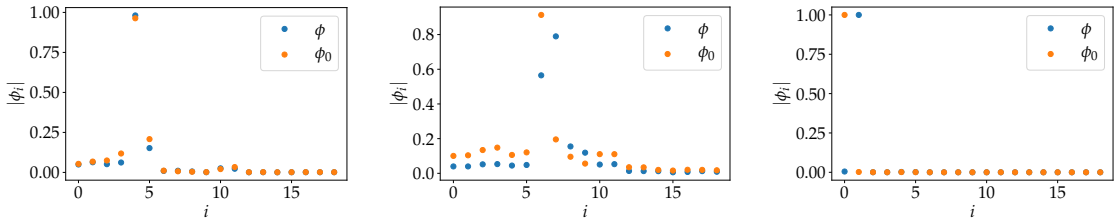

(A) $\theta \approx 0$ (B) $\theta \approx \pi/4$ (C) $\theta \approx \pi/2$

FIGURE B.2: Examples for angles between different eigenvectors. The three figures correspond to the eigenvectors of a perturbed matrix calculated with the QEP. Each figures corresponds to a typical example of the mentioned angle.

B.2 Additional Information for Chapter 5

B.2.1 Localisation in the IEEE 300 Test Case

The landscapes and resonance properties for localisation have also been performed for the IEEE 300 test case. As before, we will not show all results in the main text, to improve the flow. In general, we have found that the proposed method works well for the IEEE 300 test case. While the localisation properties might not be identical, the methods function the same. We only show two examples to highlight this behaviour here. At first, the nodes with a low spectral landscape were removed from the graph, as before. The eigenvector components for the remaining connected components for the highest modes are shown in fig. B.3a. Again, we see very large eigenvector components in some components and almost zero in the other components, which indicate successful prediction of localisation in the connected components. The interplay between resonance and localisation is shown in fig. B.3b, where all

connected subgraphs of lengths $l = 2, 3, 4$ are calculated of the IEEE 300 test case. The largest value of the resonance is plotted against the largest eigenvector component. We again see that in many cases, the largest eigenvector corresponds to the largest resonance in the system, which generally means that resonance corresponds to localisation.

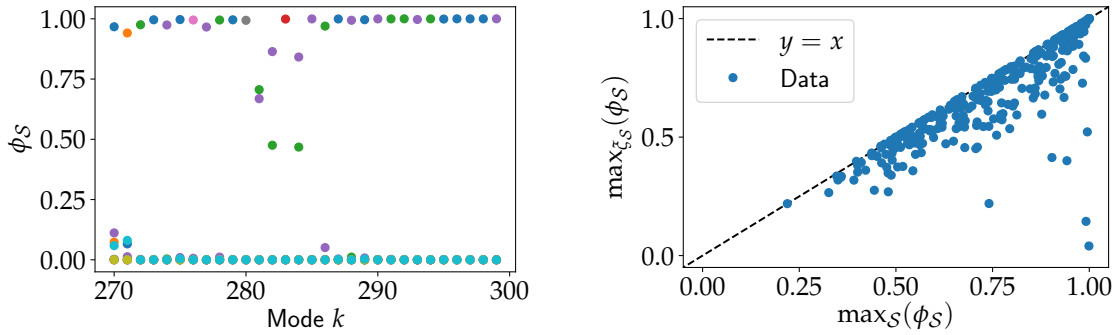

(A) Localisation connected components

(B) Resonance

FIGURE B.3: Localisation bounds on the IEEE 300 test case. Showing the eigenvector components of connected components after removing nodes with the spectral landscape and relationship between ξ and eigenvector components for all possible subgraphs.

B.2.2 Example Graphs showing Localisation

Fork

The Laplacian matrix of the graph with a fork given in section 5.1.1 is:

$$\begin{pmatrix}
1 & 0 & -1 & 0 & 0 & 0 & 0 & 0 & 0 & 0 & 0 & 0 \\
0 & 1 & -1 & 0 & 0 & 0 & 0 & 0 & 0 & 0 & 0 & 0 \\
-1 & -1 & 7 & -1 & -1 & 0 & 0 & 0 & -1 & 0 & -1 & -1 \\
0 & 0 & -1 & 4 & -1 & 0 & 0 & -1 & 0 & 0 & 0 & -1 \\
0 & 0 & -1 & -1 & 5 & -1 & -1 & -1 & 0 & 0 & 0 & 0 \\
0 & 0 & 0 & 0 & -1 & 4 & 0 & 0 & -1 & -1 & -1 & 0 \\
0 & 0 & 0 & 0 & -1 & 0 & 3 & -1 & -1 & 0 & 0 & 0 \\
0 & 0 & 0 & -1 & -1 & 0 & -1 & 4 & -1 & 0 & 0 & 0 \\
0 & 0 & -1 & 0 & 0 & -1 & -1 & -1 & 5 & -1 & 0 & 0 \\
0 & 0 & 0 & 0 & 0 & -1 & 0 & 0 & -1 & 3 & 0 & -1 \\
0 & 0 & -1 & 0 & 0 & -1 & 0 & 0 & 0 & 0 & 3 & -1 \\
0 & 0 & -1 & -1 & 0 & 0 & 0 & 0 & 0 & -1 & -1 & 4
\end{pmatrix} \tag{B.1}$$

Here, the fork are the nodes one and two, which are connected only to the third node.

High Impedance Line

The Laplacian matrix of the graph with a high impedance line, investigated in section 5.1.2 is:

$$\begin{pmatrix}
3 & -1 & 0 & 0 & 0 & 0 & 0 & 0 & 0 & 0 & 0 & 0 & 0 & 0 & 0 & 0 & 0 & -1 & -1 \\
-1 & 5 & -1 & -1 & 0 & 0 & 0 & 0 & 0 & 0 & 0 & -1 & 0 & 0 & 0 & 0 & -1 & 0 & 0 & 0 \\
0 & -1 & 3 & 0 & -1 & 0 & -1 & 0 & 0 & 0 & 0 & 0 & 0 & 0 & 0 & 0 & 0 & 0 & 0 & 0 \\
0 & -1 & 0 & 4 & -1 & -1 & 0 & 0 & 0 & 0 & 0 & 0 & 0 & 0 & 0 & 0 & 0 & 0 & -1 & 0 \\
0 & 0 & -1 & -1 & 7 & -1 & -1 & 0 & -1 & 0 & 0 & -1 & -1 & 0 & 0 & 0 & 0 & 0 & 0 & 0 \\
0 & 0 & 0 & -1 & -1 & 4 & -1 & 0 & 0 & 0 & -1 & 0 & 0 & 0 & 0 & 0 & 0 & 0 & 0 & 0 \\
0 & 0 & -1 & 0 & -1 & -1 & 5 & -1 & -1 & 0 & 0 & 0 & 0 & 0 & 0 & 0 & 0 & 0 & 0 & 0 \\
0 & 0 & 0 & 0 & 0 & 0 & -1 & 3 & 0 & -1 & 0 & 0 & 0 & 0 & -1 & 0 & 0 & 0 & 0 & 0 \\
0 & 0 & 0 & 0 & -1 & 0 & -1 & 0 & 4 & -1 & -1 & 0 & 0 & 0 & 0 & 0 & 0 & 0 & 0 & 0 \\
0 & 0 & 0 & 0 & 0 & 0 & 0 & -1 & -1 & 2 & 0 & 0 & 0 & 0 & 0 & 0 & 0 & 0 & 0 & 0 \\
0 & 0 & 0 & 0 & 0 & -1 & 0 & 0 & -1 & 0 & 2 & 0 & 0 & 0 & 0 & 0 & 0 & 0 & 0 & 0 \\
0 & -1 & 0 & 0 & -1 & 0 & 0 & 0 & 0 & 0 & 0 & 5 & -1 & -1 & 0 & 0 & 0 & 0 & 0 & -1 \\
0 & 0 & 0 & 0 & -1 & 0 & 0 & 0 & 0 & 0 & 0 & -1 & 4 & -1 & -1 & 0 & 0 & 0 & 0 & 0 \\
0 & 0 & 0 & 0 & 0 & 0 & 0 & 0 & 0 & 0 & 0 & -1 & -1 & 4 & -1 & -1 & 0 & 0 & 0 & 0 \\
0 & 0 & 0 & 0 & 0 & 0 & 0 & -1 & 0 & 0 & 0 & 0 & -1 & -1 & 5 & -1 & -1 & 0 & 0 & 0 \\
0 & 0 & 0 & 0 & 0 & 0 & 0 & 0 & 0 & 0 & 0 & 0 & 0 & -1 & -1 & 3 & 0 & -1 & 0 & 0 \\
0 & -1 & 0 & 0 & 0 & 0 & 0 & 0 & 0 & 0 & 0 & 0 & 0 & 0 & -1 & 0 & 4 & -1 & -1 & 0 \\
0 & 0 & 0 & 0 & 0 & 0 & 0 & 0 & 0 & 0 & 0 & 0 & 0 & 0 & 0 & -1 & -1 & 4 & -1 & -1 \\
-1 & 0 & 0 & -1 & 0 & 0 & 0 & 0 & 0 & 0 & 0 & 0 & 0 & 0 & 0 & 0 & -1 & -1 & 10004 & -10000 \\
-1 & 0 & 0 & 0 & 0 & 0 & 0 & 0 & 0 & 0 & 0 & -1 & 0 & 0 & 0 & 0 & 0 & -1 & -10000 & 10003
\end{pmatrix} \tag{B.2}$$

Here, the high impedance line is the edge between the nodes corresponding to the last and the second to last row.

Bibliography

[1] S Boccaletti et al. "Complex Networks: Structure and Dynamics". In: *Physics Reports* 424.4-5 (Feb. 2006), pp. 175–308. ISSN: 03701573. DOI: 10.1016/j.physrep.2005.10.009. (Visited on 10/04/2016).

[2] Duncan J. Watts and Steven H. Strogatz. "Collective Dynamics of /'small-World/' Networks". In: *Nature* 393.6684 (June 4, 1998), pp. 440–442. ISSN: 0028-0836. DOI: 10.1038/30918.

[3] Edward T. Bullmore and Danielle S. Bassett. "Brain Graphs: Graphical Models of the Human Brain Connectome". In: *Annual Review of Clinical Psychology* 7.1 (Apr. 27, 2011), pp. 113–140. ISSN: 1548-5943, 1548-5951. DOI: 10.1146/annurev-clinpsy-040510-143934. (Visited on 09/22/2019).

[4] O. Mason and M. Verwoerd. "Graph Theory and Networks in Biology". In: *IET Systems Biology* 1.2 (Mar. 1, 2007), pp. 89–119. ISSN: 1751-8849, 1751-8857. DOI: 10.1049/iet-syb:20060038. (Visited on 09/21/2019).

[5] Lauren Ancel Meyers et al. "Network Theory and SARS: Predicting Outbreak Diversity". In: *Journal of Theoretical Biology* 232.1 (Jan. 2005), pp. 71–81. ISSN: 00225193. DOI: 10.1016/j.jtbi.2004.07.026. (Visited on 09/22/2019).

[6] Pierre Brémaud. *Markov Chains: Gibbs Fields, Monte Carlo Simulation, and Queues*. Texts in Applied Mathematics 31. OCLC: 245810628. New York, NY: Springer, 1999. 444 pp. ISBN: 978-1-4419-3131-3 978-0-387-98509-1.

[7] Fan Chung and S.-T. Yau. "Discrete Green's Functions". In: *Journal of Combinatorial Theory, Series A* 91.1 (2000), pp. 191–214. ISSN: 0097-3165. DOI: https://doi.org/10.1006/jcta.2000.3094.

[8] Brooke E. Husic and Vijay S. Pande. "Markov State Models: From an Art to a Science". In: *Journal of the American Chemical Society* 140.7 (Feb. 21, 2018), pp. 2386–2396. ISSN: 0002-7863, 1520-5126. DOI: 10.1021/jacs.7b12191. (Visited on 09/23/2019).

[9] C. E. Clancy. "Na+ Channel Mutation That Causes Both Brugada and Long-QT Syndrome Phenotypes: A Simulation Study of Mechanism". In: *Circulation* 105.10 (Mar. 12, 2002), pp. 1208–1213. ISSN: 00097322, 15244539. DOI: 10.1161/hc1002.105183. (Visited on 04/08/2017).

[10] Felix Sebastian Koeth. "Complex Dynamics of Diseased Cardiac Cells". Master Thesis. Universität Göttingen, 2015.

[11] Prabha Kundur. *Power System Stability and Control*. 1st edition. New York: McGraw-Hill Education, Jan. 22, 1994. 1200 pp. ISBN: 978-0-07-035958-1.

[12] "WMO Statement on the State of the Global Climate in 2018". In: (), p. 44.

[13] Hannah Ritchie and Max Roser. "CO_2 and Greenhouse Gas Emissions". In: *Our World in Data* (2019). https://ourworldindata.org/co2-and-other-greenhouse-gas-emissions.

[14] H. Ibrahim et al. "Integration of Wind Energy into Electricity Systems: Technical Challenges and Actual Solutions". In: *Energy Procedia* 6 (2011), pp. 815–824. ISSN: 18766102. DOI: 10.1016/j.egypro.2011.05.092. (Visited on 09/24/2019).

[15] Andreas Ulbig, Theodor S. Borsche, and Göran Andersson. "Impact of Low Rotational Inertia on Power System Stability and Operation". In: *IFAC Proceedings Volumes* 47.3 (2014), pp. 7290–7297. ISSN: 14746670. DOI: 10.3182/20140824-6-ZA-1003.02615. (Visited on 09/24/2019).

[16] Adilson E. Motter and Réka Albert. "Networks in Motion". In: *Physics Today* 65.4 (2012), p. 43. ISSN: 00319228. DOI: 10.1063/PT.3.1518. (Visited on 09/09/2016).

[17] P. M Buckley and A. H Hoskyns. *Basic Electronic Circuits*. OCLC: 472752153. London: E. & F.N. Spon, 1980. ISBN: 978-0-419-11420-8.

[18] Antoni Amengual. "The Intriguing Properties of the Equivalent Resistances of *n* Equal Resistors Combined in Series and in Parallel". In: *American Journal of Physics* 68.2 (Feb. 2000), pp. 175–179. ISSN: 0002-9505, 1943-2909. DOI: 10.1119/1.19396. (Visited on 09/22/2019).

[19] F. Dörfler, J. W. Simpson-Porco, and F. Bullo. "Electrical Networks and Algebraic Graph Theory: Models, Properties, and Applications". In: *Proceedings of the IEEE* 106.5 (May 2018), pp. 977–1005. ISSN: 0018-9219. DOI: 10.1109/JPROC.2018.2821924.

[20] Florian Dorfler and Francesco Bullo. "Kron Reduction of Graphs With Applications to Electrical Networks". In: *IEEE Transactions on Circuits and Systems I: Regular Papers* 60.1 (Jan. 2013), pp. 150–163. ISSN: 1549-8328, 1558-0806. DOI: 10.1109/TCSI.2012.2215780. (Visited on 09/29/2016).

[21] Adilson E. Motter et al. "Spontaneous Synchrony in Power-Grid Networks". In: *Nature Physics* 9.3 (Feb. 10, 2013), pp. 191–197. ISSN: 1745-2473, 1745-2481. DOI: 10.1038/nphys2535. (Visited on 10/25/2016).

[22] T. Ishizaki, A. Chakrabortty, and J. Imura. "Graph-Theoretic Analysis of Power Systems". In: *Proceedings of the IEEE* 106.5 (May 2018), pp. 931–952. ISSN: 0018-9219. DOI: 10.1109/JPROC.2018.2812298.

[23] Peter W Sauer and MA Pai. "Power System Dynamics and Stability". In: *Urbana* 51 (1997), p. 61801.

[24] Takashi Nishikawa and Adilson E Motter. "Comparative Analysis of Existing Models for Power-Grid Synchronization". In: *New Journal of Physics* 17.1 (Jan. 27, 2015), p. 015012. ISSN: 1367-2630. DOI: 10.1088/1367-2630/17/1/015012. (Visited on 09/09/2016).

[25] Masud Chaichian et al. *Electrodynamics: An Intensive Course*. OCLC: 971134266. Berlin Heidelberg: Springer Berlin, 2016. 669 pp. ISBN: 978-3-642-17380-6 978-3-642-17381-3.

[26] Tom Brown, Jonas Hörsch, and David Schlachtberger. "PyPSA: Python for Power System Analysis". In: *Journal of Open Research Software* 6 (Jan. 16, 2018), p. 4. ISSN: 2049-9647. DOI: 10.5334/jors.188. (Visited on 07/16/2019).

[27] Jan Machowski, Janusz W. Bialek, and James R. Bumby. *Power System Dynamics: Stability and Control*. 2. ed., repr. with corr. OCLC: 935927371. Chichester: Wiley, 2012. 629 pp. ISBN: 978-0-470-72558-0.

[28] B. Ghaddar, J. Marecek, and M. Mevissen. "Optimal Power Flow as a Polynomial Optimization Problem". In: *IEEE Transactions on Power Systems* 31.1 (Jan. 2016), pp. 539–546. ISSN: 0885-8950. DOI: 10.1109/TPWRS.2015.2390037.

[29] P. S. R Murthy. *Power System Analysis*. OCLC: 680624912. Hyderabad [India: BS Publications, 2007. ISBN: 978-1-4416-6528-7 978-93-5043-630-1. URL: http://public.eblib.com/choice/publicfullrecord.aspx?p=588469 (visited on 09/09/2016).

[30] Federico Milano. *Power System Modelling and Scripting*. Vol. 0. Power Systems. Berlin, Heidelberg: Springer Berlin Heidelberg, 2010. ISBN: 978-3-642-13668-9 978-3-642-13669-6. DOI: 10.1007/978-3-642-13669-6. (Visited on 05/02/2017).

[31] G. Filatrella, A. H. Nielsen, and N. F. Pedersen. "Analysis of a Power Grid Using a Kuramoto-like Model". In: *The European Physical Journal B* 61.4 (Feb. 2008), pp. 485–491. ISSN: 1434-6028, 1434-6036. DOI: 10.1140/epjb/e2008-00098-8. (Visited on 09/09/2016).

[32] Florian Dorfler and Francesco Bullo. "Synchronization and Transient Stability in Power Networks and Nonuniform Kuramoto Oscillators". In: *SIAM Journal on Control and Optimization* 50.3 (2012), pp. 1616–1642. URL: http://epubs.siam.org/doi/abs/10.1137/110851584 (visited on 10/25/2016).

[33] F. Dorfler, M. Chertkov, and F. Bullo. "Synchronization in Complex Oscillator Networks and Smart Grids". In: *Proceedings of the National Academy of Sciences* 110.6 (Feb. 5, 2013), pp. 2005–2010. ISSN: 0027-8424, 1091-6490. DOI: 10.1073/pnas.1212134110. (Visited on 09/09/2016).

[34] Arthur R. Bergen and David J. Hill. "A Structure Preserving Model for Power System Stability Analysis". In: *IEEE Transactions on Power Apparatus and Systems* 1 (1981), pp. 25–35. URL: http://ieeexplore.ieee.org/abstract/document/4110445/ (visited on 05/04/2017).

[35] "Definition and Classification of Power System Stability IEEE/CIGRE Joint Task Force on Stability Terms and Definitions". In: *IEEE Transactions on Power Systems* 19.3 (Aug. 2004), pp. 1387–1401. ISSN: 0885-8950. DOI: 10.1109/TPWRS.2004.825981. (Visited on 10/21/2016).

[36] P. C. Magnusson. "The Transient-Energy Method of Calculating Stability". In: *Transactions of the American Institute of Electrical Engineers* 66.1 (Jan. 1947), pp. 747–755. DOI: 10.1109/T-AIEE.1947.5059502.

[37] M.A. Pai. "Transient Stability Studies in Power Systems Using Lyapunov-Popov Approach". In: *IFAC Proceedings Volumes* 5.1 (June 1972), pp. 287–293. ISSN: 14746670. DOI: 10.1016/S1474-6670(17)68419-2. (Visited on 10/03/2019).

[38] B. Stott. "Power System Dynamic Response Calculations". In: *Proceedings of the IEEE* 67.2 (Feb. 1979), pp. 219–241. DOI: 10.1109/PROC.1979.11233.

[39] David J Hill. "The Importance of New Theory, Computation and Data-Based Methods Research". Talks. IEEE PowerTech 2019 - Planary Session 2. June 25, 2019. URL: https://attend.ieee.org/powertech-2019/wp-content/uploads/sites/107/2019/07/p2-2.pdf (visited on 10/03/2019).

[40] Giuliano Andrea Pagani and Marco Aiello. "The Power Grid as a Complex Network: A Survey". In: *Physica A: Statistical Mechanics and its Applications* 392.11 (June 2013), pp. 2688–2700. ISSN: 03784371. DOI: 10.1016/j.physa.2013.01.023. (Visited on 09/20/2016).

[41] Arkady Pikovsky, Michael Rosenblum, and Jürgen Kurths. *Synchronization: A Universal Concept in Nonlinear Sciences*. Vol. 12. Cambridge university press, 2003. URL: https://doi.org/10.1119/1.1475332 (visited on 09/09/2016).

[42] Francisco A. Rodrigues et al. "The Kuramoto Model in Complex Networks". In: *Physics Reports* 610 (Jan. 2016), pp. 1–98. ISSN: 03701573. DOI: 10.1016/j.physrep.2015.10.008. (Visited on 04/05/2018).

[43] Louis M. Pecora and Thomas L. Carroll. "Master Stability Functions for Synchronized Coupled Systems". In: *Physical Review Letters* 80.10 (1998), p. 2109. URL: http://journals.aps.org/prl/abstract/10.1103/PhysRevLett.80.2109 (visited on 09/09/2016).

[44] Peter J. Menck et al. "How Basin Stability Complements the Linear-Stability Paradigm". In: *Nature Physics* 9.2 (Jan. 6, 2013), pp. 89–92. ISSN: 1745-2473, 1745-2481. DOI: 10.1038/nphys2516. (Visited on 09/19/2016).

[45] Dirk Witthaut and Marc Timme. "Braess's Paradox in Oscillator Networks, Desynchronization and Power Outage". In: *New Journal of Physics* 14.8 (Aug. 29, 2012), p. 083036. ISSN: 1367-2630. DOI: 10.1088/1367-2630/14/8/083036. (Visited on 09/09/2016).

[46] Hale Cetinay, Fernando A. Kuipers, and Piet Van Mieghem. "A Topological Investigation of Power Flow". In: *IEEE Systems Journal* 12.3 (Sept. 2018), pp. 2524–2532. ISSN: 1932-8184, 1937-9234, 2373-7816. DOI: 10.1109/JSYST.2016.2573851. (Visited on 05/27/2019).

[47] RICHARD STEINBERG and WILLARD I. ZANGWILL. "The Prevalence of Braess' Paradox". In: *Transportation Science* 17.3 (1983), pp. 301–318. ISSN: 00411655, 15265447. JSTOR: 25768099.

[48] Peter J. Menck et al. "How Dead Ends Undermine Power Grid Stability". In: *Nature Communications* 5 (June 9, 2014). ISSN: 2041-1723. DOI: 10.1038/ncomms4969. (Visited on 09/09/2016).

[49] Paul Schultz, Jobst Heitzig, and Jürgen Kurths. "Detours around Basin Stability in Power Networks". In: *New Journal of Physics* 16.12 (Dec. 2, 2014), p. 125001. ISSN: 1367-2630. DOI: 10.1088/1367-2630/16/12/125001. (Visited on 09/09/2016).

[50] Benjamin Schäfer et al. "Dynamically Induced Cascading Failures in Power Grids". In: *Nature Communications* 9.1 (Dec. 2018). ISSN: 2041-1723. DOI: 10.1038/s41467-018-04287-5. (Visited on 10/03/2019).

[51] Benjamin Schäfer and G. Cigdem Yalcin. "Dynamical Modelling of Cascading Failures in the Turkish Power Grid". In: (July 11, 2019). arXiv: 1907.05194 [nlin]. URL: http://arxiv.org/abs/1907.05194 (visited on 08/30/2019).

[52] Daniel Kaplan and Leon Glass. *Understanding Nonlinear Dynamics*. Nachdr. Textbooks in Mathematical Sciences. OCLC: 250023878. New York: Springer, 2003. 420 pp. ISBN: 978-0-387-94440-1.

[53] Hannele Holttinen et al. "Impacts of Large Amounts of Wind Power on Design and Operation of Power Systems, Results of IEA Collaboration". In: *Wind Energy* 14.2 (Mar. 2011), pp. 179–192. ISSN: 10954244. DOI: 10.1002/we.410. (Visited on 07/16/2019).

[54] Dan Spielman. "Spectral Graph Theory". In: *Combinatorial Scientific Computing*. CRC Press, 2012.

[55] *Spectral Graph Theory - Fall 2015 | http://www.cs.yale.edu/*. URL: http://www.cs.yale.edu/homes/spielman/561/ (visited on 09/02/2019).

[56] Andries E. Brouwer and Willem H. Haemers. *Spectra of Graphs*. Universitext. OCLC: 761381086. New York, NY Dordrecht Heidelberg London: Springer, 2012. 250 pp. ISBN: 978-1-4614-1938-9 978-1-4614-1939-6.

[57] Reinhard Diestel. *Graph Theory*. Vol. 173. Graduate Texts in Mathematics. Berlin, Heidelberg: Springer Berlin Heidelberg, 2017. ISBN: 978-3-662-53621-6 978-3-662-53622-3. DOI: 10.1007/978-3-662-53622-3. (Visited on 10/20/2017).

[58] Béla Bollobás. *Modern Graph Theory*. 5. print. Graduate Texts in Mathematics 184. OCLC: 845712663. New York, NY: Springer, 2010. 394 pp. ISBN: 978-0-387-98488-9 978-0-387-98491-9.

[59] Robin J. Wilson. *Introduction to Graph Theory*. 4. ed., [Nachdr.] OCLC: 254109274. Harlow: Prentice Hall, 1996. 171 pp. ISBN: 978-0-582-24993-6.

[60] Ronald L Breiger and Philippa E Pattison. "Cumulated Social Roles: The Duality of Persons and Their Algebras". In: *Social networks* 8.3 (1986), pp. 215–256.

[61] J. Reichardt. *Structure in Complex Networks*. Vol. 766. Lecture Notes in Physics. Berlin, Heidelberg: Springer Berlin Heidelberg, 2009. ISBN: 978-3-540-87832-2 978-3-540-87833-9. DOI: 10.1007/978-3-540-87833-9. (Visited on 10/20/2017).

[62] RB Ellis III. "Chip-Firing Games with Dirichlet Eigenvalues and Discrete Green's Functions". University of California, San Diego, 2002.

[63] Babak Ayazifar. "Graph Spectra and Modal Dynamics of Oscillatory Networks". Massachusetts Institute of Technology, 2002. URL: https://dspace.mit.edu/handle/1721.1/16913 (visited on 10/10/2017).

[64] P. Van Mieghem, K. Devriendt, and H. Cetinay. "Pseudoinverse of the Laplacian and Best Spreader Node in a Network". In: *Physical Review E* 96.3 (Sept. 15, 2017). ISSN: 2470-0045, 2470-0053. DOI: 10.1103/PhysRevE.96.032311. (Visited on 07/09/2018).

[65] Nicolás Rubido. *Energy Transmission and Synchronization in Complex Networks*. Springer Theses. Cham: Springer International Publishing, 2016. ISBN: 978-3-319-22215-8 978-3-319-22216-5. URL: http://link.springer.com/10.1007/978-3-319-22216-5 (visited on 09/12/2016).

[66] Fan RK Chung. "Laplacians of Graphs and Cheeger's Inequalities". In: *Combinatorics, Paul Erdos is Eighty* 2.157-172 (1996), pp. 13–2.

[67] Carl D. Meyer. *Matrix Analysis and Applied Linear Algebra*. Vol. 2. Siam, 2000.

[68] George B. Arfken and Hans-Jurgen Weber. *Mathematical Methods for Physicists*. 6. ed., internat. ed., [5. Nachdr.] OCLC: 551222393. Amsterdam: Elsevier, Acad. Press, 2008. 1182 pp. ISBN: 978-0-12-059876-2 978-0-12-088584-8.

[69] Leslie Hogben. *Handbook of Linear Algebra*. 2nd. 2014. ISBN: 978-1-4665-0728-9 1-4665-0728-4.

[70] Enrico Bozzo and Massimo Franceschet. "Approximations of the Generalized Inverse of the Graph Laplacian Matrix". In: *Internet Math.* 8.4 (2012), pp. 456–481. URL: https://projecteuclid.org:443/euclid.im/1354809993.

[71] Miroslav Fiedler. "Algebraic Connectivity of Graphs". In: *Czechoslovak mathematical journal* 23.2 (1973), pp. 298–305.

[72] Nair Maria Maia de Abreu. "Old and New Results on Algebraic Connectivity of Graphs". In: *Linear Algebra and its Applications* 423.1 (May 2007), pp. 53–73. ISSN: 00243795. DOI: 10.1016/j.laa.2006.08.017. (Visited on 09/09/2019).

[73] Türker Bıyıkoğlu et al. "Graph Laplacians, Nodal Domains, and Hyperplane Arrangements". In: *Linear Algebra and its Applications* 390 (Oct. 2004), pp. 155–174. ISSN: 00243795. DOI: 10.1016/j.laa.2004.04.024. (Visited on 12/20/2017).

[74] Türker Biyikoglu, Josef Leydold, and Peter F. Stadler. *Laplacian Eigenvectors of Graphs: Perron-Frobenius and Faber-Krahn Type Theorems*. Lecture Notes in Mathematics 1915. OCLC: 255682628. Berlin: Springer, 2007. 115 pp. ISBN: 978-3-540-73509-0.

[75] Ravi Kannan, Santosh Vempala, and Adrian Vetta. "On Clusterings: Good, Bad and Spectral". In: *J. ACM* 51.3 (May 2004), pp. 497–515. ISSN: 0004-5411. DOI: 10.1145/990308.990313.

[76] J. H. Chow, J. Cullum, and R. A. Willoughby. "A Sparsity-Based Technique for Identifying Slow-Coherent Areas in Large Power Systems". In: *IEEE Transactions on Power Apparatus and Systems* PAS-103.3 (Mar. 1984), pp. 463–473. DOI: 10.1109/TPAS.1984.318724.

[77] S.B. Yusof, G.J. Rogers, and R.T.H. Alden. "Slow Coherency Based Network Partitioning Including Load Buses". In: *IEEE Transactions on Power Systems* 8.3 (Aug./1993), pp. 1375–1382. ISSN: 08858950. DOI: 10.1109/59.260855. (Visited on 12/05/2018).

[78] G. N. Ramaswamy et al. "Synchrony, Aggregation, and Multi-Area Eigenanalysis". In: *IEEE Transactions on Power Systems* 10.4 (Nov. 1995), pp. 1986–1993. DOI: 10.1109/59.476067.

[79] Z. Yuan et al. "Inter-Area Oscillation Analysis Using Wide Area Voltage Angle Measurements from FNET". In: *IEEE PES General Meeting*. IEEE PES General Meeting. July 2010, pp. 1–7. DOI: 10.1109/PES.2010.5588126.

[80] R. J. Sánchez-García et al. "Hierarchical Spectral Clustering of Power Grids". In: *IEEE Transactions on Power Systems* 29.5 (Sept. 2014), pp. 2229–2237. ISSN: 0885-8950. DOI: 10.1109/TPWRS.2014.2306756.

[81] M. Tyloo, T. Coletta, and Ph. Jacquod. "Robustness of Synchrony in Complex Networks and Generalized Kirchhoff Indices". In: *Physical Review Letters* 120.8 (Feb. 22, 2018), p. 084101. ISSN: 0031-9007, 1079-7114. DOI: 10.1103/PhysRevLett.120.084101. (Visited on 10/04/2019).

[82] Laurent Pagnier and Philippe Jacquod. "Disturbance Propagation, Inertia Location and Slow Modes in Large-Scale High Voltage Power Grids". In: (Oct. 11, 2018). arXiv: 1810.04982 [cs]. URL: http://arxiv.org/abs/1810.04982 (visited on 09/03/2019).

[83] Florian Dörfler and Francesco Bullo. "Synchronization in Complex Networks of Phase Oscillators: A Survey". In: *Automatica* 50.6 (June 2014), pp. 1539–1564. ISSN: 00051098. DOI: 10.1016/j.automatica.2014.04.012. (Visited on 10/25/2016).

[84] G. Rogers. "Demystifying Power System Oscillations". In: *IEEE Computer Applications in Power* 9.3 (July 1996), pp. 30–35. DOI: 10.1109/67.526851.

[85] N. Retiére, D. T. Ha, and J. Caputo. "Spectral Graph Analysis of the Geometry of Power Flows in Transmission Networks". In: *IEEE Systems Journal* (2019), pp. 1–12. DOI: 10.1109/JSYST.2019.2928852.

[86] J. G. Caputo, A. Knippel, and N. Retiere. "Spectral Solution of Load Flow Equations". In: (Aug. 14, 2018). arXiv: 1808.06906 [physics]. URL: http://arxiv.org/abs/1808.06906 (visited on 07/22/2019).

[87] Rich Christie. "118 Bus Power Flow Test Case". In: (1993). URL: https://labs.ece.uw.edu/pstca/pf118/pg_tca118bus.htm.

[88] Françoise Tisseur and Karl Meerbergen. "The Quadratic Eigenvalue Problem". In: *SIAM review* 43.2 (2001), pp. 235–286.

[89] F. Koeth and N. Retiere. "Spectral Properties of Dynamical Power Systems". In: *2019 IEEE Milan PowerTech*. 2019 IEEE Milan PowerTech. June 2019, pp. 1–6. DOI: 10.1109/PTC.2019.8810701.

[90] D. Steven Mackey, Niloufer Mackey, and Françoise Tisseur. "Polynomial Eigenvalue Problems: Theory, Computation, and Structure". In: *Numerical Algebra, Matrix Theory, Differential-Algebraic Equations and Control Theory*. Ed. by Peter Benner et al. Cham: Springer International Publishing, 2015, pp. 319–348. ISBN: 978-3-319-15259-2 978-3-319-15260-8. DOI: 10.1007/978-3-319-15260-8_12. (Visited on 09/04/2019).

[91] Yiling You, Jose Israel Rodriguez, and Lek-Heng Lim. "Accurate Solutions of Polynomial Eigenvalue Problems". In: *arXiv preprint arXiv:1711.01301* (2017).

[92] Françoise Tisseur. "Backward Error and Condition of Polynomial Eigenvalue Problems". In: *Linear Algebra and its Applications* 309.1-3 (Apr. 2000), pp. 339–361. ISSN: 00243795. DOI: 10.1016/S0024-3795(99)00063-4. (Visited on 09/05/2019).

[93] Ray D. Zimmerman and Carlos E. Murillo-Sanchez. "Matpower 5.1-User's Manual". In: *Power Systems Engineering Research Center (PSERC)* (2015). URL: http://www.pserc.cornell.edu/matpower/docs/MATPOWER-manual-5.1.pdf (visited on 09/12/2016).

[94] Vijay Vittal et al. "Transient Stability Test Systems for Direct Stability Methods". In: *IEEE Transactions on Power Systems* 7.1 (1992), p. 37.

[95] Françoise Tisseur and Nicholas J. Higham. "Structured Pseudospectra for Polynomial Eigenvalue Problems, with Applications". In: *SIAM Journal on Matrix Analysis and Applications* 23.1 (Jan. 2001), pp. 187–208. ISSN: 0895-4798, 1095-7162. DOI: 10.1137/S0895479800371451. (Visited on 11/19/2018).

[96] Peter Benner et al. "Relative Perturbation Theory for Quadratic Eigenvalue Problems". In: *arXiv preprint arXiv:1602.03420* (2016).

[97] K. Scharnhorst. "Angles in Complex Vector Spaces". In: *Acta Applicandae Mathematica* 69.1 (Oct. 1, 2001), pp. 95–103. ISSN: 1572-9036. DOI: 10.1023/A:1012692601098.

[98] Tosio Katō. *Perturbation Theory for Linear Operators*. Classics in Mathematics. Berlin: Springer, 1995. 619 pp. ISBN: 978-3-540-58661-6.

[99] Ninoslav Truhar and Suzana Miodragović. "Relative Perturbation Theory for Definite Matrix Pairs and Hyperbolic Eigenvalue Problem". In: *Applied Numerical Mathematics* 98 (Dec. 2015), pp. 106–121. ISSN: 01689274. DOI: 10.1016/j.apnum.2015.08.006. (Visited on 09/10/2019).

[100] Anne Greenbaum, Ren-cang Li, and Michael L Overton. "First-Order Perturbation Theory for Eigenvalues and Eigenvectors". In: (2019), p. 30.

[101] Nicola Guglielmi and Michael L. Overton. "Fast Algorithms for the Approximation of the Pseudospectral Abscissa and Pseudospectral Radius of a Matrix". In: *SIAM Journal on Matrix Analysis and Applications* 32.4 (Oct. 2011), pp. 1166–1192. ISSN: 0895-4798, 1095-7162. DOI: 10.1137/100817048. (Visited on 09/15/2019).

[102] *Eigenvalue Perturbation*. In: *Wikipedia | https://en.wikipedia.org/*. Page Version ID: 858476363. Sept. 7, 2018. URL: https://en.wikipedia.org/w/index.php?title=Eigenvalue_perturbation&oldid=858476363 (visited on 09/14/2018).

[103] Jean-Guy Caputo, Arnaud Knippel, and Elie Simo. "Oscillations of Networks: The Role of Soft Nodes". In: *Journal of Physics A: Mathematical and Theoretical* 46.3 (Jan. 25, 2013), p. 035101. ISSN: 1751-8113, 1751-8121. DOI: 10.1088/1751-8113/46/3/035101. (Visited on 08/08/2019).

[104] Shigefumi Hata and Hiroya Nakao. "Localization of Laplacian Eigenvectors on Random Networks". In: *Scientific Reports* 7.1 (Dec. 2017). ISSN: 2045-2322. DOI: 10.1038/s41598-017-01010-0. (Visited on 03/06/2019).

[105] M. Filoche and S. Mayboroda. "Universal Mechanism for Anderson and Weak Localization". In: *Proceedings of the National Academy of Sciences* 109.37 (Sept. 11, 2012), pp. 14761–14766. ISSN: 0027-8424, 1091-6490. DOI: 10.1073/pnas.1120432109. (Visited on 02/14/2019).

[106] Patrick N. McGraw and Michael Menzinger. "Laplacian Spectra as a Diagnostic Tool for Network Structure and Dynamics". In: *Physical Review E* 77.3 (Mar. 4, 2008), p. 031102. ISSN: 1539-3755, 1550-2376. DOI: 10.1103/PhysRevE.77.031102. (Visited on 06/04/2019).

[107] Shant Karakashian, Berthe Y Choueiry, and Stephen G Hartke. "An Algorithm for Generating All Connected Subgraphs with k Vertices of a Graph". In: *University of Nebraska–Lincoln* (2013), p. 37.

[108] Khaled Elbassioni. "A Polynomial Delay Algorithm for Generating Connected Induced Subgraphs of a given Cardinality". In: *Journal of Graph Algorithms and Applications* 19.1 (2015), pp. 273–280. DOI: 10.7155/jgaa.00357.

[109] Peter B. Denton et al. "Eigenvectors from Eigenvalues". In: (Aug. 10, 2019). arXiv: 1908.03795 [hep-th, physics:math-ph]. URL: http://arxiv.org/abs/1908.03795 (visited on 08/15/2019).

[110] Fortunato Villella et al. "PEGASE Pan-European Test-Beds for Testing of Algorithms on Very Large Scale Power Systems". In: *2012 3rd IEEE PES Innovative Smart Grid Technologies Europe (ISGT Europe)*. 2012 3rd IEEE PES Innovative Smart Grid Technologies Europe (ISGT Europe). Oct. 2012, pp. 1–9. DOI: 10.1109/ISGTEurope.2012.6465783.

[111] Ali Ajdari Rad, Mahdi Jalili, and Martin Hasler. "A Lower Bound for Algebraic Connectivity Based on the Connection-Graph-Stability Method". In: *Linear Algebra and its Applications* 435.1 (July 2011), pp. 186–192. ISSN: 00243795. DOI: 10.1016/j.laa.2010.12.019. (Visited on 09/10/2019).

[112] Arpita Ghosh and Stephen Boyd. "Upper Bounds on Algebraic Connectivity via Convex Optimization". In: *Linear Algebra and its Applications* 418.2-3 (Oct. 2006), pp. 693–707. ISSN: 00243795. DOI: 10.1016/j.laa.2006.03.006. (Visited on 09/10/2019).

[113] Bill G Horne. "Lower Bounds for the Spectral Radius of a Matrix". In: *Linear algebra and its applications* 263 (1997), pp. 261–273.

[114] Fan Chung and Ross M. Richardson. "Weighted Laplacians and the Sigma Function of a Graph". In: *Contemporary Mathematics*. Ed. by Gregory Berkolaiko et al. Vol. 415. Providence, Rhode Island: American Mathematical Society, 2006, pp. 93–107. ISBN: 978-0-8218-3765-8 978-0-8218-8094-4. DOI: 10.1090/conm/415/07862. (Visited on 05/22/2019).

[115] Klaus Glashoff and Michael M. Bronstein. "Almost-Commuting Matrices Are Almost Jointly Diagonalizable". In: (May 7, 2013). arXiv: 1305.2135 [cs]. URL: http://arxiv.org/abs/1305.2135 (visited on 01/23/2019).

Summaries

Summary in English

This thesis investigates the fundamental properties of a simplified dynamical power system model. These models can be used to study the influence of the geometrical properties of the network describing the power system. These models and some important properties of the models are presented in chapter 1. One of the main challenges in power system research is the complexity of the system. We want to use spectral graph theory to decompose the system into different modes, which can be studied individually. The second chapter introduces the mathematical background of spectral graph theory and the applications to power systems. A simple example for the application of spectral graph theory in power system research is given in chapter 3, where the static power flow system is investigated. We can see that the eigenvalues and eigenvectors of the nodal admittance matrix of the power system can be used to calculate the phases and flows in a static system. The dynamical properties are then deeper investigated in the next chapter. Here, a quadratic eigenvalue problem has to be used to investigate the system. We introduce the fundamental properties of the quadratic eigenvalue problem and the application to power system research. An extensive investigation of the spectral properties of a dynamical power system using the quadratic eigenvalue problem is then performed. We observe short and long range interactions in the system and see that the short range interactions are more sensitive to the machine parameters and are important for the stability of the power system, as they are related to local plant modes. The emergence of this localised behaviour is investigated in chapter 5. We derive two eigenvector bounds which can be used to predict and describe localisation in a network. These bounds are then applied to simple example graphs and a power system test case, to show how they can successfully predict, explain and describe localisation.

Summary in French

Cette thèse porte sur les propriétés fondamentales d'un modèle simplifié de système d'alimentation dynamique. Ces modèles permettent d'étudier l'influence des propriétés géométriques du réseau décrivant le système électrique. Ces modèles et certaines propriétés importantes des modèles sont présentés au chapitre 1. L'un des principaux défis de la recherche sur les systèmes électriques est la complexité du système. Nous voulons utiliser la théorie du graphique spectral pour décomposer le système en différents modes, qui peuvent être étudiés individuellement. Le deuxième chapitre présente le contexte mathématique de la théorie des graphes spectraux et les applications aux systèmes d'alimentation. Un exemple simple d'application de la théorie des graphes spectraux à la recherche sur les systèmes d'alimentation est donné au chapitre 3, où l'on étudie le système d'alimentation statique. Nous pouvons voir que les valeurs propres et les vecteurs propres de la matrice d'admission nodale du système électrique peuvent être utilisés pour calculer les phases et les flux dans un système statique. Les propriétés dynamiques sont ensuite étudiées plus en profondeur dans le chapitre suivant. Ici, un problème de valeur propre quadratique doit être utilisé pour étudier le système. Nous présentons les propriétés fondamentales du problème de la valeur propre quadratique et son application à la recherche sur les systèmes d'alimentation. Une étude approfondie des propriétés spectrales d'un système de puissance dynamique utilisant le problème des valeurs propres quadratiques est ensuite réalisée. Nous observons des interactions à courte et longue portée dans le système et constatons que les interactions à courte portée sont plus sensibles aux paramètres de la machine et sont importantes pour la stabilité du système électrique, car elles sont liées aux modes locaux de la centrale. L'émergence de ce comportement localisé est étudiée au chapitre 5. Nous dérivons deux limites de vecteurs propres qui peuvent être utilisées pour prédire et décrire la localisation dans un réseau. Ces limites sont ensuite appliquées à des exemples simples de graphiques et à un cas de test de système électrique, pour montrer comment ils peuvent prédire, expliquer et décrire avec succès la localisation.

Acknowledgements

Completing this thesis has been the biggest challenge in my life thus far. The impact my time in France and my work for the INCITE project cannot be understated. It has been an amazing time which I will remember fondly. This would not have been possible without the help of many people. I might forget or not mention some of you, I am sorry in advance.

My supervisor Nicholas Retiere, thank you for accepting me as your student. Thank you for your support and time and input. Thank you for letting my do my own things at times and applying the right amount of pressure at other times. Thank you for our (way too long) meetings, where I believe we both learnt a lot. I believe that this PhD was a challenge for both of us, hopefully a fruitful ones.

I want to thank the jury of my PhD, namely Didier Georges, Ettore Bompard, Philippe Jacquod and José Luis Domínguez for their critical investigation of my manuscript and their important questions and comments about my work.

This PhD would not have been possible without the support of the INCITE Horizon 2020 project. I would like to thank all ESRs and supervisors from the INCITE project for their input and work at the project. Our workshops and summer schools have been extremely informative, helpful and fun at the same time. As part of the project, I spend four months at IREC Barcelona, which was a helpful and interesting time. Special thanks, for their roles at the INCITE project as well as for supporting me in Barcelona, to José Luis Domínguez and Marta Fonrodona.

I would like to thank my friends and other PhD students in Grenoble. There are (too) many names to mention, so I will keep this list shorter then I probably should. The complete list of names and their role for my PhD can be found in the appendix. Laurene, thank you for our time together and our friendship. Thanks to my fellow INCITE member *Νικόλαος* for the fun had in Grenoble and at various INCITE moments. And thank god you always knew the rules better then me, I don't know how I would have come thus far without you.

Finally, I would like to thank my parents and my siblings for your support, love and friendship. I found out that other PhD students call their parents much more regularly then I did, but I always felt close to you, even with all that distance.

UNIVERSITÉ GRENOBLE ALPES

Abstract

Grenoble INP
ED EEATS

Doctor of Engineering

Investigations of Spectral Graph Properties in Power Systems

by Felix Sebastian KOETH

English This thesis studies the influence of geometry on the dynamic properties of power systems. We use a mathematical technique, called spectral graph theory, to break down the system into its frequencies, which can be studied individually. Thanks to this technique, we are able to analyze the system in a fundamental way. One of the main observations concerns short-range interactions in the system, which can have a huge impact on the overall stability of the system. These interactions are studied theoretically, which leads to a method to characterise, predict and explain this localised behaviour. The developed method can be used to facilitate the design and control of power grids, but it can also be applied to different scientific fields, where location properties in networks are important.

French Cette thèse étudie l'influence de la géométrie sur les propriétés dynamiques des systèmes d'alimentation. Nous utilisons une technique mathématique, appelée théorie des graphes spectraux, pour décomposer le système en ses fréquences, qui peuvent être étudiées individuellement. Grâce à cette technique, nous sommes en mesure d'analyser le système de manière fondamentale. L'une des principales observations concerne les interactions à courte portée dans le système, qui peuvent avoir un impact énorme sur la stabilité globale du système. Ces interactions sont étudiées théoriquement, ce qui aboutit à une méthode pour caractériser, prédire et expliquer ce comportement localisé. La méthode mise au point peut être utilisée pour faciliter la conception et le contrôle des réseaux électriques, mais elle peut également s'appliquer à différents domaines scientifiques, où les propriétés de localisation dans les réseaux sont importantes.